

Hubble tension or a transition of the Cepheid SnIa calibrator parameters?

Leandros Perivolaropoulos^{1,*} and Foteini Skara^{1,†}

¹*Department of Physics, University of Ioannina, GR-45110, Ioannina, Greece*

(Dated: September 22, 2021)

We re-analyze the Cepheid data used to infer the value of the Hubble constant H_0 by calibrating Type Ia supernovae. We do not enforce a universal value of the empirical Cepheid calibration parameters R_W (Cepheid Wesenheit color-luminosity parameter) and M_H^W (Cepheid Wesenheit H-band absolute magnitude). Instead we allow for variation of either of these parameters for each individual galaxy. We also consider the case where these parameters have two universal values: one for low galactic distances $D < D_c$ and one for high galactic distances $D > D_c$ where D_c is a critical transition distance. We find hints for a 3σ level mismatch between the low and high galactic distance parameter values. We then use model selection criteria (AIC and BIC) which penalize models with large numbers of parameters, to compare and rank the following types of R_W and M_H^W parameter variations: Base models: Universal values for R_W and M_H^W (no parameter variation), I: Individual fitted galactic R_W with one universal fitted M_H^W , II: One universal fixed R_W with individual fitted galactic M_H^W , III: One universal fitted R_W with individual fitted galactic M_H^W , IV: Two universal fitted R_W (near and far) with one universal fitted M_H^W , V: One universal fitted R_W with two universal fitted M_H^W (near and far), VI: Two universal fitted R_W (near and far) with two universal fitted M_H^W (near and far). We find that the AIC and BIC model selection criteria consistently favor model IV instead of the commonly used Base model where no variation is allowed for the Cepheid empirical parameters. The best fit value of the SnIa absolute magnitude M_B and of H_0 implied by the favored model IV is consistent with the inverse distance ladder calibration based on the CMB sound horizon $H_0 = 67.4 \pm 0.5 \text{ km s}^{-1} \text{ Mpc}^{-1}$. Thus in the context of the favored model IV the Hubble crisis is not present. This model may imply the presence of a fundamental physics transition taking place at a time more recent than 100 *Myrs* ago.

I. INTRODUCTION

A number of challenges of the standard Λ CDM model has been emerging during the past few years as the accuracy of cosmological observations improves. There are signals in cosmological and astrophysical data that appear to be in some tension (2σ or larger) with the standard Λ CDM model as defined by the Planck18 parameter values [1] (for a review, see Ref. [2] and for a list of papers, see [3]).

The most intriguing large scale tension is the Hubble crisis. Using a distance ladder approach, the local (late or low redshift) measurements of the Hubble constant H_0 lead to values that are significantly higher than those inferred using the angular scale of fluctuations of the cosmic microwave background (CMB) in the context of the Λ CDM model. Local direct measurements of H_0 are in more than 4σ tension with CMB indirect measurements of H_0 (for a review, see Refs. [2, 4, 5]).

The local (late or low redshift) determination of the Hubble constant H_0 using a distance ladder approach depends on a chain of distance measurements. In the cosmic distance ladder approach each step of the distance ladder uses parallax methods and/or the known intrinsic luminosity of a standard candle source to determine the absolute (intrinsic) luminosity of a more luminous standard candle residing in the same galaxy. Thus highly

luminous standard candles are calibrated for the next step in order to reach out to high redshift luminosity distances. If one of these distance measures is subject to systematics or new physics all the subsequent rungs of the cosmic distance ladder are off.

The distance ladder approach is based on a method pioneered by Henrietta Swan Leavitt. She realized that a type of pulsating stars known as Cepheid variable has a period of pulsation that depends on its luminosity. This period–luminosity (PL) relation is called the Leavitt law [6, 7]. Knowing the luminosity of a Cepheid means that its luminosity distance can be determined just by observing its brightness which has been dimmed by that distance. Therefore the Cepheids whose luminosities are correlated with their periods of variability can be the first standard candles in the cosmic distance ladder [8–15]. Trigonometric parallax methods (geometric anchors) may be used to calibrate the Cepheid variable star standard candles at the local Universe (primary distance indicators). Then using the measured luminosity distances of the calibrated Cepheid stars, the intrinsic luminosity of nearby ($D \approx 20 - 40 \text{ Mpc}$) incredibly bright type Ia supernova (SnIa) residing in the same galaxies as the Cepheids is obtained. This calibration of the new type of standard candle SnIa fixes its absolute magnitude M_B and is then used for SnIa at more distant galaxies (in the Hubble flow) to measure H_0 ($z \in [0.01, 0.1]$) and $H(z)$ ($z \in [0.01, 2.3]$) via the measurement of their luminosity distances.

The angular diameter distance of standard rulers can also be used for the estimation of $H(z)$. The Λ CDM best fit value obtained from the sound horizon at recombina-

* leandros@uoi.gr

† f.skara@uoi.gr

tion standard ruler calibrated by the CMB anisotropy spectrum peaks, leads to the measurement $H_0 = 67.4 \pm 0.5 \text{ km s}^{-1} \text{ Mpc}^{-1}$ [1]. The local measurements based on Cepheid calibrators indicate the value $H_0 = 74.03 \pm 1.42 \text{ km s}^{-1} \text{ Mpc}^{-1}$ [16] (4.4σ , 9%). A more recent analysis by the Supernovae H_0 for the Equation of State (SH0ES) Team [16–18] using the recently released Gaia Early Data Release 3 (EDR3) parallaxes [19] has reached 1.8% precision by improving the calibration. Thus, a value of $H_0 = 73.2 \pm 1.3$ was obtained [20]. This is in a 4.2σ tension with the prediction from Planck18 CMB observations [1].

The values of H_0 determined in the late Universe with a calibration based on the Cepheid distance scale and the derived values of H_0 from analysis of the CMB anisotropy spectrum data are shown in Fig. 1. The uncertainties in these values have been decreasing for both methods and the recent measurements disagree beyond 4σ . The Hubble constant H_0 values at 68% CL through direct and indirect measurements obtained by the different methods are illustrated in Fig. 2, from which is evident that the SnIa distance scale calibrated by Cepheid variables is in tension with the CMB sound horizon scale.

If the Hubble tension is not due to systematic errors [4, 33–38], it could be an indication of incorrect estimate of the sound horizon scale due e.g. to early dark energy [39] or to late phantom dark energy [40]. A Gpc scale underdensity [41] has also been proposed as a possible cause of the Hubble tension. Theoretical models addressing this discrepancy utilize either a recalibration of the Λ CDM standard ruler (the sound horizon) assuming new physics before the time of recombination [42–45] or a deformation of the Hubble expansion rate $H(z)$ at late times [40, 46, 47] or an abrupt transition of the SnIa absolute luminosity due to late time new physics [48] (for a review, see Refs. [2, 4, 5], for approaches, see Refs. [49, 50] and for a relevant talk, see Ref. [51]).

The authors of Ref. [48] have pointed out that the H_0 crisis may be viewed as a mismatch between the SnIa absolute magnitude calibrated by Cepheids at $z < 0.01$ [52, 53]

$$M_B^< = -19.244 \pm 0.037 \text{ mag} \quad (1.1)$$

and the SnIa absolute magnitude obtained using the parametric free inverse distance ladder calibrating SnIa absolute magnitude using the sound horizon scale [54]

$$M_B^> = -19.401 \pm 0.027 \text{ mag} \quad (1.2)$$

Since the two measurements are obtained at different redshifts they may indicate a transition in the absolute magnitude with amplitude $\Delta M_B = M_B^> - M_B^< \simeq -0.2 \text{ mag}$ at a transition redshift $z_t \lesssim 0.01$ (roughly 100-150 million years ago) [48, 55]. Note that hints of a possible weak evolution of the absolute magnitude M_B have been recently pointed out in Refs. [56, 57].

Such a transition may occur due to a transition of the strength of the gravitational interactions G_{eff} which modifies the SnIa intrinsic luminosity L by changing the value

of the Chandrasekhar mass M_{Ch} . The simplest assumption leads to [58, 59]

$$L \sim M_{Ch} \sim G_{\text{eff}}^{-3/2} \quad (1.3)$$

even though corrections may be required to the above simplistic approach [60].

Using the normalized effective Newton constant $\mu_G \equiv G_{\text{eff}}/G_N$ (where G_N is the locally measured Newton's constant and $\mu_G = 1$ for $z < z_t \lesssim 0.01$) and assuming the power law dependence Eq. (1.3) the absolute magnitude of SnIa M_B is expected to change as [59, 61–63]

$$\Delta M_B = \frac{15}{4} \log_{10}(\Delta \mu_G - 1) \quad (1.4)$$

Thus for $\Delta M_B \simeq -0.2 \text{ mag}$ it is straightforward to show that the change of μ_G [48]

$$\Delta \mu_G \equiv \mu_G^> - \mu_G^< \simeq -0.12 \quad (1.5)$$

where $\mu_G^>$ corresponds to $z > z_t$ and $\mu_G^<$ corresponds to $z < z_t$ in the context of a Λ CDM background $H(z)$.

This connection indicates that a 10% smaller G_{eff} for $z > z_t$ could potentially provide the required decrease of the absolute magnitude (increase of luminosity) at early times for the resolution of the Hubble tension. In fact such a decrease would also lower the growth rate of cosmological perturbations thus helping in the resolution of the growth tension [48, 64]. Thus, the smaller G_{eff} ($G_{\text{eff}} < 1$) for $z > z_t$ hints towards weaker gravity as indicated by studies discussing the growth tension [65–71].

Interestingly, an analysis of recent Tully-Fisher data [72] has identified hints for a transition of the values of the Tully-Fisher parameters which depend on gravitational physics at a distance scale close to 20 Mpc . The magnitude and sign of the transition are consistent with the proposed mechanism albeit at somewhat more recent times: about 70 million years ago, corresponding to $z_t \simeq 0.005$.

A recent analysis [73], has analyzed the color-luminosity relation of Cepheids in anchor galaxies and SnIa host galaxies by identifying the color-luminosity relation for each individual galaxy instead of enforcing a universal color-luminosity relation to correct the near infrared (NIR) Cepheid magnitudes. This analysis finds a systematic brightening of Cepheids at distances larger than about 20 Mpc (see Fig. 4 in Ref. [73]). As pointed out in [73] this brightening could be enough to resolve the Hubble tension. The authors attribute it to variation of dust properties but there is currently a debate on the actual cause of this brightening.

In the present study we reproduce and extend the analysis of Ref. [73] by considering a varying among individual galaxies color-luminosity relation and (in a separate analysis) allowing the Cepheid absolute magnitude M_H^W to vary among individual galaxies instead of enforcing a universal absolute magnitude. We also explore the possibility that there are two universal absolute magnitudes: one applicable for low distance D Cepheids ($M_H^{W,<}$ for

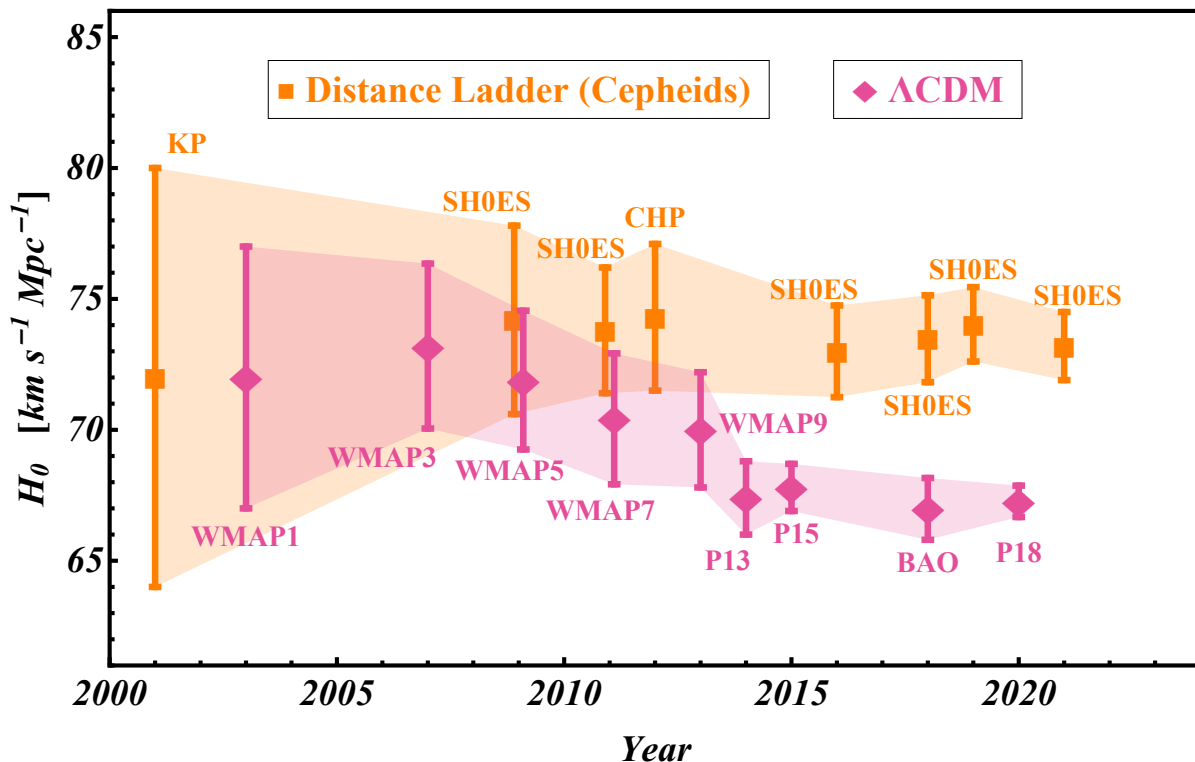


FIG. 1. The Hubble constant as a function of publication date, using a set of different tools. Symbols in orange denote the values of H_0 determined in the late Universe with a calibration based on the Cepheid distance scale (Key Project (KP) [21], SH0ES [16–18, 20, 22, 23], Carnegie Hubble Program (CHP) [24]). Symbols in purple denote the derived values of H_0 from analysis of the CMB data based on the sound horizon standard ruler (First Year WMAP (WMAP1) [25], Three Year WMAP (WMAP3) [26], Five Year WMAP (WMAP5) [27], Seven Year WMAP (WMAP7) [28], Nine Year WMAP (WMAP9) [29], Planck13 (P13) [30], Planck15 (P15) [31], Planck18 (P18) [1], BAO [32]). The orange and purple shaded regions demonstrate the evolution of the uncertainties in these values which have been decreasing for both methods. The most recent measurements disagree at greater than 4σ (from Ref. [2]).

$D < D_c$) and a second, applicable for high distance D Cepheids ($M_H^{W,>}$ for $D > D_c$). We then test the consistency among the two absolute magnitudes searching for hints of a physics transition at some critical distance (time) D_c (D_c/c).

We thus address the following questions:

- Are there indications for variation of the color-luminosity relation and of the Cepheid absolute magnitude among individual galaxies?
- Is the color-luminosity relation and/or absolute magnitude of nearby Cepheids consistent with the corresponding properties of Cepheids in more distant galaxies?
- Are there indications for a Cepheid luminosity transition similar to the one required for the resolution of the Hubble tension?

In order to address these questions we use the same data and similar method as those used in Ref. [73] but in addition we extend the types of parameter variations allowed while implementing model selection criteria in

order to compare the different allowed types of parameter variations (models) with the Base model which assumes universal Cepheid empirical parameter values. The data are obtained from Refs. [16, 18, 20] and displayed in the Appendix B. Our generalized approach is based on two extensions

- We break the assumption of universality not only on the color-luminosity relation but also on the absolute magnitude of Cepheids.
- In addition to fitting the Cepheid color-luminosity relation (or the absolute magnitude) for each galaxy separately, we also consider the case of two universality classes one for nearby and one for more distant galaxies thus introducing only one new parameter in each case compared to the standard universal approach.

The structure of this paper is the following: In the next Section II we present a brief review of the theoretical background and we describe the method used in our analysis as well as the data considered. In Section III we present our results focusing on the consistency of nearby

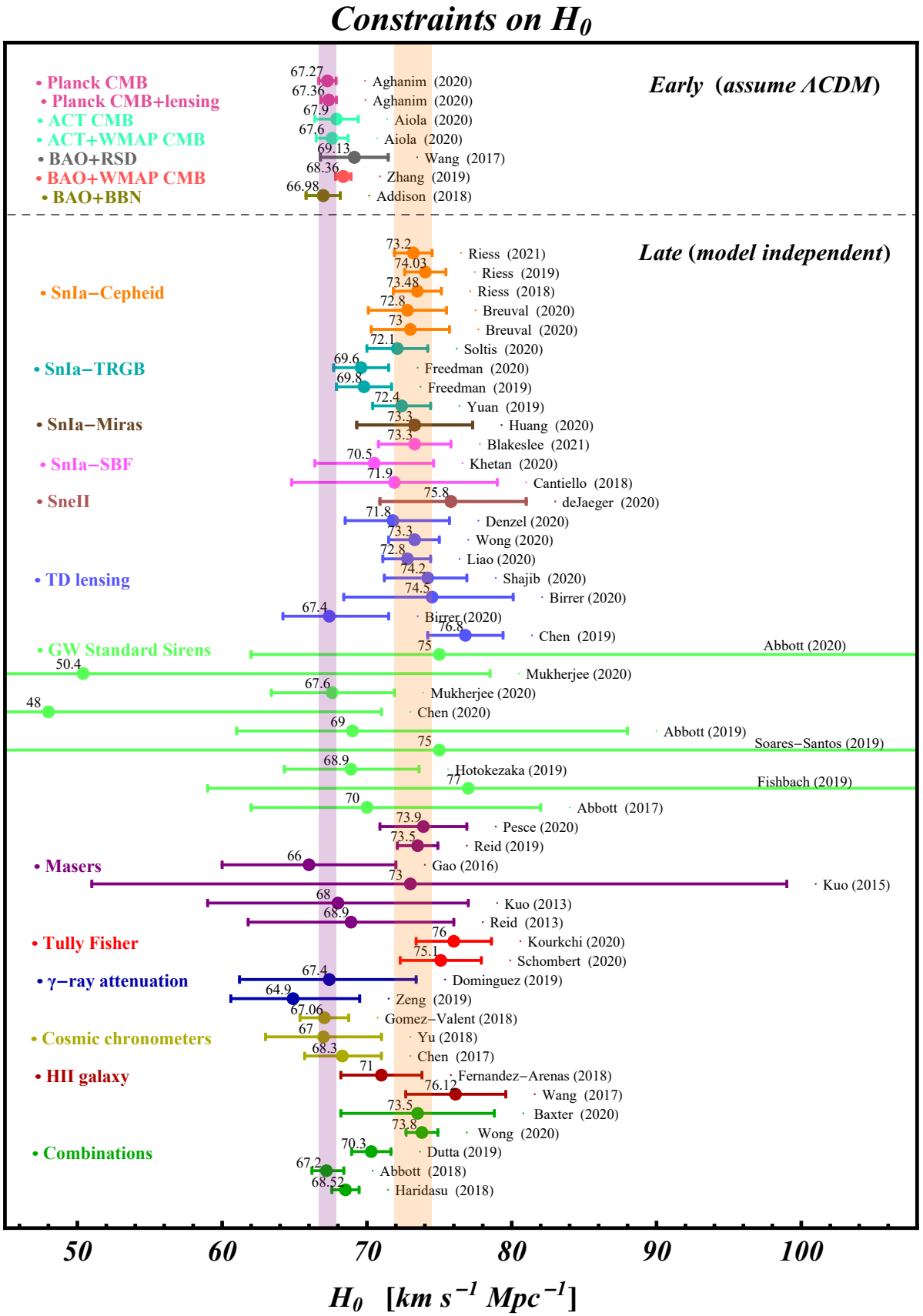


FIG. 2. The Hubble constant H_0 values with the 68% CL constraints derived by recent measurements. The value of the Hubble constant H_0 is derived by early time approaches based on sound horizon, under the assumption of a Λ CDM background. The shaded orange and purple bands show the tension between the values inferred from Cepheid calibrated SnIa and CMB observation (from Ref. [2]).

and more distant samples with each other. We also compare with a Monte Carlo uniformized dataset in order to verify that any observed peculiar signal disappears in a Monte Carlo constructed homogeneous dataset. In Section IV we consider various cases (models) allowing for different types of empirical parameter variation and use criteria for model selection and model comparison. In Section V we investigate the impact of the allowed types of parameter variation on the SnIa absolute magnitude M_B and on the corresponding derived value of H_0 . Finally in Section VI we summarize our methods and results and discuss possible extensions of our analysis. We also compare our results with previous analyses searching for similar transition effects in different datasets.

II. THEORETICAL BACKGROUND-METHOD-DATA

In this section, we present a brief review of the theoretical expressions and describe the method and the dataset used.

II.1. Standard candles

In an expanding flat Universe, where the energy is not conserved due to the increase of the photon wavelength and period with time, the luminosity distance can be expressed as [74, 75]

$$d_L(z) = c(1+z) \int_0^z \frac{dz'}{H(z')} \quad (2.1)$$

The luminosity distance is an important cosmological observable that is measured using standardizable candles like SnIa ($z < 2.3$) [76] and gamma-ray bursts (GRBs) ($0.1 < z \lesssim 9$) [77–82].

Surveys can indicate the distance-redshift relation of SnIa by measuring their peak luminosity that is tightly correlated with the shape of their characteristic light curves (luminosity as a function of time after the explosion) [83] and the redshifts of host galaxies.

The use of SnIa in the measurement of H_0 and $H(z)$ relies on a basic assumption that they are standardizable and after proper calibration they have a fixed absolute magnitude independent of redshift in the redshift range $z \in [0.01, 2.3]$ [83]. This assumption has been tested in Refs. [49, 56, 57, 84–90]. The possibility for intrinsic luminosity evolution of SnIa with redshift was first highlighted by Ref. [91]. Also, the assumption that the luminosity of SnIa is independent of host galaxy properties (e.g. host age, host morphology, host mass) and local star formation rate has been discussed in Refs. [92–96].

The apparent magnitude m_B of SnIa at redshift z with absolute magnitude M_B in the context of a specified form of $H(z)$, is related to their luminosity distance $d_L(z)$ in

Mpc as

$$m_B(z) = M_B + 5 \log_{10} \left[\frac{d_L(z)}{\text{Mpc}} \right] + 25 \quad (2.2)$$

Using now the dimensionless Hubble free luminosity distance

$$D_L(z) = \frac{H_0 d_L(z)}{c} \quad (2.3)$$

the apparent magnitude can be written as

$$m_B(z) = M_B + 5 \log_{10} [D_L(z)] + 5 \log_{10} \left[\frac{c/H_0}{\text{Mpc}} \right] + 25 \quad (2.4)$$

Using the degenerate combination

$$\mathcal{M} = M_B + 5 \log_{10} \left[\frac{c/H_0}{\text{Mpc}} \right] + 25 \quad (2.5)$$

into Eq. (2.4) we obtain

$$m_B(z) = \mathcal{M} + 5 \log_{10} [D_L(z)] \quad (2.6)$$

The use of Eq. (2.4) to measure H_0 using the measured apparent magnitudes of SnIa requires knowledge of the value of the SnIa absolute magnitude M_B . This can be obtained using calibrators of local SnIa at $z < 0.01$ (closer than the start of the Hubble flow) in the context of a distance ladder approach (e.g. [97]). Calibrators like Cepheid stars which are bright, variable supergiants are used in this context.

II.2. Cepheid calibration

The Milky Way (MW), the Large Magellanic Cloud (LMC) and NGC 4258 are used as distance anchor galaxies. For Cepheids in the anchor galaxies there are three different ways of geometric distance calibration of their luminosities: parallaxes in the MW [20, 23, 98–103], detached eclipsing binary stars (DEBs) in the LMC [104] and water masers¹ in NGC 4258 [107]. The DEBs method relies on surface-brightness relations and is one-step distance determination to nearby galaxies independent from Cepheids [108]. The Andromeda galaxy (M31) could serve as an anchor in the cosmic distance ladder but the uncertainty in its distance measurements is difficult to reduce [109].

The empirically-determined period-magnitude relationship of a Cepheid can be expressed as (e.g. [36])

$$m_H - R_H E(V - I) = \mu + M_H + b_H [P] + Z_H [M/H] \quad (2.7)$$

¹ Very long baseline interferometric (VLBI) observations of water megamasers which are found in the accretion disks around supermassive black holes (SMBHs) in active galactic nuclei (AGN) have been demonstrated to be powerful one-step geometric probes for measuring extragalactic distances [105, 106].

where m_H is the observed apparent magnitude in the near-infrared H (F160W) band which is centered at $\lambda_H \sim 1.63 \mu m$, V (F555W) and I (F814W) are the optical mean apparent magnitudes which are centered at $\lambda_V \sim 0.555 \mu m$ and $\lambda_I \sim 0.79 \mu m$ respectively, in the HST system², $E(V - I)$ is the color excess, R_H is the total to selective extinction parameter at H band³, $\mu \equiv 5 \log_{10} [d_L(z)/Mpc] + 25$ is the inferred distance modulus to the Cepheid, M_H is the absolute magnitude of a period $P = 10 d$ Cepheid (d for days), b_H and Z_H are the slope parameters that represent the dependence of magnitude on both period and metallicity.

The $[M/H]$ is a measure of the metallicity of the Cepheid. The usual bracket shorthand notation for the metallicity $[M/H]$ represents the Cepheid metal abundance compared to that of the Sun

$$[M/H] \equiv \log(M/H) - \log(M/H)_\odot = \Delta \log(M/H) \quad (2.8)$$

where M and H is the number of metal (any element other than hydrogen or helium) and hydrogen atoms per unit of volume respectively. The unit often used for metallicity is the dex (decimal exponent) defined as $n \text{ dex} = 10^n$.

Also, the bracket shorthand notation for the period $[P]$ is used as (P in units of days)

$$[P] \equiv \log P - 1 \quad (2.9)$$

The color excess characterizes the amount of reddening associated with interstellar extinction, a combined effect of absorption and scattering of blue more than red light by dust and other matter [110, 111]. The color excess depends on the properties of dust and is defined as

$$E(V - I) \equiv A_V - A_I = (V - I) - (V - I)_0 \quad (2.10)$$

where $V - I$ and $(V - I)_0$ are the observed and the intrinsic (normal) Cepheid color respectively. The latter is the hypothetical true Cepheid color which would be observed if there was no extinction.

Following the same formulation used by the SHOES team [16, 18] in order to minimize the impact of extinction correction uncertainties for distance measurements and determination of the Hubble constant H_0 , we use the replacement $E(V - I) \rightarrow V - I$ in Eq. (2.7), the Hubble Space Telescope (HST) NIR H-band and the reddening-free "Wesenheit" magnitudes [112]

$$m_H^W \equiv m_H - R_W(V - I) = \mu + M_H^W + b_W[P] + Z_W[M/H] \quad (2.11)$$

where the empirical parameter R_W is the reddening-free "Wesenheit" color ratio and is different from R_H which

can be derived from a dust law (e.g. the Fitzpatrick law [113]). The parameter R_W corrects for both dust and intrinsic variations applied to observed blackbody colors $V - I$. Eq. (2.11) can be derived from Eq. (2.7) using Eq. (2.10) with a constant fixed parameter R_W under the important assumption that the intrinsic Cepheid color $(V - I)_0$ can be assumed to have the same distribution for all galaxies. This allows the absorption of the term $R_H(V - I)_0$ by the Cepheid absolute magnitude M_H thus defining the Cepheid Wesenheit H-band absolute magnitude M_H^W in Eq. (2.11). An additional logarithmic dependence of the intrinsic color on the Cepheid period is also allowed and would be absorbed by the parameter b_H leading to the parameter b_W . Thus, if there was a transition in the intrinsic Cepheid color $(V - I)_0$ at a given galactic distance, this transition would manifest itself as a shift of any or all of the parameters M_H^W , b_W and/or R_W at the same distance.

For distances based on NIR ($1 < \lambda < 2.5 \mu m$) measurements, both the impact of extinction by dust (gauged using the observed color $V - I$) and the impact of metallicity on the luminosities and colors of Cepheids, are less significant compared to the corresponding optical measurements [8, 114–116] (for the metallicity effects which are still largely debated, see Refs. [117–121]). However the NIR measurements of Cepheids still suffer from crowding and blending (photometric contamination) from redder Red Giant Branch (RGB) and Asymptotic Giant Branch (AGB) disk stars, particularly as the distance increases [122–124].

Wesenheit magnitudes have the advantage of smaller dispersion in the PL relation caused by differential extinction and the nonzero temperature width of the Cepheid instability strip⁴ (see e.g. Ref. [128]).

Following Ref. [18] and breaking the slope of the Leavitt law at a period of 10 days ($P = 10 d$) we include two different slopes b_W^s and b_W^l parameters in Eq. (2.11) for short and long period Cepheids with $P < 10 d$ and $P > 10 d$ respectively (for a discussion about the presence of a broken PL slope at $P = 10 d$, see Refs. [129–134]).

Ref. [18] considers a universal reddening law in all galaxies and thus assume a global fixed value $R_W = 0.386$. This value is derived from the reddening law of Ref. [113] using a ratio of total to selective extinction at the B and V bands⁵ of the Johnson-Morgan or UB V (Ultraviolet, Blue, Visual) photometric system [135] $R_V = 3.3$ to parameterize the shape of the extinction curve. In the literature the parameter R_W ranges

² HST uses the same three-band photometric system with the Wide Field Camera 3 (WFC3) with two optical filters (F555W and F814W) and one near-infrared filter (F160W).

³ The total to selective extinction parameter at H band R_H is defined as $R_H \equiv A_H/(A_V - A_I) = A_H/E(V - I)$ (where A_H is the extinction due to dust along the line of sight).

⁴ The instability strip refers to a narrow, almost vertical temperature (spectral type) region on the Hertzsprung-Russell (H-R) diagram which contains several types of pulsating variable stars including Cepheid variables (see e.g. Refs. [125–127]). The Classical Cepheids (Population I Cepheids) are F6-K2 type supergiants ($\sim 4 - 20 M_\odot$) with a period of 1 to 70 days with an amplitude variation of 0.1 to 2.0 magnitudes.

⁵ The total to selective extinction at B and V bands R_V is defined as $R_V \equiv A_V/E(B - V)$

from 0.3 to 0.5 at H band (e.g. $R_W = 0.41$ in Ref. [17]) and the universal parameter R_V ranges from 1 to 6 (the average value for the MW is $R_V = 3.1$) [136–146] depending on the reddening law [147–149].

As noted recently by Ref. [73] a global fixed value for parameter R_W could result in a systematic error in distance measurements and the determination of the Hubble constant H_0 . Refs. [73, 150] motivated by the observed variation in dust properties allowing for the parameter R_W to vary between galaxies. However these studies make no attempt to search for possible transitions within the low z galaxy data. In the present analysis we search for transition effects in Cepheid data at $z \lesssim 0.01$ ($\lesssim 40$ Mpc).

II.3. Datasets

We use a sample of 1630 Cepheids in the anchor galaxies and in the SnIa host galaxies. For 74 MW Cepheids including GAIA parallax measurements we use the dataset from Table 1 in Ref. [20] and for 70 LMC Cepheids we use the dataset from Table 2 in Ref. [16]. These data are shown in Tables IV and V of the Appendix B. Fitting the distance ladder with the system of equations for the 70 LMC Cepheids an intrinsic scatter of 0.08 mag is added to the error estimates given in Table 2 of Ref. [16] (note that Ref. [16] include a intrinsic LMC dispersion of 0.07 mag) which is necessary in order to obtain a reduced chi-square of unity $\chi_{red}^2 = \chi_{min}^2/dof = 1$ [151].

We obtain data for 1486 Cepheids in the anchor galaxy NGC 4258, in the M31 galaxy and in the 19 SnIa host galaxies from Table 4 in Ref [18] (for details, see Ref. [152]). This data are shown in Table VI of the Appendix B.

We consider the revised distance modulus to NGC 4258 of $\mu_{N4258} = 29.397 \pm 0.032$ mag (7.576 ± 0.112 Mpc) reported by Ref. [107] using water masers data. Also we consider the distance modulus to the LMC of $\mu_{LMC} = 18.477 \pm 0.0263$ mag derived by Ref. [104] with 1% precision based on enhanced samples of late-type DEBs. This distance modulus is increased from that in Ref. [18] by 0.5%.

Finally for SnIa B-band magnitudes we adopt the data from Table 5 in Ref. [18], derived from the version 2.4 of SALT2⁶ modeling of SnIa light curves by Ref. [158]. These data are shown in Table VII of the Appendix B.

Following Ref. [16] for all LMC Cepheids we adopt the mean metallicity of -0.33 dex from Ref. [159] and -0.27 dex from Ref. [160], $[Fe/H] = -0.30$ dex which is slightly different than the value of -0.25 dex adopted

by Ref. [18]. Also following Ref. [16] we adopt $[O/H] = [Fe/H]$ (where O and Fe is the number of oxygen and iron atoms per unit of volume respectively) and we measure the metallicity in units of $Z = 12 + \log(O/H)$ (with Solar metallicity in these units $Z_\odot = 12 + \log(O/H)_\odot = 8.824$ [150]).

Note that since we use the datasets from Refs. [16, 18, 20] with the same filters we do not need to apply further corrections. The full datasets are available in [161].

III. SEARCH FOR TRANSITION

Our analysis is closely related to the results of study by Ref. [73]. Using the same datasets that were used by Ref. [73] we first reproduce their results and then we search for a transition signal of the best fit parameter values R_W and M_H^W between data subsamples at low and high distances.

From Eq. (2.11) using the Wesenheit magnitude of the j th Cepheid in the i th galaxy, including the host and the anchor galaxies, here MW, NGC 4258 and the LMC, separating PL relations for short and long period Cepheids we have

$$\begin{aligned} m_{H,i,j}^W &\equiv m_{H,i,j} - R_{W,i}(V - I)_{i,j} \\ &= \mu_i + M_{H,i}^W + b_W^s [P]_{i,j}^s + b_W^l [P]_{i,j}^l + Z_W [M/H]_{i,j} \end{aligned} \quad (3.1)$$

where $[P]_{i,j}^s = 0$ for Cepheids with $P > 10$ d and $[P]_{i,j}^l = 0$ for Cepheids with $P < 10$ d.

In the case where i th galaxy is the MW the distance modulus for the j th Cepheid is estimated using parallaxes in units of mas (mas for milliarcsec)

$$\pi_j + zp = 10^{-0.2(\mu_j - 10)} \quad (3.2)$$

where zp is a residual parallax calibration offset.

Thus

$$\begin{aligned} \mu_j &= 10 - \frac{5}{\ln 10} \left[\ln \pi_j + \ln \left(1 + \frac{zp}{\pi_j} \right) \right] \\ &\simeq 10 - \frac{5}{\ln 10} \left[\ln \pi_j + \frac{zp}{\pi_j} \right] \end{aligned} \quad (3.3)$$

where higher order terms $\mathcal{O}(zp/\pi_j)^2$ are negligible. Using Eq. (3.3) into Eq. (3.1) in the case of MW Cepheids we obtain

$$\begin{aligned} m_{\pi,j}^W &= m_{\pi,j} - R_W(V - I)_j \\ &= M_H^W + b_W^s [P]_j^s + b_W^l [P]_j^l + Z_W [M/H]_j + \frac{5}{\ln 10} \frac{zp}{\pi_j} \end{aligned} \quad (3.4)$$

where we use

$$m_{\pi,j}^W = m_{H,j}^W - 10 + \frac{5}{\ln 10} \ln \pi_j \quad (3.5)$$

⁶ Spectral Adaptive Light Curve Template (SALT) is an empirical spectro-photometric model that is used in SnIa light curve fitting [153–155] (for SALT tests with simulations, see [156]). SALT is publicly available at [157].

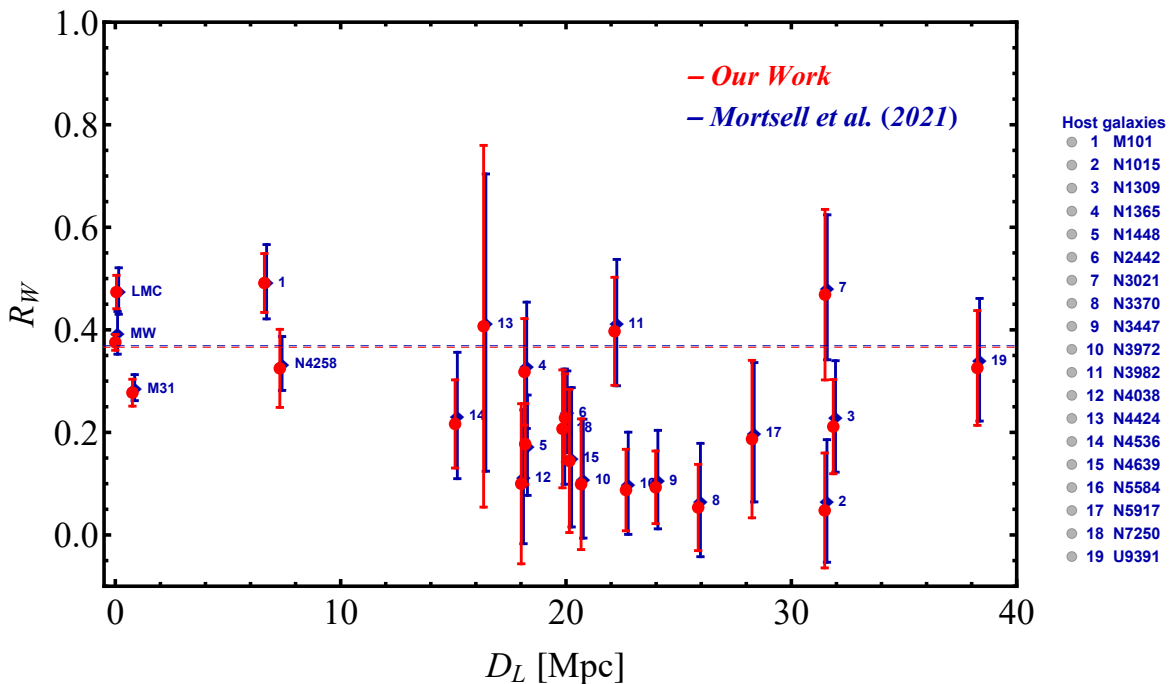


FIG. 3. Fitting individual R_W to Cepheid data as derived from our work (red points) and from Ref. [73] (blue points). For illustration purposes, the D_L axis has been shifted slightly for our values so that the error bars do not overlap. The red and blue dotted lines correspond to $R_W = 0.366$ and $R_W = 0.369$ respectively. These R_W values are taken using the derived individual parameters of anchor galaxies and M31 (due to its proximity) $R_{W,k}$.

and

$$m_{\pi,j} = m_{H,j} - 10 + \frac{5}{\ln 10} \ln \pi_j \quad (3.6)$$

Also in order to combine the measurements of SnIa and Cepheids we use the calibrated SnIa B-band peak magnitude in the i th host

$$m_{B,i} = \mu_i + M_B \quad (3.7)$$

Using the data (see Section II.3) for observed Cepheid magnitudes m_H , colors $V - I$, periods $[P]$, metallicities $[M/H]$, MW Cepheid parallaxes π , anchor distances μ_k together with the SnIa magnitudes m_B , we can fit simultaneously for R_W , b_W^s , b_W^l , Z_W , the host and the anchor galaxy distances μ_i , the parallax offset zp , the Cepheid absolute magnitude M_H^W and the SnIa absolute magnitude M_B .

Combining the equations for apparent magnitudes for Cepheids, Eqs. (3.1), (3.4), and for SnIa, Eq. (3.7), we relate data and parameters through the matrix equation

$$\mathbf{Y} = \mathbf{A}\mathbf{X} \quad (3.8)$$

with \mathbf{Y} the matrix of measurements, \mathbf{X} the matrix of parameters and \mathbf{A} the equation (or design) matrix. Using these matrices with the measurement error matrix \mathbf{C} we fit the data by minimizing the chi squared χ^2 statistic expressed as

$$\chi^2 = (\mathbf{Y} - \mathbf{A}\mathbf{X})^T \mathbf{C}^{-1} (\mathbf{Y} - \mathbf{A}\mathbf{X}) \quad (3.9)$$

Note that we can solve the following expression for the maximum likelihood parameters \mathbf{X} analytically:

$$\mathbf{X}_{\text{best}} = (\mathbf{A}^T \mathbf{C}^{-1} \mathbf{A})^{-1} \mathbf{A}^T \mathbf{C}^{-1} \mathbf{Y} \quad (3.10)$$

The standard errors for the parameters in \mathbf{X}_{best} are given by the covariance matrix

$$\Sigma = (\mathbf{A}^T \mathbf{C}^{-1} \mathbf{A})^{-1} \quad (3.11)$$

In the Appendix A we present the schematic form of the \mathbf{C} , \mathbf{Y} , \mathbf{X} and \mathbf{A} matrices. We adopt 2D fit including errors in the error matrix \mathbf{C} in both \mathbf{Y} and \mathbf{X} "axes". In particular we do not neglect to include in the error matrix \mathbf{C} the errors in the colors V and I . These errors for MW and LMC Cepheids as provided by the SH0ES team (see in Table 1 of Ref. [20] and in Table 2 of Ref. [16]) are shown in Table IV and in Table V of the Appendix B respectively. For Cepheids in galaxies (other than MW and LMC) where the SH0ES team does not provide separate color errors we use total statistical uncertainties where the color errors are included. These total statistical uncertainties derived by the SH0ES team (see in column 8 of the Table 4 of Ref. [18]) are shown in Table VI of the Appendix B).

In the following subsections we study three cases where the questions mentioned in Introduction I will be addressed.

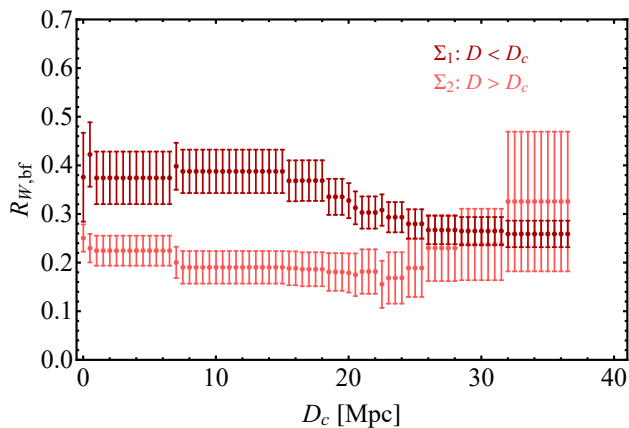


FIG. 4. The best fit $R_{W,bf}$ for various Σ_1 and Σ_2 datasets as a function of the critical dividing distance $D_c \in [0.01, 37] Mpc$ as derived using the individual R_W (red points in Fig. 3). The dark red points correspond to the dataset with galaxies that have distance below D_c , whereas the red points regard galaxies with distances above D_c .

III.1. Case I: Fitting individual R_W and global M_H^W

We first allow, as done in Ref. [73], the parameter R_W to vary between galaxies and we consider a global value of the Cepheid absolute magnitude M_H^W . Despite slight differences in the analysis method, the results are in very good agreement with the results in Ref. [73] as illustrated in Fig. 3. Fitting individual parameters of galaxies $R_{W,i}$ to Cepheid data as derived from our work and from Ref. [73] correspond to red and blue points respectively. The inferred best fit value of the Cepheid absolute magnitude is $M_H^W = -5.958 \pm 0.028 mag$. The red and blue dotted lines correspond to $R_W = 0.365$ and $R_W = 0.369$. These R_W values are taken using the derived individual parameters of anchor galaxies (here MW, NGC 4258, and LMC) and M31 (due to its proximity) $R_{W,k}$ and minimizing the $\chi^2(R_W)$ with respect to the R_W

$$\chi^2(R_W) = \sum_{k=1}^N \frac{(R_{W,k} - R_W)^2}{\sigma_{R_{W,k}}^2 + \sigma_s^2} \quad (3.12)$$

where $N = 4$. We fix the scatter to $\sigma_s = 0.08$ obtained by demanding that $\chi_{min}^2/N = 1$ (where χ_{min}^2 is the minimized value of χ^2).

Using the obtained best fit individual values for all galaxies $R_{W,i}$ (see red points in Fig. 3) we focus on a particular type of evolution, sharp transition of these best fit values at low and high distances. We thus use the Distance Split Sample (DSS) method which consists of the following steps:

- We consider a critical dividing distance $D_c \in [0.01, 37] Mpc$ and split the sample of galaxies in two subsamples Σ_1 and Σ_2 with distances $D < D_c$ and $D > D_c$ respectively.

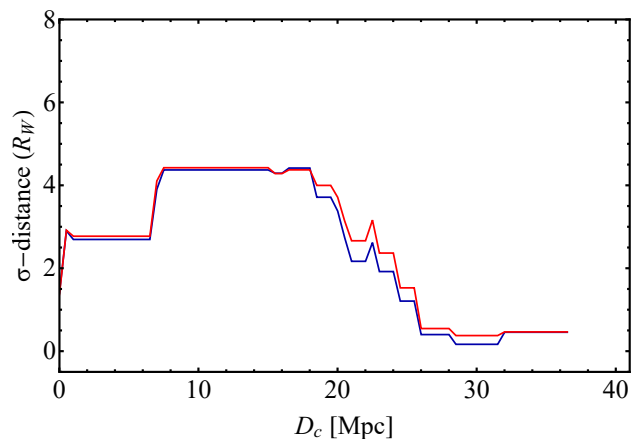


FIG. 5. The σ -distances between the various Σ_1 and Σ_2 datasets as a function of the critical dividing distance D_c as derived using the individual values of R_W . The red and blue lines correspond to the red (our results) and blue (the results in Ref. [73]) points of Fig. 4 respectively. A transition of the σ -distance at $D_c \simeq 22 Mpc$ is apparent.

- For each subsample we use the maximum likelihood method to find the best fit parameters $R_{W,bf}$ ($R_W^<$ and $R_W^>$) by minimizing $\chi_1^2(R_W^<)$ and $\chi_2^2(R_W^>)$ using a similar equation as Eq. (3.12). The best fit values $R_{W,bf}$ for various Σ_1 and Σ_2 datasets as a function of the critical distances D_c are shown in Fig. 4.
- We evaluate the $\Delta\chi_{12}^2(D_c)$ of the best fit of each subsample Σ_1 with respect to the likelihood of the other subsample Σ_2 and vice versa

$$\Delta\chi_{12}^2(D_c) \equiv \chi_2^2(R_W^<)(D_c) - \chi_{2,min}^2(R_W^>)(D_c) \quad (3.13)$$

$$\Delta\chi_{21}^2(D_c) \equiv \chi_1^2(R_W^>)(D_c) - \chi_{1,min}^2(R_W^<)(D_c) \quad (3.14)$$

- Using these values we evaluate the distances $d_{\sigma,12}(D_c)$ and $d_{\sigma,21}(D_c)$ as a solution of the equation

$$\Delta\chi_{ij}^2 = 2Q^{-1} \left[\frac{M}{2}, 1 - \text{Erf} \left(\frac{d_{\sigma,ij}}{\sqrt{2}} \right) \right] \quad (3.15)$$

where $ij = 12, 21$, M is the number of parameters to fit i.e $M = 1$, Q^{-1} is the inverse regularized incomplete Gamma function and Erf is the error function.

- We then define the σ -distance $d_\sigma(D_c)$ as the minimum of the distances $d_{\sigma,12}(D_c)$ and $d_{\sigma,21}(D_c)$ i.e.

$$d_\sigma(D_c) \equiv \text{Min} [d_{\sigma,12}(D_c), d_{\sigma,21}(D_c)] \quad (3.16)$$

The anticipated value of d_σ is in the range of 1 – 2 in the context of a homogeneous sample as verified below using Monte Carlo simulations. We thus address the question: 'Does the real Cepheid sample have this property?'

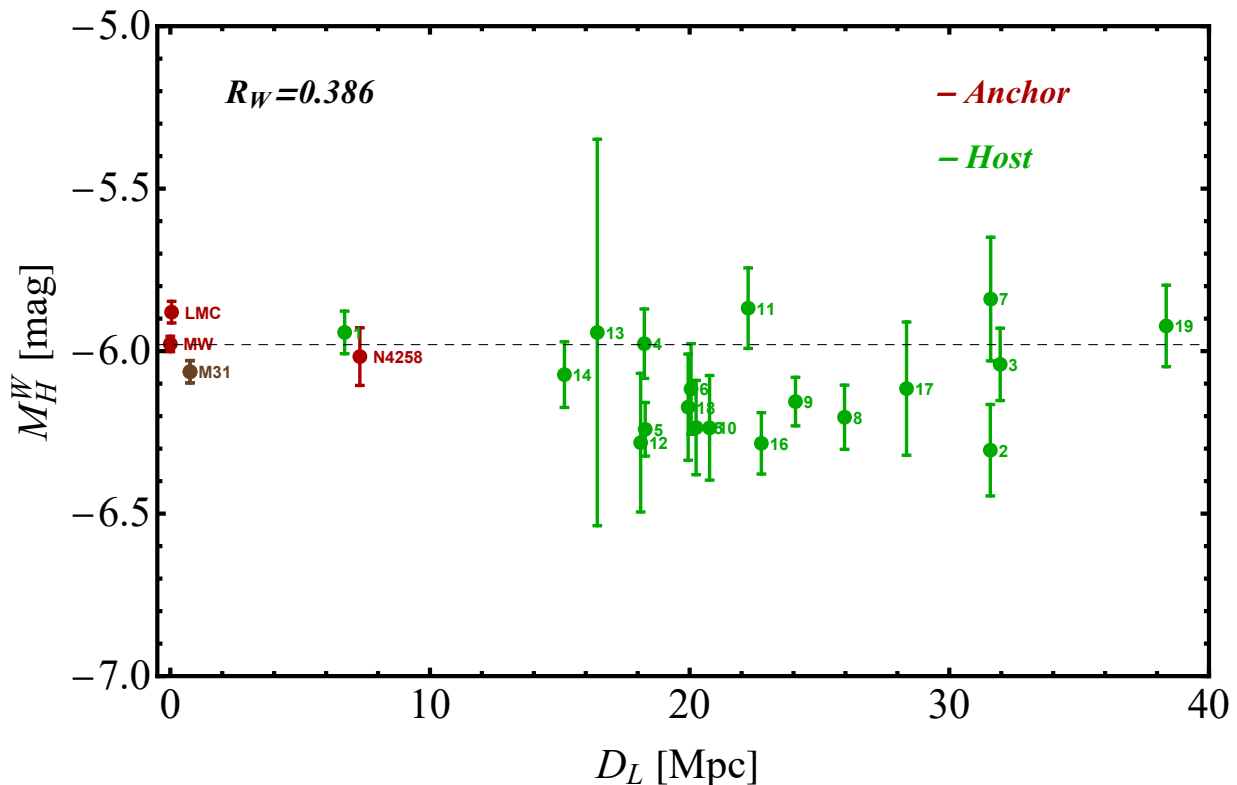


FIG. 6. Fitting individual M_H^W to Cepheid data for global R_W with a fixed value 0.386. Anchor galaxies are denoted with dark red points and SNIa host galaxies with green points. The dotted line corresponds to $M_H^W = -5.98 \text{ mag}$ as derived using the individual values of anchor galaxies and M31 (due to its proximity) $M_{H,k}^W$.

Fig. 5 shows the σ -distance $d_\sigma(D_c)$ between the various Σ_1 and Σ_2 datasets as a function of the critical distances D_c as derived using the individual values of R_W . The red and blue lines correspond to the red (our results) and blue (the results in Ref. [73]) points of Fig. 4 respectively.

Clearly, the Cepheid best fit $R_{W,bf}$ parameter indicates the presence of a transition at a critical distance D_c in the range between 8 Mpc and 18 Mpc or at a time between 25 Myrs and 55 Myrs ago. For this range of D_c the best fit value of $R_W^< = 0.388 \pm 0.042$ differs from the best fit value of $R_W^> = 0.206 \pm 0.033$ at a level more than 4σ with $\Delta R_W \equiv R_W^> - R_W^< = -0.182 \pm 0.056$.

III.2. Case II: Fitting individual M_H^W with fixed global R_W

In this case we allow the value of the Cepheid absolute magnitude M_H^W to vary between galaxies and we consider a global fixed parameter $R_W = 0.386$ in agreement with Refs. [16, 18, 20].

The results of fitting individual M_H^W to Cepheid data are illustrated in Fig. 6. Anchor galaxies are denoted with dark red points and SNIa host galaxies with green points. We see that Cepheids in nearby galaxies are fainter. The dotted line corresponds to $M_H^W =$

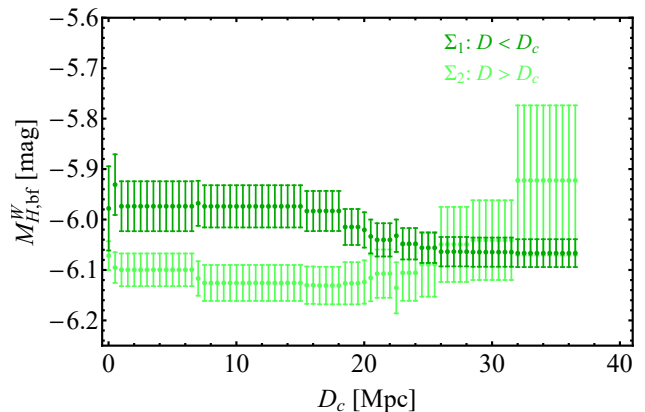


FIG. 7. The best fit $M_{H,bf}^W$ for various Σ_1 and Σ_2 datasets as a function of the critical distances D_c as derived using the individual values of M_H^W (points in Fig. 6). The dark green points correspond to the dataset with galaxies that have distance below D_c , whereas the green points regard galaxies with distances above D_c .

-5.98 mag as derived using the individual parameters of anchor galaxies (here MW, NGC 4258, and LMC) and M31 (due to its proximity) $M_{H,k}^W$ and minimizing

$\chi^2(M_H^W)$ with respect to the M_H^W

$$\chi^2(M_H^W) = \sum_{k=1}^N \frac{(M_{H,k}^W - M_H^W)^2}{\sigma_{M_{H,k}^W}^2 + \sigma_s^2} \quad (3.17)$$

where $N = 4$. We fix the scatter to $\sigma_s = 0.08$ obtained by demanding that $\chi_{min}^2/N = 1$.

Using the obtained best fit individual values for all galaxies $M_{H,i}^W$ (see Fig. 6) we focus on a particular type of evolution, sharp transition of these best fit values at low and high distances. We follow the same DSS method as in the previous subsection. Thus

- First we consider a critical dividing distance $D_c \in [0.01, 37] Mpc$ and split the sample of galaxies in two subsamples Σ_1 and Σ_2 with distances $D < D_c$ and $D > D_c$ respectively.
- For each subsample we use the maximum likelihood method to find the best fit parameters $M_{H,bf}^W$ ($M_H^{W,<}$ and $M_H^{W,>}$) by minimizing $\chi_1^2(M_H^{W,<})$ and $\chi_2^2(M_H^{W,>})$. The best fit values of the $M_{H,bf}^W$ for various Σ_1 and Σ_2 datasets as a function of the critical distances D_c are shown in Fig. 7.
- We consider the $\Delta\chi_{12}^2(D_c)$ of the best fit of each subsample Σ_1 with respect to the likelihood of the other subsample Σ_2 and vice versa

$$\Delta\chi_{12}^2(D_c) \equiv \chi_2^2(M_H^{W,<})(D_c) - \chi_{2,min}^2(M_H^{W,>})(D_c) \quad (3.18)$$

$$\Delta\chi_{21}^2(D_c) \equiv \chi_1^2(M_H^{W,>})(D_c) - \chi_{1,min}^2(M_H^{W,<})(D_c) \quad (3.19)$$

- We evaluate the distances $d_{\sigma,12}(D_c)$ and $d_{\sigma,21}(D_c)$ as a solution of the corresponding Eq. (3.15).
- We then find the σ -distances $d_\sigma(D_c)$ as the minimum of the distances $d_{\sigma,12}(D_c)$ and $d_{\sigma,21}(D_c)$.

In Fig. 8 with the green line we show the σ -distances $d_\sigma(D_c)$ between the various Σ_1 and Σ_2 datasets as a function of the critical distances D_c as derived using the individual values of M_H^W . As in the previous case we see that the Cepheid best fit $M_{H,bf}^W$ parameter indicates the presence of a transition at a critical distance D_c in the range between $8Mpc$ and $18Mpc$. For this range of D_c the best fit value of $M_H^{W,<} = -5.974 \pm 0.042 mag$ differs from the best fit value of $M_H^{W,>} = -6.126 \pm 0.036 mag$ at a level more than 3σ with $\Delta M_H^W \equiv M_H^{W,>} - M_H^{W,<} = -0.152 \pm 0.055 mag$.

In order to secure the robustness of our approach we use a Monte Carlo simulation allowing the galactic distances to vary randomly using their error bars. In particular, the simulations have been performed for randomly varying galaxy distance values with a Gaussian probability distribution (normal distribution) with mean equal to the measured distance and standard deviation equal

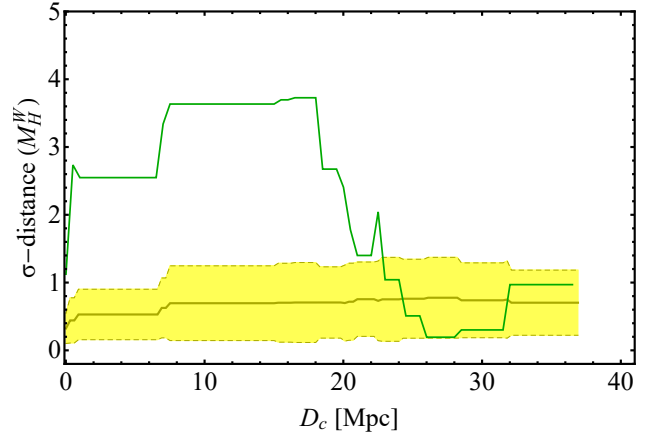


FIG. 8. The green line represents the σ -distances between the various Σ_1 and Σ_2 datasets as a function of the critical distances D_c as derived using the individual values of M_H^W . In contrast the yellow lines correspond to 68% (one standard deviation) range of the σ -distances as a function of the critical distances D_c produced by a Monte Carlo simulation of 100 sample datasets assuming artificial homogeneity of the M_H^W data. The simulations have been performed for randomly varying M_H^W values with a Gaussian probability distribution with mean $M_H^W = -6 mag$ provided by the full M_H^W data-points and standard deviation equal to the corresponding 1σ error.

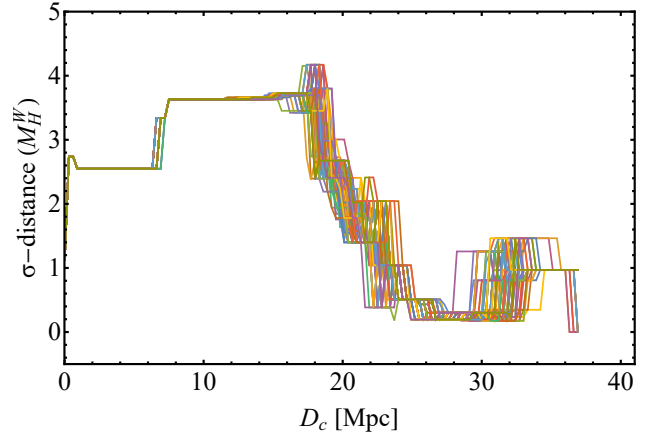


FIG. 9. The σ -distances as a function of the critical distances D_c for 100 sample datasets with random distance values, normally distributed inside their individual $1\text{-}\sigma$ range as derived using the individual values of M_H^W . A transition of the σ -distance at $D_c \simeq 22Mpc$ remains present for practically all of the Monte Carlo samples.

to the corresponding 1σ error. In Fig. 9 we show the σ -distances as a function of the critical distances D_c for 100 sample datasets with random distance values, normally distributed inside their individual $1\text{-}\sigma$ range as derived using the individual values of M_H^W . Clearly, the random variation of the galactic distances does not change the transition effect. The 68% (one standard deviation) range of the σ -distances as a function of the critical dis-

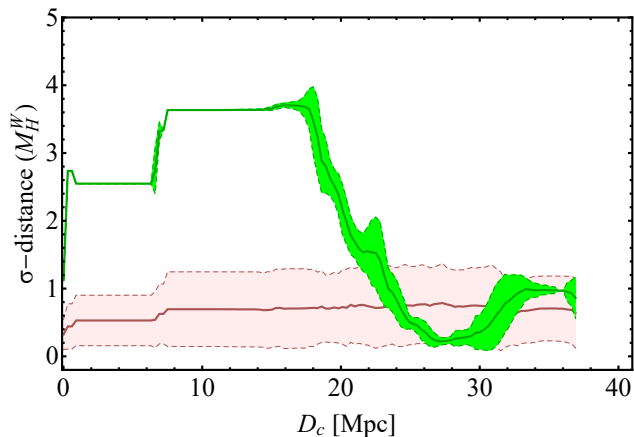


FIG. 10. The green lines represent the 68% range of the σ -distances as a function of the critical distances D_c produced by a Monte Carlo simulation of 100 sample datasets. The simulations have been performed for randomly varying galaxy distance values with a Gaussian probability distribution with mean equal to the measured distance and standard deviation equal to the corresponding 1σ error. In contrast the pink region correspond to a Monte Carlo simulation of 100 sample datasets assuming artificial homogeneity of the M_H^W data. In addition to this homogeneity the simulations have been performed for randomly varying galaxy distance values with a Gaussian probability distribution.

tances D_c produced by the Monte Carlo simulation of 100 sample datasets is shown in Fig. 10 with the green lines. Evidently, the Monte Carlo simulation demonstrates the robustness of the identified transition with respect to variation of galactic distances.

We now test if the effect would disappear in the context of homogenized Monte-Carlo Cepheid datasets. In Fig. 8, we examine if this obvious transition of this case could be due to a systematic uncertainty of the Cepheid absolute magnitude value. Thus, the yellow region corresponds to the 68% range of the σ -distances as a function of the critical distances D_c produced by a Monte Carlo simulation of 100 sample datasets assuming artificial homogeneity of the M_H^W data. The simulations have been performed by randomly varying the M_H^W values with a Gaussian probability distribution with mean $M_H^W = -6 mag$ as obtained by the full dataset with a universal M_H^W and standard deviation of each global universal fit which is equal to the corresponding 1σ error. For this Monte Carlo uniformized data there is no transition. This demonstrates that the observed transition is due to the actual Cepheid data and not to the method we used. As expected the same result persists if in addition to homogenizing the sample with respect to M_H^W we also randomly vary the galactic distances as described above assuming a Gaussian distribution (pink region in Fig. 10). Thus the observed transition effect as illustrated in Figs. 8 and 10 is robust with respect to random variation of the galactic distances and disappears only if we artificially homogenize the data in the context of Monte

Carlo simulations.

III.3. Case III: Fitted individual M_H^W and a global R_W

In this case we assume a free to fit global parameter R_W and allow the value of the Cepheid absolute magnitude M_H^W to vary between galaxies. The results of fitting individual M_H^W to Cepheid data are illustrated in Fig. 11. The dotted line corresponds to $M_H^W = -5.90 mag$ as derived using the individual parameters of anchor galaxies and M31 (due to its proximity) $M_{H,k}^W$ and minimizing $\chi^2(M_H^W)$ in Eq. (3.17) with respect to the M_H^W .

In this case we obtain the best fit value of the parameter $R_W = 0.310 \pm 0.021$ which is smaller than the global fixed value $R_W = 0.386$ used by Refs. [16, 18, 20]. We attribute this difference to the fact that we have used the full Cepheid sample for its determination and not just the anchor galaxies and we have not used a global value of the absolute magnitude M_H^W common for all Cepheids.

Using the same DSS method as in the two previous cases we find the best fit values of the $M_{H,bf}^W$ ($M_H^{W,<}$ and $M_H^{W,>}$) for various Σ_1 and Σ_2 datasets as a function of the critical distances D_c . As the previous cases the presence of a transition at a critical distance D_c in the range between $8 Mpc$ and $18 Mpc$ is obvious. For this range of D_c the best fit value of $M_H^{W,<} = -5.904 \pm 0.042 mag$ differs from the best fit value of $M_H^{W,>} = -6.092 \pm 0.035 mag$ at a level more than 4σ with $\Delta M_H^W \equiv M_H^{W,>} - M_H^{W,<} = -0.188 \pm 0.055 mag$.

In this case, we do not plot here the result since it is very similar to that plotted in the figures of previous cases but are available in our publicly available numerical analysis files [161].

IV. MODEL SELECTION

As pointed out in the previous subsections where we study three cases (I, II, and III) both the Cepheid best fit absolute magnitude and color luminosity parameters indicate the presence of a transition effect at a critical distance D_c in the range between $8 Mpc$ and $18 Mpc$ (see Fig. 12). This transition however becomes apparent when additional parameters are introduced (the individual R_W or M_H^W for each galaxy). Thus the questions we address in this section is the following:

- Is the introduction of additional parameters favored by model selection criteria like the Akaike Information Criterion (AIC) [168] and the Bayesian Information Criterion (BIC) [169]?

Model	Best Fit Parameters (with 1σ ranges) $\sigma_{LMC} = 0.08$ ($\sigma_{LMC} = 0$)	Model Selection Criteria	Intrinsic scatter of LMC Cepheids	
			$\sigma_{LMC} = 0$	$\sigma_{LMC} = 0.08$
Base-SH0ES	$R_W = 0.386$ (fixed) Global R_W Global M_H^W $N = 1650$ $M = 28$ $dof = 1622$	χ_{min}^2 χ_{red}^2 AIC ΔAIC BIC ΔBIC	1767.48 1.089 1823.48 7.65 (0) 1974.92 2.25 (0)	1644.79 1.014 1700.79 17.97 (0) 1852.23 12.57 (0)
Base	$R_W = 0.309 \pm 0.021$ Global R_W Global M_H^W $N = 1650$ $M = 29$ $dof = 1621$	χ_{min}^2 χ_{red}^2 AIC ΔAIC BIC ΔBIC	1759.47 1.084 1815.83 0 (-7.65) 1972.67 0 (-2.25)	1624.82 1.002 1682.82 0 (-17.97) 1839.66 0 (-12.57)
I	$R_{W,i}$ red points in Fig. 3 Individual R_W Global M_H^W $N = 1650$ $M = 51$ $dof = 1599$	χ_{min}^2 χ_{red}^2 AIC ΔAIC BIC ΔBIC	1676.76 1.049 1778.76 -37.07 (-44.72) 2054.59 81.92 (79.67)	1564.06 0.978 1666.06 -16.76 (-34.73) 1941.9 102.24 (89.74)
II	$R_W = 0.386$ (fixed) Global R_W Individual M_H^W $N = 1650$ $M = 50$ $dof = 1600$	χ_{min}^2 χ_{red}^2 AIC ΔAIC BIC ΔBIC	1732.05 1.083 1832.05 16.22 (8.57) 2102.48 129.81 (127.56)	1611.04 1.007 1711.04 28.22 (10.25) 1981.47 141.81 (129.24)
III	$R_W = 0.310 \pm 0.021$ Global R_W Individual M_H^W $N = 1650$ $M = 51$ $dof = 1599$	χ_{min}^2 χ_{red}^2 AIC ΔAIC BIC ΔBIC	1726.7 1.079 1828.7 12.87 (5.22) 2104.53 131.86 (129.61)	1592.09 0.996 1694.09 11.27 (-6.7) 1969.93 130.27 (117.7)
IV	$R_W^< = 0.325 \pm 0.018$ Two universal R_W Global M_H^W $N = 1650$ $M = 30$ $dof = 1620$	χ_{min}^2 χ_{red}^2 AIC ΔAIC BIC ΔBIC	1744.19 1.077 1804.19 -13.34 (-18.99) 1966.44 -6.23 (-8.48)	1611.65 0.995 1671.46 -11.36 (-29.33) 1833.91 -5.75 (-18.32)
V	$R_W = 0.308 \pm 0.021$ Global R_W Two universal M_H^W $N = 1650$ $M = 30$ $dof = 1620$	χ_{min}^2 χ_{red}^2 AIC ΔAIC BIC ΔBIC	1757.15 1.085 1817.15 1.32 (-6.33) 1979.41 6.74 (4.49)	1621.98 1.001 1681.98 -0.84 (-18.81) 1844.23 4.57 (-8.0)
VI	$R_W^< = 0.329 \pm 0.018$ Two universal R_W Two universal M_H^W $N = 1650$ $M = 31$ $dof = 1619$	χ_{min}^2 χ_{red}^2 AIC ΔAIC BIC ΔBIC	1743.26 1.077 1805.26 -10.57 (-18.22) 1972.93 0.26 (-1.99)	1612.09 0.996 1674.09 -8.73 (-26.7) 1841.75 2.09 (-10.48)

TABLE I. Fitting results and model comparison tests for different models. For the ΔAIC and ΔBIC the comparisons are made respect to base (base-SH0ES) models. The value of H_0 derived using the Eq. (5.1) (black font) and the Eq. (5.3) (green font). The best fit parameters of SnIa absolute magnitude M_B and the value of H_0 in the parentheses correspond to intrinsic scatter of LMC Cepheids $\sigma_{LMC} = 0$.

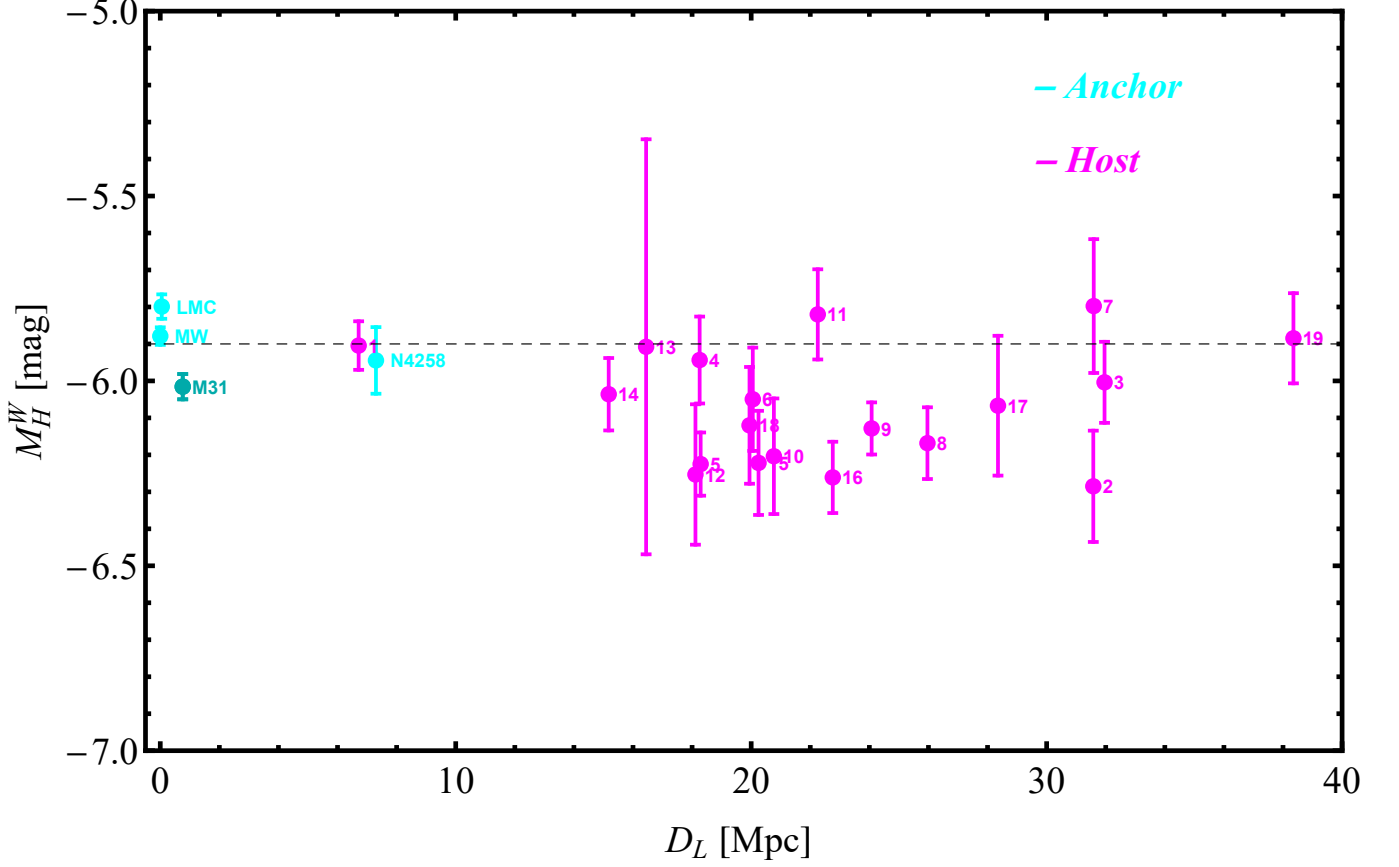


FIG. 11. Fitting individual M_H^W to Cepheid data with a free global R_W . Anchor galaxies are denoted with cyan points and SNIa host galaxies with magenta points. The dotted line corresponds to $M_H^W = -5.90 \text{ mag}$ as derived using the individual values of anchor galaxies and M31 (due to its proximity) $M_{H,k}^W$.

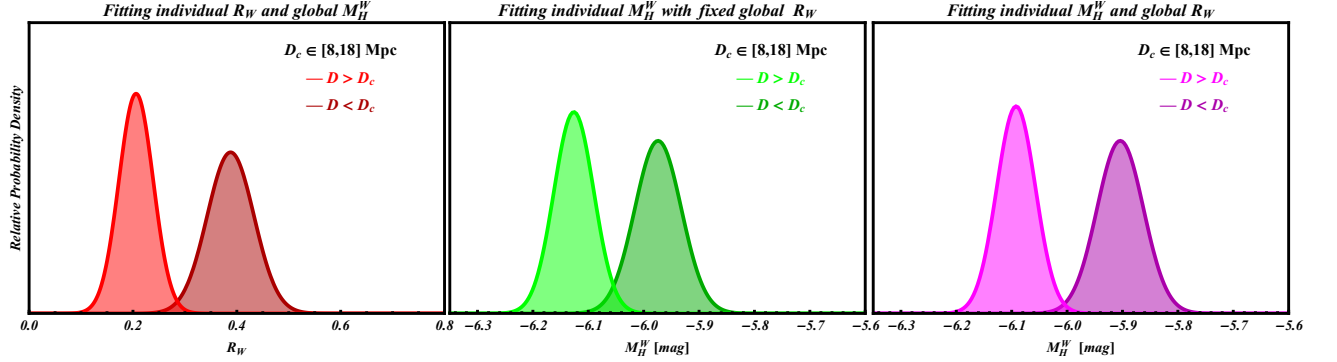


FIG. 12. The one dimensional relative probability density values of the color luminosity parameter and the Cepheid absolute magnitude as derived using the DSS method for the cases I, II, and III. All measurements are shown as normalized Gaussian distributions. Notice that the best fit values one for galaxies at distances $D < D_c$ and one for galaxies at $D > D_c$ are inconsistent with each other at a level larger than 3σ .

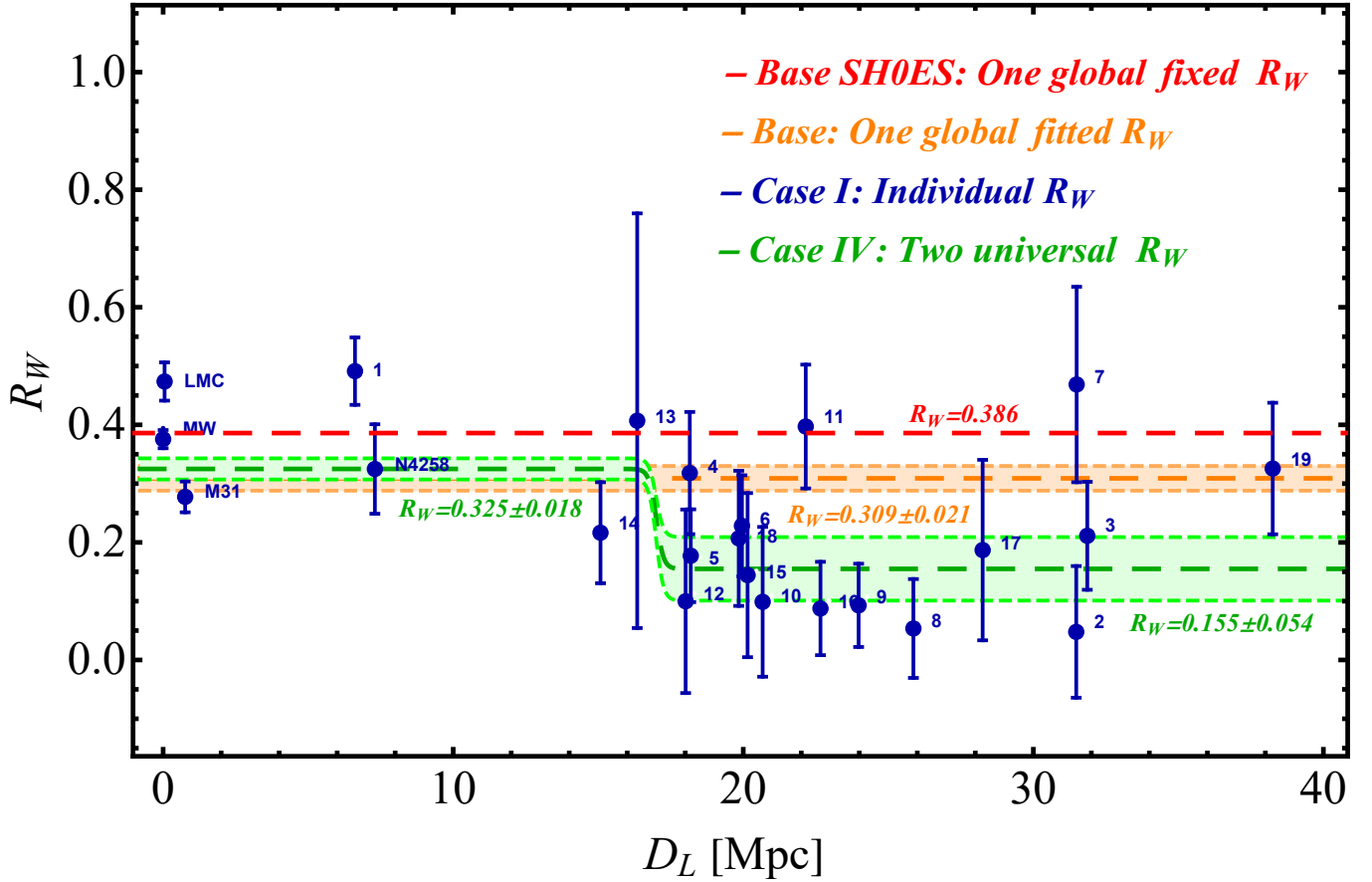


FIG. 13. The best fit values of the parameter R_W for base/base-SH0ES, I and IV models as derived using Cepheid data. Note that in terms of the AIC and BIC, fitting for two universal values of R_W with global M_H^W is the preferred model (case IV, green region).

ΔAIC			ΔBIC			
Level of empirical support for the model with the smaller AIC			Evidence against the model with the larger BIC			
0-2	4-7	> 10	0-2	2-6	6-10	> 10
Substantial	Strong	Very strong	Weak	Positive	Strong	Very strong

TABLE II. The interpretation of differences ΔAIC and ΔBIC according to the calibrated Jeffreys' scale [162] (see also Refs. [163–167]). However, it should be noted that the Jeffreys' scale has to be interpreted with care [164] because has been shown to lead to different qualitative conclusions.

- Could the introduction of a smaller number of parameters lead to more favored phenomenological models?

following⁷:

- **Base-SH0ES:** Like previous studies of SH0ES team we consider universality on the color-luminosity relation with a global fixed parameter

In order to address these questions we use model selection tests for eight cases with different number of free parameters. The additional five considered cases are the

⁷ Note that for all cases we fit other 27 additional parameters (see the schematic form of the matrix of parameters \mathbf{X} in Appendix A)

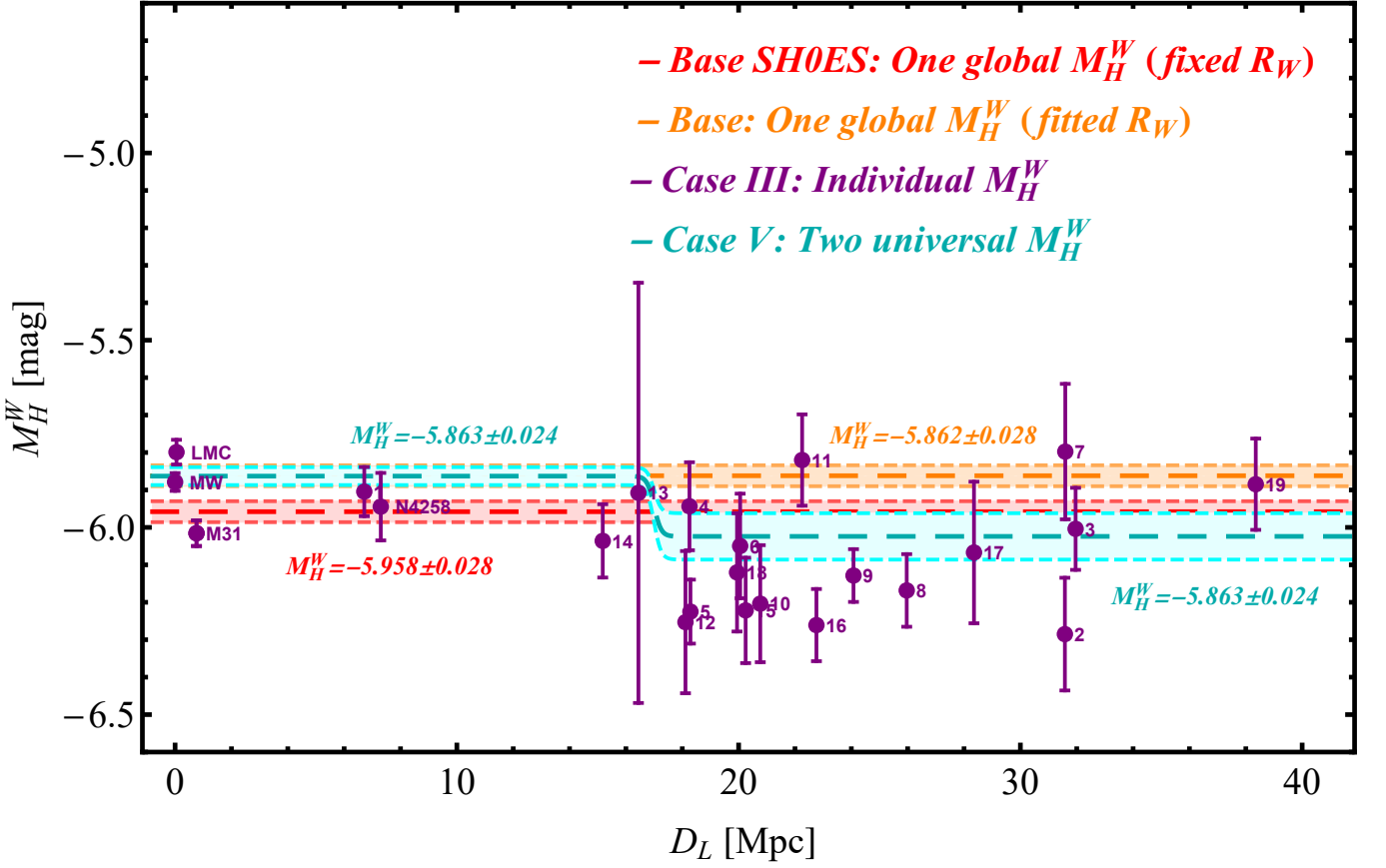


FIG. 14. The best fit values of the parameter M_H^W for base/base-SH0ES, III and V models as derived using the Cepheid data. Note that in terms of the AIC and BIC, fitting for two universal values of M_H^W with global R_W is the preferred model among the models shown (case V, cyan region).

Ranking	AIC		BIC	
	$\sigma_{LMC} = 0$	$\sigma_{LMC} = 0.08$	$\sigma_{LMC} = 0$	$\sigma_{LMC} = 0.08$
1	I	I	IV	IV
2	IV	IV	Base	Base
3	VI	VI	VI	VI
4	Base	V	Base-SH0ES	V
5	V	Base	V	Base-SH0ES
6	Base-SH0ES	III	I	I
7	III	Base-SH0ES	II	III
8	II	II	III	II

TABLE III. Ranking of models according to *AIC* and *BIC* criteria. We see that in terms of the AIC and BIC fitting for two universal values of R_W with global M_H^W is the preferred model (case IV).

$R_W = 0.386$ [16, 18, 20] and universality on the absolute magnitude of Cepheids SnIa calibrators with a global M_H^W to be fit by the Cepheid data. Thus in this case we use the base, commonly used parameter set in the field.

- **Base:** We consider universality on the color-luminosity relation with a global parameter R_W

to be fit by data and universality on the absolute magnitude of Cepheids SnIa calibrators with global M_H^W .

- **IV:** We consider a global M_H^W and two universal R_W ($R_W^<$ for galaxies at distances $D < 16$ Mpc and $R_W^>$ for galaxies at distances $D > 16$ Mpc).
- **V:** We consider a global R_W and two universal M_H^W

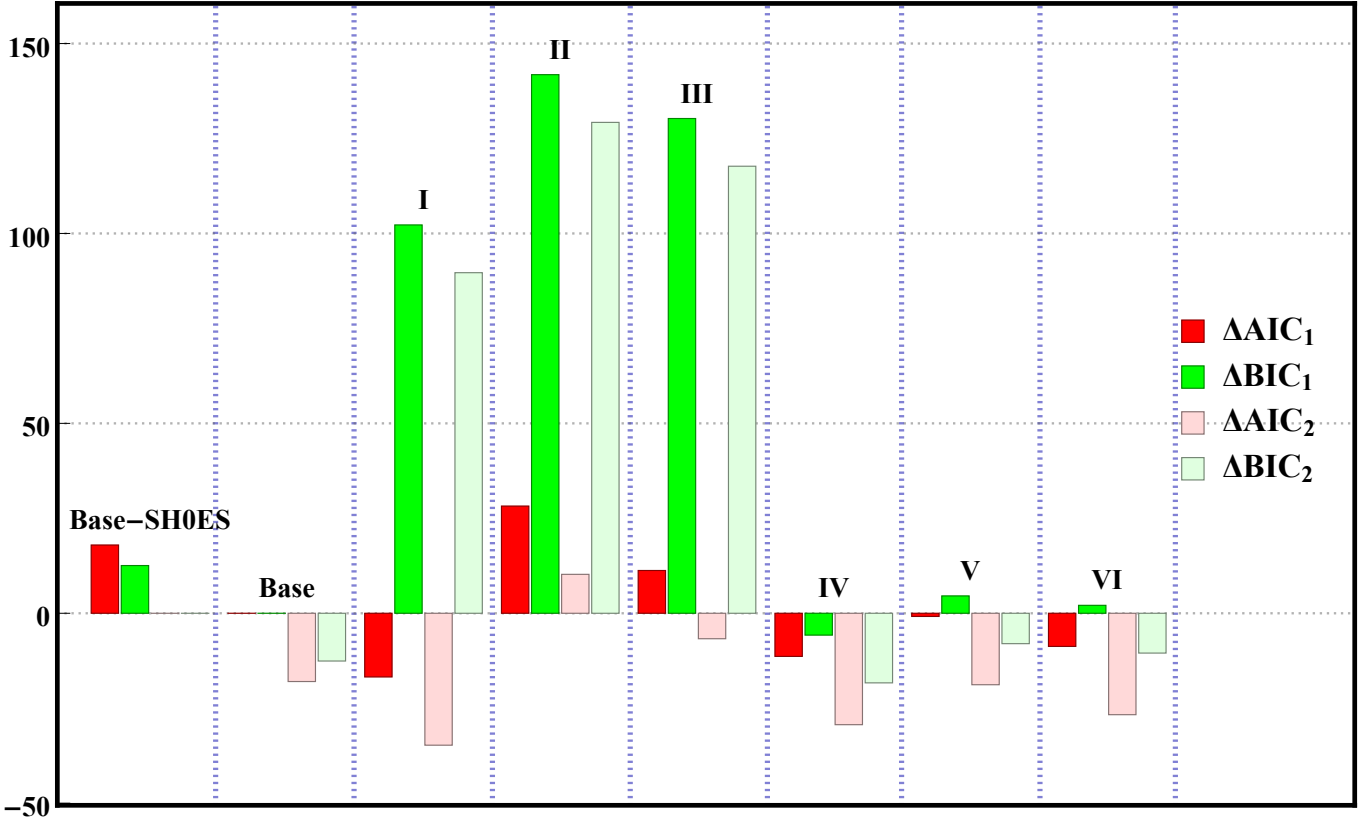


FIG. 15. The ΔAIC and ΔBIC of models with different free parameter set compared to base (subindex 1) and base-SHOES (subindex 2) models. Clearly, the case IV (two universal R_W and a global M_H^W) is the best model and on the other hand, the case II (a global R_W and individual M_H^W) is the worst one.

($M_H^{W,<}$ for galaxies at distances $D < 16 Mpc$ and $M_H^{W,>}$ for galaxies at distances $D > 16 Mpc$).

- **VI:** We consider two universal R_W ($R_W^<$ for galaxies at distances $D < 16 Mpc$ and $R_W^>$ for galaxies at distances $D > 16 Mpc$) and two universal M_H^W ($M_H^{W,<}$ for galaxies at distances $D < 16 Mpc$ and $M_H^{W,>}$ for galaxies at distances $D > 16 Mpc$).

In order to compare the models we construct Table I with the fitting parameters for all cases. The best fit values of the parameter R_W for base/base-SHOES, I and IV models are shown in Fig. 13 and the best fit values of the parameter M_H^W for base/base-SHOES, III and V models are shown in Fig. 14. Various methods for model selection have been developed and model comparison techniques used [163, 170–172]. In table I we show the value of the minimum χ^2 (χ_{min}^2) for all cases and the reduced chi-squared which is a very popular method for model comparison. This is defined by

$$\chi_{red}^2 = \frac{\chi_{min}^2}{dof} \quad (4.1)$$

where $dof = N - M$ is typically the number of degrees of freedom (with N is the number of datapoints used in

the fit and M is the number of free parameters) for each model.

We also use the model selection methods like Akaike Information Criterion (AIC) [168] and the Bayesian Information Criterion (BIC) [169] that penalize models with additional parameters. For a model with M parameters and a dataset with N total observations these are defined through the relations [163, 170, 171]

$$AIC = -2\ln\mathcal{L}_{max} + 2M = \chi_{min}^2 + 2M \quad (4.2)$$

$$BIC = -2\ln\mathcal{L}_{max} + M\ln N = \chi_{min}^2 + M\ln N \quad (4.3)$$

where $\mathcal{L}_{max} \equiv e^{-\chi_{min}^2/2}$ (e.g. [164, 173]) is the maximum likelihood of the model under consideration. Note that a version of the AIC corrected for small sample sizes is important [174, 175]. This version is given by [176] (see also Refs. [170, 177])

$$AIC_{cor} = AIC + \frac{2M(M+1)}{N-M-1} \quad (4.4)$$

For large samples as in our case ($N \gg M$) the correction term disappears but for small samples gives a more accurate answer.

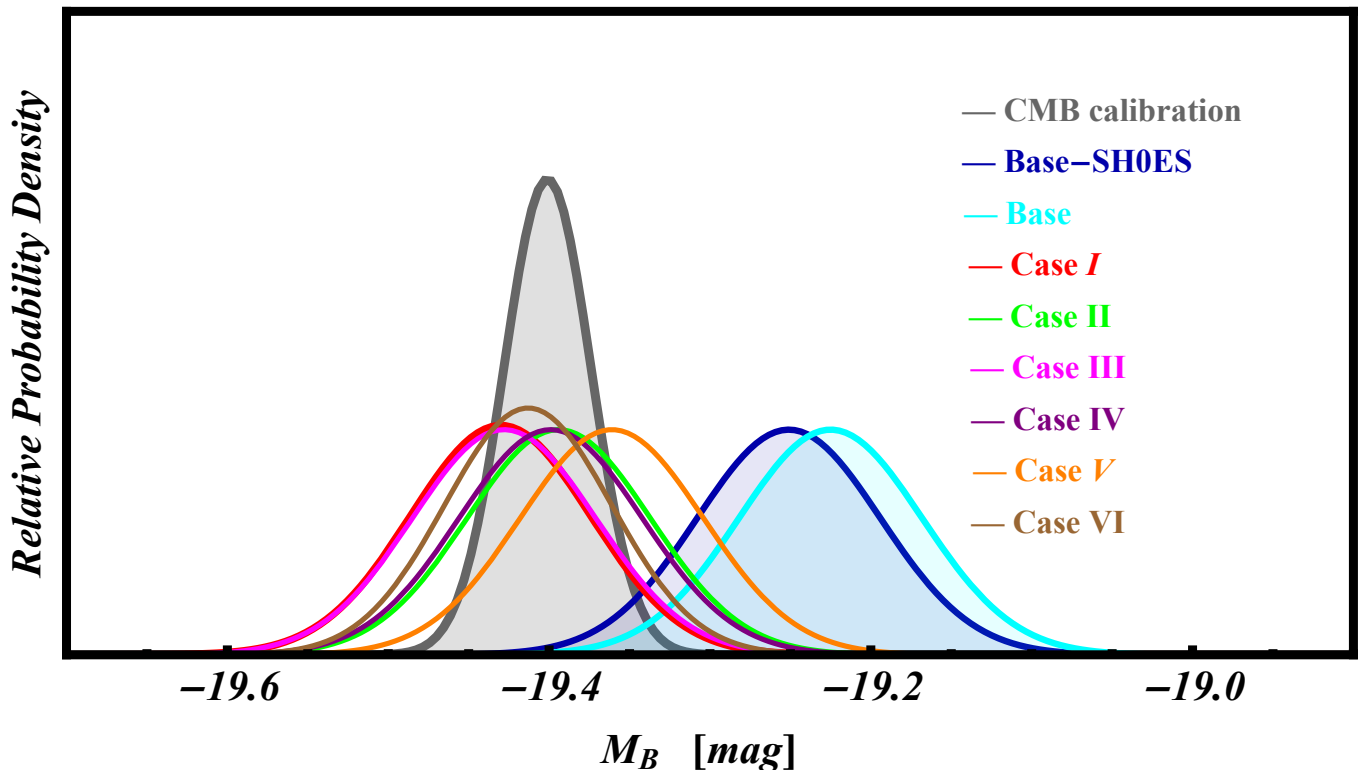


FIG. 16. The one dimensional relative probability density value of SnIa absolute magnitude M_B for all cases studied in this paper compared to that obtained using CMB calibration. All measurements are shown as normalized Gaussian distributions. Clearly, for all cases where we do not consider the universality of parameters R_W and M_H^W (i.e. I, II, III, IV, V, VI) the M_B is consistent with the CMB determination value.

The results for each candidate model are shown in Table I and the "preferred model" is the one which minimizes AIC and BIC. The absolute values of the AIC and BIC are not informative. Only the relative values between different competing models are relevant. Hence when comparing one model versus the base/base-SH0ES we can use the model differences ΔAIC and ΔBIC .

The differences ΔAIC and ΔBIC with respect to the base/base-SH0ES model defined as

$$\Delta AIC = AIC_i - AIC_s = \Delta\chi_{min}^2 + 2\Delta M \quad (4.5)$$

$$\Delta BIC = BIC_i - BIC_s = \Delta\chi_{min}^2 + \Delta M(\ln N) \quad (4.6)$$

where the subindex i refers to value of AIC (BIC) for the model i and AIC_s (BIC_s) is the value of AIC (BIC) for the base/base-SH0ES model. The resulting ΔAIC and ΔBIC are shown in Table I and in Fig. 15. Note that a positive value of ΔAIC or ΔBIC means a preference for base/base-SH0ES model.

According to the calibrated Jeffreys' scales [162] showed in the Table II (see also Refs. [163–167]) a range $0 < |\Delta AIC| < 2$ means that the two comparable models have about the same support from the data, a range $4 < |\Delta AIC| < 7$ means this support is considerably less for the model with the larger AIC while for $|\Delta AIC| > 10$ the model with the larger AIC have no support i.e. the

model is practically irrelevant. Similarly, for two competing models a range $0 < |\Delta BIC| < 2$ is regarded as weak evidence, a range $2 < |\Delta BIC| < 6$ is regarded as positive evidence, while for $|\Delta BIC| > 6$ the evidence is strong against the model with the larger value.

Ranking of the models considered according to AIC and BIC criteria are presented in Table III. Clearly, in terms of the AIC and BIC, fitting for two universal values of R_W with global M_H^W is the preferred model (case IV). Base/base-SH0ES model is considerable less supported by data with respect to the IV model (ΔAIC) and there is a positive/very strong evidence against it (ΔBIC). We attribute the difference between ΔAIC and ΔBIC for the models considered to the fact that the BIC penalizes additional parameters more strongly than the AIC as inferred by the Eqs. (4.2) and (4.3) for the used dataset with $\ln N > 2$ (see Refs. [163, 171, 178]).

V. TRANSITION AS A POSSIBLE SOLUTION OF HUBBLE TENSION

In this section, we investigate whether the existence of transition of the Cepheid parameters can impact on the inferred value of Hubble constant H_0 and its corresponding uncertainties. Using the best fit values of SnIa

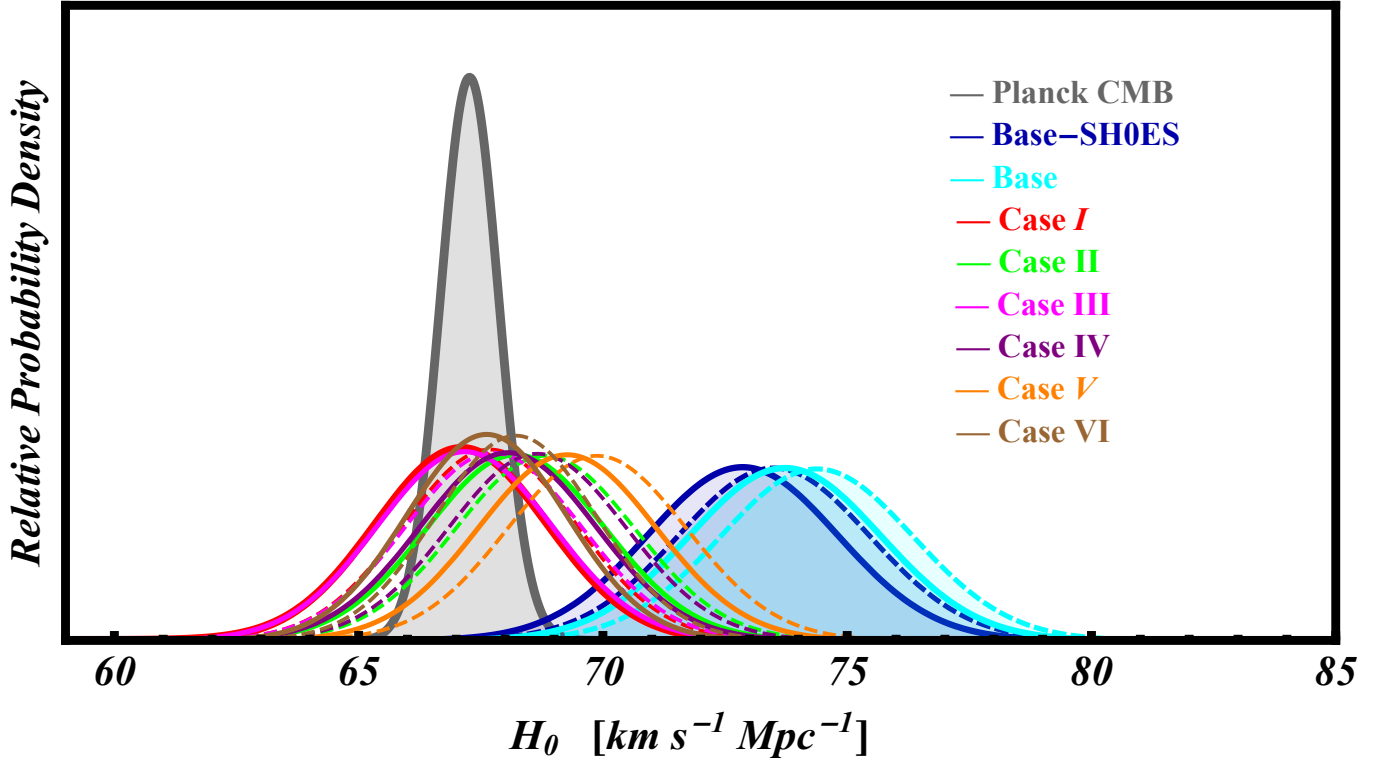


FIG. 17. The one dimensional relative probability density value of H_0 as derived using the Eq. (5.1) (solid lines) and the Eq. (5.3) (dashed lines) for all cases studied in this paper compared to that from the Planck CMB measurement (grey line). All measurements are shown as normalized Gaussian distributions. It is evident that for all cases where we break the assumption of universality of the parameters R_W and M_H^W (i.e. I, II, III, IV, V, VI) the derived values of H_0 are consistent with the corresponding predicted Planck CMB best fit value.

absolute magnitude M_B the Hubble constant is given by

$$H_0 = 10^{0.2M_B + \alpha_B + 5} \quad (5.1)$$

where the term α_B is the intercept of the SnIa magnitude-redshift relation defined as [18]

$$\alpha_B = \log \left[cz \left(1 + \frac{1}{2}(1 - q_0)z - \frac{1}{6}(1 - q_0 - 3q_0^2 + j_0)z^2 + \mathcal{O}(z^3) \right) \right] - 0.2m_B \quad (5.2)$$

where $q_0 \equiv -\frac{1}{H_0^2} \frac{d^2 a(t)}{dt^2} \Big|_{t=t_0}$ and $j_0 \equiv \frac{1}{H_0^3} \frac{d^3 a(t)}{dt^3} \Big|_{t=t_0}$ are the deceleration and jerk parameters respectively.

The intercept α_B using 217 observed SnIa at redshifts $0.023 < z < 0.15$ with the deceleration and jerk parameters set to $q_0 = -0.55$ and $j_0 = 1$ is determined to be $\alpha_B = 0.71273 \pm 0.00176$ by Ref. [18].

Alternatively, using the the best fit value of degenerate combination $\mathcal{M} = 23.803 \pm 0.007$ as derived by Ref. [57] for full Pantheon dataset in Eq. (2.5) the Hubble constant can be estimated

$$H_0 = c 10^{0.2(M_B - \mathcal{M}) + 5} \quad (5.3)$$

In Table I we show the best fit value of SnIa absolute magnitude M_B and the corresponding Hubble constant H_0 as derived using the Eq. (5.1) and the Eq. (5.3) (the values in the parentheses) for all cases studied in this paper. Also the one dimensional relative probability density values of M_B and H_0 as derived using the Eq. (5.1) and the Eq. (5.3) (the values in the parentheses of table I) compared to that from the Planck CMB measurement assuming flat Λ CDM are shown in Fig. 16 and Fig. 17 respectively.

Clearly, for all cases which break the assumption of universality of the parameters R_W and M_H^W (i.e. I, II, III, IV, V, VI) the best fit value of SnIa absolute magnitude M_B and the derived values of H_0 decrease and become consistent with the corresponding predicted CMB best fit values. For the preferred model (case IV) we obtain $H_0 = 68.06 \pm 1.80 \text{ km s}^{-1} \text{ Mpc}^{-1}$ with Planck tension $< 1\sigma$. Therefore the transition in the Cepheid calibrator parameters at $D_c \simeq 16 \text{ Mpc}$ can provide a resolution of the Hubble tension.

VI. CONCLUSION-DISCUSSION

In the present study we have used Cepheid SnIa calibrator data to investigate the effects of variation of

the Cepheid calibration empirical parameters. We have shown that models where such a variation is allowed are favored on the basis of model selection criteria AIC and BIC. The models that are consistently favored by both AIC and BIC involve a transition in either the color-luminosity parameter R_W or the Cepheid absolute magnitude M_H^W , at a distance in the range between 10 and 20 Mpc . In the context of a homogeneous Universe where the cosmological principle is respected this would be a transition in time between about 25 $Myrs$ and 70 $Myrs$ ago. Models involving a transition in R_W are slightly favored over models where there is a transition in M_H^W . Both classes of models, lead to values of H_0 that are consistent with the CMB inferred values thus eliminating the Hubble tension.

Such a transition of Cepheid parameters could be induced by a fundamental physics transition. The magnitude of the transition is consistent with the magnitude required for the resolution of the Hubble tension in the context of a fundamental gravitational transition occurring by a sudden increase of the strength of the gravitational interactions G_{eff} by about 10% [48] at a redshift $z_t \lesssim 0.01$ ($\lesssim 150$ million years). Such a transition would abruptly increase the SnIa absolute magnitude by $\Delta M_B \simeq 0.2$ [48, 55] (from $M_B = -19.401 \pm 0.027 mag$ for $z > z_t$ [54] to $M_B = -19.244 \pm 0.037 mag$ for $z < z_t$ [52, 53]). The distance range/timescale corresponding to this transition is consistent with a recent analysis indicating a similar transition in the context of the Tully-Fisher data [72].

An alternative origin of the observed effect is based on a scenario where the parameter R_W could vary across different sightlines and different galaxy distances, morphologies, environments and properties. Dust extinction differences between galaxies could be the origin for a systematic "mass step" (at $\sim 10^{10} M_\odot$) in the data [179, 180]: after standardization, SnIa in a high-mass galaxy appear brighter than those in a low-mass galaxy [76, 181–185]. Such an alternative scenario is testable using the methods presented here and it could also lead to a resolution of the Hubble tension. Such an extension is beyond the goals of the present analysis.

Other interesting extensions of the present analysis include the following:

- The search for transition in other parameters that can be constrained using the Cepheid data (for example the SnIa absolute magnitude M_B and its effect on the estimation of H_0).
- If the transition is physical and due to fundamental gravitational physics it would be interesting to search for possible constraints or remnants of such a transition in the solar system. For example what could be the relevance of such a transition on the observed increased rate of impactors on Earth and Moon by a factor of 2-3 during the past 290 Myrs [186] which may also be related with the Cretaceous–Paleogene (K-Pg) extinction event (also

known as the Cretaceous–Tertiary (K–T) extinction) (e.g. [187]) that eliminated several species on Earth about 66 Myrs ago [188] including dinosaurs (e.g. [189]). According to the impact hypothesis or Alvarez hypothesis [190, 191] this extinction event was caused by an asteroid impact producing the $\sim 200 km$ wide Chicxulub impact crater.

- It would be interesting to search for a similar transition in the other SnIa calibrator such as the Tip (a sharp discontinuity) of the Red Giant Branch (TRGB) in the Hertzsprung-Russell diagram [192]. The Red Giant stars have nearly exhausted the hydrogen in their cores and have just began helium burning by the triple- α process (helium flash phase). The brightness of TRGB stars can be standardized using DEBs combined with parallax calibration. They can serve as excellent alternative standard candles [193] visible in the local Universe for the subsequent calibration of SnIa [194–197] and thereby provide an independent determination of the Hubble constant H_0 [198, 199].

The indicated transition at a distance of about 10 – 20 Mpc could be interpreted as violating the cosmological principle according to which the distance of any galaxy from us should not impact its properties. The cosmological principle however is not necessarily violated in the transition models because a spatial transition can not be observationally distinguished from a temporal transition. If the transition is temporal and occurred at a specific time then there is no violation of the cosmological principle.

Even if the transition is spatial it could be interpreted as a result of a first order phase transition occurring very recently due to a decay of the false vacuum [200]. Then we could live in 20 Mpc true vacuum bubble where a first order scalar-tensor physics transition has occurred. If the bubble was created at recent cosmological times (e.g. last 100 $Myrs$) in the context of a decay of a false vacuum (see e.g. Ref. [200]) then we would not have been able to see the other true vacuum bubbles since light from them may not have reached us yet. Thus even in that case there would be no apparent large-scale violation of the cosmological principle. The phenomenology of such recent false vacuum decay in the context of scalar-tensor theories is another interesting extension of our analysis. In this context it may be shown that for a transition energy scale similar to the present Hubble constant the typical scale of the true vacuum bubbles produced would be 15 – 20 Mpc . Fine tuning questions also arise in the context of the indicated transition: 'What is special about the scale of 15 – 20 Mpc where the transition signal appears to exist?'. In the context of a false vacuum decay bubble there is no more fine tuning than in the Λ CDM. If we accept the scale of the cosmological constant and the fact that there is a first order phase transition to another vacuum of a similar energy scale ($\sim 0.002 eV$) then the predicted spatial scale of the produced bubbles is theo-

retically predicted to be about $15 Mpc$. If we allow for some true vacuum bubble growth (they expand with the speed of light) it could increase to the scale of $20 Mpc$. This generic result may be demonstrated as follows [200–203]: For a very recent false vacuum decay with vacuum energy comparable to the cosmological constant the scale of the produced bubbles is

$$R_b = \delta/H_0 \quad (6.1)$$

where δ depends logarithmically on the ratio of the Planck mass M_P to the transition temperature energy scale $T_c = 2.7^\circ K \simeq 2 \times 10^{-4} eV$ as [201]

$$\delta \simeq [4B_1 \ln(M_P/T_c)]^{-1} \quad (6.2)$$

where B_1 is a constant of $O(1)$. Using Eqs. (6.1) and (6.2) with $H_0 = 70 km s^{-1} Mpc^{-1}$ we obtain $R_b \simeq 15 Mpc$ which is clearly within the range of transition scales favored by the Cepheid data by the present analysis and by the Tully-Fisher data as indicated by Ref. [200, 202, 203].

In conclusion the revolutionary improvement in the quality and quantity of data from existing and upcoming missions/experiments raises the expectation of determining the origin of the existing transition effect shown in our analysis. One possible origin would be the presence of systematic errors affecting the adopted calibration method. Alternatively, if the source of the demonstrated transition is physical it could lead to new cosmological physics beyond the standard model which

may include a very recent false vacuum decay.

NUMERICAL ANALYSIS FILES

The numerical files for the reproduction of the figures can be found in the [Cepheid SnIa Calibrator Data Transition](#) Github repository under the MIT license.

ACKNOWLEDGEMENTS

We thank Adam Riess and Dan Scolnic for interesting and useful comments. This research is co-financed by Greece and the European Union (European Social Fund-ESF) through the Operational Programme "Human Resources Development, Education and Lifelong Learning 2014-2020" in the context of the project MIS 5047648.

Appendix A: MATRICES OF SYSTEM OF EQUATIONS

In this Appendix we present the schematic form of the error matrix \mathbf{C} , the matrix of measurements \mathbf{Y} , the matrix of parameters \mathbf{X} and the equation (or design) matrix \mathbf{A} used in the system of equations of our analysis (see Eqs. (3.8), (3.9), (3.10) and (3.11) in Section III).

The schematic form of the error matrix \mathbf{C} is

$$\mathbf{C} = \begin{pmatrix} \sigma_{MW,j}^2 & 0 & \dots & & & & & & & 0 \\ 0 & \sigma_{tot,j}^2 & 0 & \dots & & & & & & \vdots \\ 0 & 0 & \sigma_{LMC,j}^2 & 0 & \dots & & & & & \vdots \\ \vdots & & & & \ddots & & & & & \\ & & & & & \sigma^2(\mu_{N4258}) & & & & \\ & & & & & & \sigma^2(\mu_{LMC}) & & & \\ & & & & & & & \sigma^2(m_{B,1}) & & \\ & & & & & & & & \ddots & \\ 0 & & & & & & & & & \sigma^2(m_{B,19}) \end{pmatrix} \quad (A1)$$

where $\sigma(\mu_{LMC}) = 0.0263$ is the error of the distance modulus to the LMC reported by Ref. [104], $\sigma(\mu_{N4258}) = 0.032$ is the error of the distance modulus to the NGC 4258 reported by Ref. [107] and $\sigma(m_{B,k})$ ($k = 1, \dots, 19$) are the errors of SnIa B-band magnitudes obtained from Table 5 in Ref. [18] (see our Table VII of the Appendix B).

For MW j th Cepheid we use a total statistical uncertainty arising from the quadrature sum of four terms (higher order terms $\mathcal{O}(zp/\pi_j)^2$ are negligible)

$$\sigma_{MW,j}^2 = \sigma^2(m_{H,j}) + \left(\frac{5}{\ln 10} \frac{1}{\pi_j}\right)^2 \sigma^2(\pi_j) + R_W^2 \sigma^2(V_j) + R_W^2 \sigma^2(I_j) \quad (A2)$$

and for LMC Cepheids we use a total statistical uncertainty arising from the quadrature sum of four terms:

$$\sigma_{LMC,j}^2 = \sigma^2(m_{H,j}) + \sigma^2(\mu) + R_W^2 \sigma^2(V_j) + R_W^2 \sigma^2(I_j) \quad (A3)$$

We see that for the MW and LMC Cepheids where the color errors are provided by SH0ES team (see in Table 1 of Ref. [20] and in Table 2 of Ref. [16] or our Table IV and our Table V of the Appendix B respectively) we have included them in the error matrix \mathbf{C} in the proper 2D manner (i.e. 2D fit including errors in both \mathbf{Y} and \mathbf{X} "axes").

For the j th Cepheid in the i th galaxy (other than MW and LMC) where SH0ES does not provide separate color errors we use a total statistical uncertainty σ_{tot} arising from the quadrature sum of four terms: NIR photometric error, color error, intrinsic width and random-phase as derived by SH0ES team and shown in column 8 of Table 4 of Ref. [18]

$$\sigma_{tot,j}^2 = \sigma_{sky}^2 + \sigma_{col}^2 + \sigma_{int}^2 + (f_{pf}\sigma_{ph})^2 \quad (\text{A4})$$

These total statistical uncertainties σ_{tot} are shown in our Table VI of the Appendix B. Note that even though the color errors are included implicitly in our fit, in order to make a full 2D fit we will need the separate color errors which are not publicly available for these Cepheids by SH0ES team.

The schematic form of the matrix of measurements \mathbf{Y} and the matrix of parameters \mathbf{X} are

$$\mathbf{Y} = \begin{pmatrix} m_{\pi,j} \\ m_{H,1,j} \\ \vdots \\ m_{H,19,j} \\ m_{H,N4258,j} \\ m_{H,M31,j} \\ m_{H,LMC,j} \\ \mu_{N4258} \\ \mu_{LMC} \\ m_{B,1} \\ \vdots \\ m_{B,19} \end{pmatrix}, \quad \mathbf{X} = \begin{pmatrix} R_{W,LMC} \\ R_{W,MW} \\ R_{W,1} \\ \vdots \\ R_{W,19} \\ R_{W,N4258} \\ R_{W,M31} \\ \mu_1 \\ \vdots \\ \mu_{19} \\ \mu_{N4258} \\ \mu_{M31} \\ \mu_{LMC} \\ M_{H,MW}^W \\ M_{H,1}^W \\ \vdots \\ M_{H,19}^W \\ M_{H,N4258}^W \\ M_{H,M31}^W \\ M_{H,LMC}^W \\ b_W^s \\ b_W^l \\ Z_W \\ z_p \\ M_B \end{pmatrix} \quad (\text{A5})$$

The schematic form of the equation (or design) matrix \mathbf{A} is

$$\mathbf{A} = \begin{pmatrix}
 0 & (V-I)_{MW,1} & 0 & \cdot & \cdot & \cdot & 0 & \dots & 1 & 0 & \dots & [P]_{MW,1}^s & [P]_{MW,1}^l & [M/H]_1 & \frac{-5\pi_1}{\ln 10} & 0 \\
 \vdots & \vdots & \vdots & \vdots & \vdots & \vdots & \vdots & \vdots & \vdots & \vdots & \vdots & \vdots & \vdots & \vdots & \vdots & \vdots \\
 0 & (V-I)_{MW,N} & 0 & \cdot & \cdot & \cdot & 0 & \dots & 1 & 0 & \dots & [P]_{MW,N}^s & [P]_{MW,N}^l & [M/H]_{19} & \frac{-5\pi_N}{\ln 10} & 0 \\
 0 & 0 & (V-I)_{1,1} & 0 & \dots & \dots & 1 & 0 & \dots & 0 & 1 & \dots & [P]_{1,1}^l & [M/H]_{1,1} & 0 & 0 \\
 \vdots & \vdots & \vdots & \vdots & \vdots & \vdots & \vdots & \vdots & \vdots & \vdots & \vdots & \vdots & \vdots & \vdots & \vdots & \vdots \\
 0 & 0 & (V-I)_{1,N} & 0 & \dots & \dots & 1 & 0 & \dots & 0 & 1 & \dots & [P]_{1,N}^l & [M/H]_{1,N} & 0 & 0 \\
 0 & 0 & 0 & (V-I)_{2,1} & 0 & \dots & 0 & 1 & 0 & \dots & 0 & 0 & [P]_{2,1}^l & [M/H]_{2,1} & 0 & 0 \\
 \vdots & \vdots & \vdots & \vdots & \vdots & \vdots & \vdots & \vdots & \vdots & \vdots & \vdots & \vdots & \vdots & \vdots & \vdots & \vdots \\
 0 & 0 & 0 & (V-I)_{2,N} & 0 & \dots & 0 & 1 & 0 & \dots & 0 & 0 & [P]_{2,N}^l & [M/H]_{2,N} & 0 & 0 \\
 \vdots & \vdots & \vdots & \vdots & \vdots & \vdots & \vdots & \vdots & \vdots & \vdots & \vdots & \vdots & \vdots & \vdots & \vdots & \vdots \\
 0 & 0 & 0 & \cdot & \cdot & \cdot & (V-I)_{M31,1} & 0 & \dots & 1 & 0 & \dots & [P]_{M31,1}^l & [M/H]_{M31,1} & 0 & 0 \\
 \vdots & \vdots & \vdots & \vdots & \vdots & \vdots & \vdots & \vdots & \vdots & \vdots & \vdots & \vdots & \vdots & \vdots & \vdots & \vdots \\
 0 & 0 & 0 & \cdot & \cdot & \cdot & (V-I)_{M31,N} & 0 & \dots & 1 & 0 & \dots & [P]_{M31,N}^l & [M/H]_{M31,N} & 0 & 0 \\
 (V-I)_{LMC,1} & 0 & 0 & \cdot & \cdot & \cdot & 0 & \dots & 0 & 1 & 0 & \dots & [P]_{LMC,1}^l & [M/H]_{LMC,1} & 0 & 0 \\
 \vdots & \vdots & \vdots & \vdots & \vdots & \vdots & \vdots & \vdots & \vdots & \vdots & \vdots & \vdots & \vdots & \vdots & \vdots & \vdots \\
 (V-I)_{LMC,N} & 0 & 0 & \cdot & \cdot & \cdot & 0 & \dots & 0 & 1 & 0 & \dots & [P]_{LMC,N}^l & [M/H]_{LMC,N} & 0 & 0 \\
 0 & \cdot & \cdot & \cdot & \cdot & \cdot & 0 & \dots & 1 & 0 & 0 & \dots & \cdot & \cdot & \cdot & \cdot \\
 0 & \cdot & \cdot & \cdot & \cdot & \cdot & 0 & \dots & 0 & 0 & 1 & 0 & \dots & \cdot & \cdot & \cdot \\
 0 & \cdot & \cdot & \cdot & \cdot & \cdot & 1 & 0 & \dots & 0 & 1 & 0 & \dots & \cdot & \cdot & \cdot \\
 0 & \cdot & \cdot & \cdot & \cdot & \cdot & 0 & 1 & 0 & \dots & 0 & 1 & 0 & \dots & \cdot & \cdot \\
 \vdots & \vdots & \vdots & \vdots & \vdots & \vdots & \vdots & \vdots & \vdots & \vdots & \vdots & \vdots & \vdots & \vdots & \vdots & \vdots \\
 0 & \cdot & \cdot & \cdot & \cdot & \cdot & 0 & \dots & 1 & 0 & 0 & \dots & \cdot & \cdot & \cdot & \cdot
 \end{pmatrix}$$

(A6)

Appendix B: DATA USED IN THE ANALYSIS

In this appendix we present the data used in the analysis.

TABLE IV: Photometric data for MW Cepheids from Table 1 in Ref. [20].

Cepheid	log P	F 555W [mag]	σ [mag]	F 814W [mag]	σ [mag]	F 160W [mag]	σ [mag]	m_H^W [mag]	σ [mag]	[Fe/H]	π [mas]	σ [mas]	π_{EDR3} [mas]	σ [mas]
AA-GEM	1.053	9.9130	0.029	8.542	0.025	7.348	0.017	6.860	0.023	-0.080	0.259	0.008	0.311	0.019
AD-PUP	1.133	10.015	0.028	8.675	0.023	7.488	0.020	7.011	0.024	-0.060	0.214	0.006	0.254	0.018
AQ-CAR	0.990	8.9836	0.020	7.854	0.009	6.766	0.007	6.373	0.011	0.013	0.354	0.010	0.361	0.017
AQ-PUP	1.479	8.8671	0.018	7.120	0.014	5.487	0.013	4.859	0.016	0.060	0.340	0.010	0.294	0.025
BK-AUR	0.903	9.5609	0.036	8.220	0.038	7.015	0.021	6.539	0.029	0.070	0.371	0.011	0.426	0.016
BN-PUP	1.136	10.051	0.033	8.505	0.017	7.198	0.015	6.642	0.021	0.030	0.251	0.007	0.301	0.016
CD-CYG	1.232	9.1207	0.011	7.468	0.012	5.900	0.012	5.307	0.014	0.120	0.398	0.011	0.394	0.018
CP-CEP	1.252	10.757	0.015	8.638	0.052	6.871	0.022	6.095	0.030	0.050	0.270	0.008	0.279	0.022
CR-CAR	0.989	11.750	0.019	9.973	0.018	8.384	0.014	7.736	0.017	-0.080	0.190	0.005	0.194	0.016
CY-AUR	1.141	12.052	0.012	9.953	0.020	8.106	0.025	7.334	0.027	-0.150	0.183	0.006
DD-CAS	0.992	10.036	0.007	8.523	0.011	7.108	0.012	6.566	0.013	0.160	0.319	0.009	0.346	0.014
DL-CAS	0.903	9.1059	0.019	7.569	0.022	6.238	0.018	5.689	0.021	0.050	0.550	0.016
DR-VEL	1.049	9.7083	0.034	7.770	0.020	6.183	0.021	5.479	0.026	0.024	0.488	0.015	0.520	0.015
GQ-ORI	0.935	8.7199	0.020	7.632	0.024	6.523	0.032	6.146	0.034	0.250	0.418	0.013	0.408	0.023
HW-CAR	0.964	9.2782	0.016	8.007	0.013	6.798	0.005	6.350	0.009	0.060	0.370	0.010	0.397	0.013
KK-CEN	1.086	11.598	0.017	9.862	0.021	8.292	0.015	7.660	0.018	0.210	0.167	0.005	0.152	0.017
KN-CEN	1.532	10.062	0.023	7.924	0.017	5.856	0.006	5.076	0.013	0.550	0.273	0.008	0.251	0.020
RW-CAM	1.215	8.8673	0.015	7.044	0.014	5.451	0.021	4.794	0.022	0.080	0.519	0.015
RW-CAS	1.170	9.3719	0.021	7.863	0.016	6.483	0.022	5.944	0.024	0.280	0.322	0.010	0.334	0.021
RY-CAS	1.084	10.075	0.019	8.333	0.040	6.715	0.010	6.085	0.020	0.320	0.342	0.010	0.359	0.016
RY-SCO	1.308	8.2067	0.012	6.206	0.010	4.408	0.010	3.685	0.012	0.010	0.757	0.021	0.764	0.035
RY-VEL	1.449	8.5234	0.036	6.757	0.016	5.211	0.017	4.576	0.023	0.090	0.403	0.012	0.376	0.023
S-NOR	0.989	6.5779	0.011	5.410	0.012	4.391	0.012	3.990	0.014	0.100	1.054	0.030	1.099	0.024
S-VUL	1.839	9.1668	0.008	6.862	0.012	4.885	0.010	4.043	0.011	0.090	0.287	0.008	0.237	0.022
SS-CMA	1.092	10.121	0.012	8.444	0.008	6.894	0.011	6.289	0.012	0.012	0.315	0.009	0.308	0.014
SV-PER	1.046	9.2186	0.016	7.760	0.014	6.435	0.027	5.916	0.028	0.030	0.400	0.012
SV-VEL	1.149	8.7316	0.026	7.302	0.009	6.024	0.010	5.517	0.015	0.090	0.411	0.012	0.434	0.019
SV-VUL	1.653	7.2675	0.047	5.648	0.033	4.214	0.027	3.639	0.035	0.110	0.457	0.015	0.402	0.023
SY-NOR	1.102	9.8284	0.023	7.925	0.038	6.214	0.013	5.523	0.022	0.230	0.435	0.013
SZ-CYG	1.179	9.6209	0.013	7.756	0.017	6.004	0.008	5.329	0.012	0.150	0.426	0.012	0.445	0.014
T-MON	1.432	6.0680	0.023	4.828	0.016	3.725	0.021	3.298	0.024	0.040	0.749	0.022	0.745	0.057
U-CAR	1.589	6.3852	0.038	4.967	0.023	3.768	0.019	3.272	0.026	0.250	0.589	0.018	0.561	0.025
UU-MUS	1.066	9.9212	0.024	8.457	0.025	7.108	0.010	6.584	0.017	0.190	0.282	0.008	0.306	0.013
V-339-CEN	0.976	8.8402	0.024	7.321	0.016	5.990	0.024	5.448	0.026	-0.080	0.557	0.017	0.568	0.023
V-340-ARA	1.318	10.460	0.024	8.554	0.014	6.808	0.012	6.115	0.016	-0.080	0.245	0.007	0.239	0.022
VW-CEN	1.177	10.379	0.031	8.718	0.023	7.158	0.010	6.558	0.018	0.410	0.238	0.007	0.260	0.017
VX-PER	1.037	9.4589	0.008	7.906	0.006	6.470	0.009	5.914	0.010	0.030	0.407	0.011	0.392	0.019
VY-CAR	1.276	7.6162	0.014	6.253	0.007	4.991	0.004	4.513	0.007	0.080	0.539	0.015	0.565	0.018
VZ-PUP	1.365	9.7715	0.033	8.262	0.022	6.931	0.017	6.390	0.023	-0.010	0.200	0.006	0.220	0.016
WX-PUP	0.951	9.1909	0.030	7.944	0.012	6.807	0.010	6.368	0.016	-0.010	0.376	0.011	0.387	0.017
WZ-SGR	1.339	8.2021	0.012	6.481	0.013	4.858	0.009	4.242	0.011	0.280	0.547	0.015	0.612	0.031
X-CYG	1.214	6.5295	0.020	5.230	0.049	4.080	0.033	3.629	0.039	0.160	0.883	0.029	0.910	0.022
X-PUP	1.414	8.6949	0.019	7.128	0.010	5.628	0.008	5.069	0.012	0.020	0.341	0.010	0.397	0.022
XX-CAR	1.196	9.4627	0.027	8.067	0.015	6.833	0.022	6.337	0.025	0.010	0.264	0.008	0.305	0.016
XY-CAR	1.095	9.4660	0.011	7.927	0.009	6.455	0.006	5.904	0.008	0.012	0.375	0.010	0.390	0.015
XZ-CAR	1.221	8.7725	0.017	7.217	0.006	5.770	0.007	5.215	0.010	0.026	0.425	0.012	0.473	0.020
YZ-CAR	1.259	8.8644	0.016	7.401	0.007	5.991	0.013	5.471	0.015	-0.030	0.359	0.010	0.358	0.020
YZ-SGR	0.980	7.4662	0.021	6.176	0.014	5.103	0.020	4.653	0.022	0.120	0.786	0.023	0.860	0.027
Z-LAC	1.037	8.5686	0.022	7.157	0.015	5.917	0.018	5.417	0.021	0.070	0.509	0.015	0.510	0.023
AG-CRU	0.584	8.3175	0.013	7.307	0.011	6.414	0.027	6.068	0.028	0.020	0.748	0.023	0.758	0.022
AP-PUP	0.706	7.4560	0.016	6.412	0.014	5.534	0.027	5.177	0.028	-0.020	0.941	0.029	0.924	0.022

AP-SGR	0.704	7.1056	0.028	6.036	0.013	5.094	0.027	4.729	0.030	0.160	1.145	0.035	1.217	0.026
BF-OPH	0.609	7.5091	0.018	6.347	0.010	5.374	0.027	4.972	0.028	0.110	1.184	0.036	1.189	0.026
BG-VEL	0.840	7.7827	0.010	6.299	0.009	5.054	0.019	4.529	0.020	0.040	1.033	0.030	1.045	0.019
ER-CAR	0.888	6.9095	0.011	5.916	0.012	5.078	0.027	4.742	0.028	0.120	0.867	0.026	0.869	0.016
R-CRU	0.765	6.8479	0.017	5.856	0.016	4.984	0.027	4.649	0.028	0.100	1.088	0.033	1.078	0.031
R-MUS	0.876	6.4568	0.009	5.447	0.008	4.609	0.019	4.268	0.020	-0.110	1.117	0.033	1.076	0.019
R-TRA	0.530	6.7236	0.013	5.794	0.014	5.025	0.019	4.714	0.020	0.160	1.497	0.044	1.560	0.018
RV-SCO	0.783	7.1616	0.010	5.871	0.007	4.773	0.019	4.323	0.020	0.080	1.234	0.036	1.257	0.023
RX-CAM	0.898	7.8310	0.016	6.215	0.013	4.791	0.028	4.216	0.029	0.080	1.090	0.034
RY-CMA	0.670	8.2358	0.015	7.111	0.013	6.045	0.027	5.656	0.028	0.140	0.787	0.024	0.825	0.032
S-CRUe	0.671	6.6700	0.050	5.698	0.011	4.843	0.027	4.516	0.033	0.080	1.335	0.042	1.342	0.026
S-TRA	0.801	6.5171	0.013	5.553	0.012	4.752	0.027	4.429	0.028	0.010	1.150	0.035	1.120	0.024
SS-SCT	0.565	8.3122	0.010	7.073	0.005	6.034	0.019	5.600	0.019	0.110	0.948	0.028	0.934	0.025
T-VEL	0.667	8.1205	0.009	6.915	0.007	5.839	0.019	5.419	0.020	-0.160	0.904	0.026	0.940	0.018
TX-CYG	1.168	9.6108	0.024	7.083	0.015	4.789	0.027	3.862	0.029	0.260	0.844	0.026	0.829	0.020
U-AQL	0.847	6.5396	0.019	5.168	0.029	4.115	0.027	3.636	0.030	0.140	1.531	0.047
U-SGR	0.829	6.8864	0.018	5.388	0.011	4.143	0.027	3.615	0.028	0.140	1.588	0.049	1.605	0.025
V-CAR	0.826	7.4753	0.009	6.403	0.008	5.463	0.019	5.096	0.020	0.080	0.810	0.024	0.797	0.015
V-VEL	0.641	7.5198	0.013	6.555	0.010	5.693	0.027	5.366	0.028	0.000	0.951	0.029	0.953	0.019
V0386-CYG	0.721	9.8126	0.015	7.748	0.014	5.944	0.027	5.192	0.028	0.170	0.901	0.028	0.894	0.014
V0482-SCO	0.656	8.0697	0.013	6.773	0.013	5.697	0.027	5.242	0.028	0.019	0.982	0.030	0.993	0.028
V0636-SCO	0.832	6.8167	0.009	5.618	0.008	4.568	0.020	4.154	0.021	0.070	1.239	0.036	1.180	0.037
W-GEM	0.898	7.0841	0.057	5.899	0.018	4.863	0.027	4.454	0.036	-0.010	0.984	0.032	1.006	0.031

TABLE V: Photometric data for LMC Cepheids from Table 2 in Ref. [16].

Cepheid	RA	DEC	Geo	log Period	F 555W [mag]	σ [mag]	F 814W [mag]	σ [mag]	F 160W [mag]	σ [mag]	m_H^W [mag]	σ [mag]
OGL0434	74.114583	-69.379611	0.028	1.482	13.131	0.028	12.208	0.011	11.321	0.018	10.966	0.021
OGL0501	74.462625	-69.958250	0.034	1.367	13.623	0.022	12.693	0.012	11.770	0.021	11.406	0.023
OGL0510	74.523208	-69.454333	0.027	1.566	13.457	0.037	12.299	0.021	11.232	0.042	10.787	0.045
OGL0512	74.545000	-69.949694	0.033	1.595	13.134	0.025	12.005	0.017	11.038	0.017	10.598	0.020
OGL0528	74.636583	-70.346028	0.038	1.553	13.175	0.052	12.156	0.021	11.226	0.020	10.824	0.029
OGL0545	74.696292	-70.061583	0.034	1.199	14.414	0.045	13.349	0.010	12.311	0.018	11.895	0.025
OGL0590	74.921417	-69.456111	0.025	1.502	13.470	0.025	12.382	0.014	11.311	0.038	10.895	0.039
OGL0594	74.937833	-69.493194	0.025	0.828	15.279	0.012	14.352	0.011	13.525	0.030	13.171	0.030
OGL0648	75.201500	-69.531861	0.025	1.134	14.740	0.012	13.675	0.009	12.714	0.028	12.308	0.029
OGL0683	75.353917	-70.071750	0.031	1.166	14.446	0.009	13.350	0.009	12.481	0.020	12.056	0.021
OGL0712	75.477375	-68.904028	0.016	1.316	13.771	0.033	12.862	0.009	11.889	0.038	11.552	0.040
OGL0716	75.503958	-68.922833	0.016	1.085	14.958	0.012	13.895	0.011	12.938	0.023	12.541	0.024
OGL0727	75.542667	-69.539917	0.023	1.161	14.208	0.010	13.231	0.010	12.375	0.033	12.004	0.034
OGL0757	75.629333	-69.397056	0.021	0.924	15.153	0.012	14.214	0.012	13.364	0.023	13.010	0.024
OGL0770	75.714750	-68.784806	0.013	1.035	14.698	0.012	13.757	0.010	12.913	0.029	12.566	0.030
OGL0787	75.787750	-69.223333	0.018	1.243	14.243	0.009	13.186	0.009	12.281	0.042	11.884	0.042
OGL0798	75.848542	-69.000889	0.015	1.029	14.891	0.011	13.860	0.009	12.934	0.020	12.550	0.021
OGL0800	75.854417	-68.772500	0.012	1.101	14.541	0.018	13.584	0.011	12.712	0.043	12.359	0.044
OGL0812	75.908167	-69.063083	0.015	1.086	14.670	0.011	13.691	0.010	12.733	0.024	12.369	0.025
OGL0819	75.942333	-68.876778	0.013	1.348	14.162	0.014	13.013	0.010	11.987	0.029	11.560	0.030
OGL0821	75.956250	-68.934083	0.014	1.411	13.770	0.009	12.714	0.010	11.706	0.024	11.314	0.025
OGL0831	75.988583	-68.840056	0.012	0.987	14.761	0.012	13.827	0.010	12.969	0.023	12.625	0.024
OGL0844	76.064458	-69.026778	0.014	1.235	13.967	0.019	13.010	0.011	12.146	0.034	11.791	0.035
OGL0847	76.081833	-68.930306	0.013	1.314	14.437	0.009	13.317	0.011	12.320	0.030	11.904	0.031
OGL0848	76.087833	-68.728556	0.010	1.203	14.262	0.013	13.341	0.011	12.444	0.027	12.107	0.028
OGL0888	76.316875	-68.723472	0.009	0.971	14.889	0.010	13.960	0.010	13.135	0.022	12.796	0.022
OGL0915	76.424875	-68.851472	0.010	0.868	15.125	0.013	14.216	0.011	13.359	0.021	13.027	0.022
OGL0936	76.504708	-68.627361	0.007	0.920	15.046	0.015	14.101	0.012	13.260	0.023	12.917	0.024
OGL0949	76.570375	-68.676028	0.007	1.111	14.519	0.016	13.549	0.011	12.670	0.018	12.317	0.019
OGL0966	76.699875	-70.037056	0.024	1.676	12.944	0.026	11.861	0.014	10.896	0.023	10.483	0.025
OGL0969	76.720250	-68.723639	0.007	1.104	14.727	0.013	13.691	0.012	12.725	0.028	12.347	0.029

OGL0970	76.720708	-68.659889	0.006	1.242	14.369	0.014	13.249	0.011	12.260	0.031	11.850	0.032
OGL0975	76.742833	-68.611417	0.006	1.101	14.628	0.015	13.617	0.011	12.749	0.023	12.382	0.024
OGL0978	76.748792	-68.723972	0.007	1.022	14.855	0.011	13.817	0.010	12.908	0.021	12.529	0.022
OGL0986	76.782542	-68.888750	0.009	1.492	13.471	0.018	12.403	0.008	11.445	0.045	11.053	0.045
OGL0992	76.816583	-68.883500	0.009	1.723	12.305	0.016	11.297	0.011	10.436	0.073	10.067	0.073
OGL1001	76.840375	-68.338417	0.002	1.160	14.464	0.009	13.447	0.009	12.485	0.023	12.119	0.024
OGL1031	76.925542	-69.246694	0.013	1.266	14.455	0.011	13.348	0.009	12.284	0.021	11.873	0.022
OGL1058	77.076125	-68.779750	0.006	1.482	13.564	0.016	12.452	0.008	11.467	0.021	11.060	0.022
OGL1080	77.183292	-68.757778	0.005	1.270	14.135	0.014	13.061	0.011	12.097	0.025	11.706	0.026
OGL1109	77.316417	-68.741556	0.005	1.074	14.520	0.008	13.592	0.009	12.744	0.053	12.410	0.053
OGL1112	77.326458	-68.299556	-0.000	0.899	14.713	0.010	13.907	0.011	13.134	0.053	12.853	0.054
OGL1313	78.580750	-69.490056	0.008	0.834	15.128	0.012	14.278	0.012	13.529	0.026	13.222	0.027
OGL1374	78.857208	-69.340917	0.005	0.838	15.386	0.011	14.438	0.012	13.582	0.031	13.240	0.031
OGL1389	78.909875	-69.255500	0.004	0.862	14.965	0.011	14.139	0.012	13.382	0.019	13.088	0.020
OGL1411	78.991833	-69.712083	0.009	0.897	15.324	0.010	14.324	0.011	13.468	0.026	13.102	0.026
OGL1417	79.000917	-69.538167	0.007	0.938	14.879	0.009	13.954	0.010	13.138	0.031	12.803	0.031
OGL1424	79.016000	-69.247889	0.003	0.830	15.663	0.013	14.622	0.015	13.686	0.030	13.310	0.031
OGL1431	79.041083	-69.544306	0.007	1.010	14.829	0.010	13.841	0.009	13.028	0.027	12.669	0.027
OGL1463	79.228708	-69.330667	0.003	0.876	15.098	0.011	14.171	0.011	13.339	0.024	13.007	0.025
OGL1466	79.244417	-69.393889	0.004	0.789	15.581	0.012	14.607	0.013	13.719	0.031	13.368	0.032
OGL1490	79.353083	-69.349333	0.003	0.912	14.690	0.014	13.876	0.010	13.160	0.023	12.872	0.024
OGL1526	79.515792	-69.426639	0.003	0.828	15.147	0.012	14.287	0.011	13.475	0.025	13.169	0.026
OGL1539	79.592125	-69.363139	0.002	1.130	14.636	0.016	13.620	0.011	12.671	0.019	12.306	0.021
OGL1578	79.811667	-69.605028	0.005	1.123	14.329	0.017	13.379	0.010	12.590	0.023	12.248	0.024
OGL1587	79.865750	-69.508389	0.003	1.334	14.151	0.008	12.959	0.009	11.925	0.034	11.491	0.034
OGL1616	79.999708	-69.173722	-0.001	1.191	14.894	0.017	13.693	0.012	12.631	0.033	12.198	0.034
OGL1637	80.095833	-69.038194	-0.003	1.504	13.337	0.025	12.251	0.014	11.314	0.035	10.928	0.036
OGL1641	80.119292	-69.025500	-0.003	1.144	14.180	0.010	13.272	0.010	12.428	0.026	12.111	0.027
OGL1647	80.155792	-69.515722	0.002	0.939	14.833	0.019	13.957	0.015	13.157	0.028	12.846	0.030
OGL1677	80.301958	-69.052111	-0.004	1.372	13.717	0.013	12.716	0.017	11.816	0.020	11.463	0.022
OGL1862	81.056042	-69.500444	-0.001	1.118	14.868	0.013	13.763	0.010	12.753	0.028	12.357	0.028
OGL1939	81.370042	-69.912361	0.002	0.782	15.498	0.021	14.583	0.015	13.683	0.029	13.356	0.031
OGL1940	81.370625	-69.834194	0.001	0.972	16.659	0.022	15.055	0.017	13.509	0.026	12.917	0.028
OGL1941	81.372000	-69.920167	0.003	0.832	15.642	0.015	14.538	0.013	13.593	0.029	13.193	0.030
OGL1945	81.381000	-69.834361	0.001	0.885	16.166	0.020	14.832	0.016	13.610	0.023	13.123	0.025
OGL1994	81.594042	-69.602056	-0.002	0.889	14.779	0.022	13.946	0.011	13.229	0.019	12.939	0.022
OGL2012	81.708292	-69.764667	-0.000	0.872	15.061	0.011	14.136	0.010	13.327	0.025	13.000	0.025
OGL2019	81.732917	-69.980222	0.002	1.448	13.615	0.018	12.581	0.014	11.697	0.025	11.325	0.027
OGL2043	81.845667	-69.849444	0.000	0.867	15.246	0.011	14.320	0.012	13.495	0.038	13.167	0.039

TABLE VI: WFC3-IR data for 1486 Cepheids in the anchor galaxy NGC 4258 and in the host galaxies from Table 4 in Ref. [18]. An electronic version of the complete table is available at [161].

Galaxy Name	α	δ	ID [mag]	P [days]	$V - I$ [mag]	H [mag]	σ_{tot} [mag]	Z^8 [dex]
N1309	50.513050	-15.412250	154632	38.10	1.08	25.46	0.22	8.582
N1309	50.514080	-15.405860	149317	39.31	1.34	25.31	0.42	8.722
N1309	50.537010	-15.412090	42756	39.42	1.14	25.28	0.24	8.793
N1309	50.536140	-15.385790	40303	39.50	1.00	25.19	0.24	8.758
N1309	50.534050	-15.388290	50270	39.83	1.22	25.56	0.26	8.866
N1309	50.520380	-15.397210	119907	40.84	1.40	24.57	0.55	8.974
N1309	50.516100	-15.386090	136479	41.02	1.15	25.07	0.18	8.646
N1309	50.531470	-15.406890	67093	41.77	1.23	24.45	0.45	9.037
N1309	50.528230	-15.408650	82654	41.94	1.05	24.24	0.50	8.987
N1309	50.540170	-15.394110	27150	42.11	1.03	24.49	0.28	8.860

⁸ $Z = 12 + \log(O/H)$

N1309	50.533920	-15.386930	50545	44.14	1.11	25.34	0.57	8.825
N1309	50.534590	-15.392310	48826	44.32	1.65	24.54	0.34	8.975
N1309	50.522460	-15.384870	103930	44.60	0.89	24.95	0.22	8.739
N1309	50.520140	-15.408020	2099043	44.30	1.39	24.12	0.45	8.866
N1309	50.535980	-15.411540	47351	45.45	1.02	24.64	0.24	8.828
N1309	50.516850	-15.403490	2108877	47.59	1.34	24.78	0.53	8.841
N1309	50.513220	-15.403900	152242	47.82	0.95	24.76	0.33	8.715
N1309	50.514140	-15.404030	2117990	48.18	1.23	24.88	0.43	8.745
N1309	50.517600	-15.403870	134187	47.87	1.31	23.84	0.62	8.862
N1309	50.513500	-15.398810	150120	48.45	1.52	24.85	0.30	8.743
N1309	50.541640	-15.396450	22773	49.57	1.35	25.16	0.23	8.840
N1309	50.523070	-15.400960	105535	50.82	1.25	24.92	0.49	9.074
N1309	50.530380	-15.386750	66971	51.38	1.14	24.75	0.24	8.849
N1309	50.519300	-15.403510	126515	51.43	0.80	24.60	0.60	8.922
N1309	50.532360	-15.415870	65208	52.02	1.41	24.34	0.18	8.734
N1309	50.526790	-15.409480	89446	52.50	1.11	24.57	0.40	8.950
N1309	50.523400	-15.407320	105633	54.07	0.89	24.65	0.65	8.963
N1309	50.531490	-15.389480	62523	56.82	1.13	24.77	0.25	8.934
N1309	50.530220	-15.390540	68651	58.92	1.31	25.03	0.33	8.978
N1309	50.520230	-15.406500	122991	58.97	1.66	24.83	0.43	8.902
N1309	50.515030	-15.407650	145875	64.63	1.54	24.58	0.33	8.726
N1309	50.520350	-15.400180	120871	64.84	1.32	23.75	0.54	8.983
N1309	50.528410	-15.417520	83989	64.20	1.32	24.32	0.19	8.688
N1309	50.540600	-15.394620	25808	67.70	1.18	24.61	0.19	8.854
N1309	50.528080	-15.409230	83493	57.92	1.40	24.53	0.35	8.967
N1309	50.536050	-15.412330	47225	69.33	1.11	24.57	0.22	8.804
N1309	50.537880	-15.406430	37762	69.30	1.09	24.31	0.21	8.914
N1309	50.535540	-15.414100	49918	71.48	1.08	24.12	0.23	8.758
N1309	50.527070	-15.408140	87828	73.62	0.97	24.31	0.30	8.996
N1309	50.519710	-15.404750	124934	75.76	1.50	24.21	0.40	8.918
N1309	50.518570	-15.394630	127649	84.54	1.07	24.27	0.50	8.885
N1309	50.526840	-15.407730	88762	84.89	1.27	23.90	0.40	9.007
N1309	50.540840	-15.390800	24251	90.59	1.31	24.01	0.18	8.781
N1309	50.526100	-15.405700	91743	90.91	1.06	24.08	0.36	9.061
N1365	53.428340	-36.168310	111818	15.90	0.71	25.07	0.63	8.814
N1365	53.468230	-36.154760	140975	16.45	1.27	25.25	0.32	8.420
N1365	53.435410	-36.169560	123989	16.72	0.88	24.53	0.40	8.715
N1365	53.448980	-36.163290	132389	17.00	1.07	25.29	0.33	8.613
N1365	53.444760	-36.149450	103384	17.01	0.91	25.82	0.44	8.796
N1365	53.440820	-36.157210	111940	19.69	0.67	24.86	0.40	8.784
N1365	53.465100	-36.152740	136735	25.70	0.89	24.48	0.18	8.480
N1365	53.426190	-36.165250	101154	26.08	0.99	23.98	0.70	8.878
N1365	53.445370	-36.136230	63449	26.96	1.36	24.16	0.36	8.858
N1365	53.462490	-36.157290	138773	26.98	1.01	24.40	0.19	8.481
N1365	53.443040	-36.160620	120972	27.45	1.04	24.41	0.24	8.720
N1365	53.446770	-36.135500	65336	27.94	0.87	24.82	0.32	8.839
N1365	53.438940	-36.166810	124631	29.33	1.02	24.11	0.24	8.705
N1365	53.458140	-36.153810	130859	29.37	0.98	24.48	0.23	8.571
N1365	53.460390	-36.153990	133465	29.45	1.35	24.29	0.23	8.538
N1365	53.431590	-36.162200	105797	30.34	1.29	24.07	0.48	8.851
N1365	53.427620	-36.166050	106470	30.39	0.91	23.83	0.42	8.851
N1365	53.438980	-36.153370	100027	31.37	0.67	24.33	0.30	8.845
N1365	53.431200	-36.158650	94995	32.42	1.02	24.35	0.45	8.897
N1365	53.449180	-36.155960	122163	34.10	1.21	24.19	0.19	8.680
N1365	53.449310	-36.140060	87703	35.11	1.21	23.54	0.26	8.786
N1365	53.427540	-36.151730	61628	37.01	1.61	24.27	0.38	9.018
N1365	53.433170	-36.155410	90510	39.06	1.06	24.04	0.41	8.905
N1365	53.437550	-36.170950	128912	40.73	1.14	23.47	0.20	8.673
N1365	53.440360	-36.153510	103704	40.85	1.43	24.26	0.23	8.825
N1365	53.432210	-36.161310	104907	42.90	1.10	23.44	0.36	8.854
N1365	53.431420	-36.172780	123489	43.00	0.97	23.96	0.32	8.720
N1365	53.437390	-36.155420	101731	47.24	0.91	23.03	0.22	8.848
N1365	53.435220	-36.154740	94055	51.45	1.33	23.91	0.25	8.884
N1365	53.438630	-36.170270	129336	57.13	0.95	23.42	0.16	8.668

N1365	53.432110	-36.155840	88821	63.17	1.32	23.35	0.26	8.915
N1365	53.427080	-36.156250	75575	68.46	1.25	22.90	0.32	8.976

TABLE VII: Approximations for distance parameters from Table 5 in Ref. [18].

Host Galaxy	SnIa	$m_{B,i}^0 + 5\alpha_B$ [mag]	σ [mag]	μ_{ceph} [mag]	σ [mag]	$M_{B,i}^0$ [mag]	σ [mag]
M101	2011fe	13.310	0.117	29.135	0.045	-19.389	0.125
N1015	2009ig	17.015	0.123	32.497	0.081	-19.047	0.147
N1309	2002fk	16.756	0.116	32.523	0.055	-19.331	0.128
N1365	2012fr	15.482	0.125	31.307	0.057	-19.390	0.137
N1448	2001el	15.765	0.116	31.311	0.045	-19.111	0.125
N2442	2015F	15.840	0.142	31.511	0.053	-19.236	0.152
N3021	1995al	16.527	0.117	32.498	0.090	-19.535	0.147
N3370	1994ae	16.476	0.115	32.072	0.049	-19.161	0.125
N3447	2012ht	16.265	0.124	31.908	0.043	-19.207	0.131
N3972	2011by	16.048	0.116	31.587	0.070	-19.103	0.136
N3982	1998aq	15.795	0.115	31.737	0.069	-19.507	0.134
N4038	2007sr	15.797	0.114	31.290	0.112	-19.058	0.160
N4424	2012cg	15.110	0.109	31.080	0.292	-19.534	0.311
N4536	1981B	15.177	0.124	30.906	0.053	-19.293	0.135
N4639	1990N	15.983	0.115	31.532	0.071	-19.113	0.135
N5584	2007af	16.265	0.115	31.786	0.046	-19.085	0.124
N5917	2005cf	16.572	0.115	32.263	0.102	-19.255	0.154
N7250	2013dy	15.867	0.115	31.499	0.078	-19.196	0.139
U9391	2003du	17.034	0.114	32.919	0.063	-19.449	0.130

-
- [1] N. Aghanim *et al.* (Planck), “Planck 2018 results. VI. Cosmological parameters,” *Astron. Astrophys.* **641**, A6 (2020), [arXiv:1807.06209](https://arxiv.org/abs/1807.06209) [astro-ph.CO].
- [2] Leandros Perivolaropoulos and Foteini Skara, “Challenges for Λ CDM: An update,” (2021), [arXiv:2105.05208](https://arxiv.org/abs/2105.05208) [astro-ph.CO].
- [3] <https://cosmology.physics.uoi.gr>.
- [4] L. Verde, T. Treu, and A. G. Riess, “Tensions between the Early and the Late Universe,” *Nature Astron.* **3**, 891 (2019), [arXiv:1907.10625](https://arxiv.org/abs/1907.10625) [astro-ph.CO].
- [5] Eleonora Di Valentino, Olga Mena, Supriya Pan, Luca Visinelli, Weiqiang Yang, Alessandro Melchiorri, David F. Mota, Adam G. Riess, and Joseph Silk, “In the realm of the Hubble tension—a review of solutions,” *Class. Quant. Grav.* **38**, 153001 (2021), [arXiv:2103.01183](https://arxiv.org/abs/2103.01183) [astro-ph.CO].
- [6] Henrietta S. Leavitt, “1777 variables in the Magellanic Clouds,” *Harvard Obs. Annals* **60**, 87–108 (1908).
- [7] Henrietta S. Leavitt and Edward C. Pickering, “Periods of 25 Variable Stars in the Small Magellanic Cloud,” *Harvard Obs. Circ.* **173**, 1–3 (1912).
- [8] Barry F. Madore and Wendy L. Freedman, “The Cepheid distance scale,” *Publ. Astron. Soc. Pac.* **103**, 933–957 (1991).
- [9] George H. Jacoby, David Branch, Robin Ciardullo, Roger L. Davies, William E. Harris, Michael J. Pierce, Christopher J. Pritchet, John L. Tonry, and Douglas L. Welch, “A Critical Review of Selected Techniques for Measuring Extragalactic Distances,” *Publ. Astron. Soc. Pac.* **104**, 599 (1992).
- [10] Michael Feast, “Cepheids as Distance Indicators,” *Publ. Astron. Soc. Pac.* **111**, 775–793 (1999).
- [11] George Wallerstein, “The cepheids of population ii and related stars,” *Publ. Astron. Soc. Pac.* **114**, 689–699 (2002).
- [12] Allan Sandage and Gustav A. Tammann, “Absolute magnitude calibrations of population i and ii cepheids and other pulsating variables in the instability strip of the hertzsprung-russell diagram,” *Annu. Rev. Astron. Astrophys.* **44**, 93–140 (2006), <https://doi.org/10.1146/annurev.astro.43.072103.150612>.
- [13] Pascal Fouque, Jesper Storm, and Wolfgang Gieren, “Calibration of the distance scale from Cepheids,” *Lect. Notes Phys.* **635**, 21–44 (2003), [arXiv:astro-ph/0301291](https://arxiv.org/abs/astro-ph/0301291).
- [14] P. Fouque *et al.*, “A new calibration of Galactic Cepheid Period-Luminosity relations from B to K bands and a comparison to LMC PL relations,” *Astron. Astrophys.* **476**, 73–81 (2007), [arXiv:0709.3255](https://arxiv.org/abs/0709.3255) [astro-ph].
- [15] Wendy L. Freedman and Barry F. Madore, “The Hubble

- Constant,” *Ann. Rev. Astron. Astrophys.* **48**, 673–710 (2010), [arXiv:1004.1856 \[astro-ph.CO\]](#).
- [16] Adam G. Riess, Stefano Casertano, Wenlong Yuan, Lucas M. Macri, and Dan Scolnic, “Large Magellanic Cloud Cepheid Standards Provide a 1% Foundation for the Determination of the Hubble Constant and Stronger Evidence for Physics beyond Λ CDM,” *Astrophys. J.* **876**, 85 (2019), [arXiv:1903.07603 \[astro-ph.CO\]](#).
- [17] Adam G. Riess, Lucas Macri, Stefano Casertano, Hubert Lampeitl, Henry C. Ferguson, Alexei V. Filippenko, Saurabh W. Jha, Weidong Li, and Ryan Chornock, “A 3% Solution: Determination of the Hubble Constant with the Hubble Space Telescope and Wide Field Camera 3,” *Astrophys. J.* **730**, 119 (2011), [Erratum: *Astrophys. J.* 732, 129 (2011)], [arXiv:1103.2976 \[astro-ph.CO\]](#).
- [18] Adam G. Riess *et al.*, “A 2.4% Determination of the Local Value of the Hubble Constant,” *Astrophys. J.* **826**, 56 (2016), [arXiv:1604.01424 \[astro-ph.CO\]](#).
- [19] Gaia Collaboration and A. G. A. Brown *et al.*, “Gaia Early Data Release 3. Summary of the contents and survey properties,” *Astron. Astrophys.* **649**, A1 (2021), [arXiv:2012.01533 \[astro-ph.GA\]](#).
- [20] Adam G. Riess, Stefano Casertano, Wenlong Yuan, J. Bradley Bowers, Lucas Macri, Joel C. Zinn, and Dan Scolnic, “Cosmic Distances Calibrated to 1% Precision with Gaia EDR3 Parallaxes and Hubble Space Telescope Photometry of 75 Milky Way Cepheids Confirm Tension with Λ CDM,” *Astrophys. J. Lett.* **908**, L6 (2021), [arXiv:2012.08534 \[astro-ph.CO\]](#).
- [21] W. L. Freedman *et al.* (HST), “Final results from the Hubble Space Telescope key project to measure the Hubble constant,” *Astrophys. J.* **553**, 47–72 (2001), [arXiv:astro-ph/0012376](#).
- [22] Adam G. Riess *et al.*, “A Redetermination of the Hubble Constant with the Hubble Space Telescope from a Differential Distance Ladder,” *Astrophys. J.* **699**, 539–563 (2009), [arXiv:0905.0695 \[astro-ph.CO\]](#).
- [23] Adam G. Riess *et al.*, “New Parallaxes of Galactic Cepheids from Spatially Scanning the Hubble Space Telescope: Implications for the Hubble Constant,” *Astrophys. J.* **855**, 136 (2018), [arXiv:1801.01120 \[astro-ph.SR\]](#).
- [24] Wendy L. Freedman, Barry F. Madore, Victoria Scowcroft, Chris Burns, Andy Monson, S. Eric Persson, Mark Seibert, and Jane Rigby, “Carnegie Hubble Program: A Mid-Infrared Calibration of the Hubble Constant,” *Astrophys. J.* **758**, 24 (2012), [arXiv:1208.3281 \[astro-ph.CO\]](#).
- [25] D. N. Spergel *et al.* (WMAP), “First year Wilkinson Microwave Anisotropy Probe (WMAP) observations: Determination of cosmological parameters,” *Astrophys. J. Suppl.* **148**, 175–194 (2003), [arXiv:astro-ph/0302209](#).
- [26] D. N. Spergel *et al.* (WMAP), “Wilkinson Microwave Anisotropy Probe (WMAP) three year results: implications for cosmology,” *Astrophys. J. Suppl.* **170**, 377 (2007), [arXiv:astro-ph/0603449](#).
- [27] J. Dunkley *et al.* (WMAP), “Five-Year Wilkinson Microwave Anisotropy Probe (WMAP) Observations: Likelihoods and Parameters from the WMAP data,” *Astrophys. J. Suppl.* **180**, 306–329 (2009), [arXiv:0803.0586 \[astro-ph\]](#).
- [28] E. Komatsu *et al.* (WMAP), “Seven-Year Wilkinson Microwave Anisotropy Probe (WMAP) Observations: Cosmological Interpretation,” *Astrophys. J. Suppl.* **192**, 18 (2011), [arXiv:1001.4538 \[astro-ph.CO\]](#).
- [29] C. L. Bennett *et al.* (WMAP), “Nine-Year Wilkinson Microwave Anisotropy Probe (WMAP) Observations: Final Maps and Results,” *Astrophys. J. Suppl.* **208**, 20 (2013), [arXiv:1212.5225 \[astro-ph.CO\]](#).
- [30] P. A. R. Ade *et al.* (Planck), “Planck 2013 results. XVI. Cosmological parameters,” *Astron. Astrophys.* **571**, A16 (2014), [arXiv:1303.5076 \[astro-ph.CO\]](#).
- [31] P.A.R. Ade *et al.* (Planck), “Planck 2015 results. xiii. cosmological parameters,” *Astron. Astrophys.* **594**, A13 (2016), [arXiv:1502.01589 \[astro-ph.CO\]](#).
- [32] G.E. Addison, D.J. Watts, C.L. Bennett, M. Halpern, G. Hinshaw, and J.L. Weiland, “Elucidating Λ CDM: Impact of Baryon Acoustic Oscillation Measurements on the Hubble Constant Discrepancy,” *Astrophys. J.* **853**, 119 (2018), [arXiv:1707.06547 \[astro-ph.CO\]](#).
- [33] George Efstathiou, “H0 Revisited,” *Mon. Not. Roy. Astron. Soc.* **440**, 1138–1152 (2014), [arXiv:1311.3461 \[astro-ph.CO\]](#).
- [34] Wilmar Cardona, Martin Kunz, and Valeria Pettorino, “Determining H_0 with Bayesian hyper-parameters,” *JCAP* **1703**, 056 (2017), [arXiv:1611.06088 \[astro-ph.CO\]](#).
- [35] Bonnie R. Zhang, Michael J. Childress, Tamara M. Davis, Natallia V. Karpenka, Chris Lidman, Brian P. Schmidt, and Mathew Smith, “A blinded determination of H_0 from low-redshift Type Ia supernovae, calibrated by Cepheid variables,” *Mon. Not. Roy. Astron. Soc.* **471**, 2254–2285 (2017), [arXiv:1706.07573 \[astro-ph.CO\]](#).
- [36] Brent Follin and Lloyd Knox, “Insensitivity of the distance ladder Hubble constant determination to Cepheid calibration modelling choices,” *Mon. Not. Roy. Astron. Soc.* **477**, 4534–4542 (2018), [arXiv:1707.01175 \[astro-ph.CO\]](#).
- [37] Stephen M. Feeney, Daniel J. Mortlock, and Nicolò Dalmaso, “Clarifying the Hubble constant tension with a Bayesian hierarchical model of the local distance ladder,” *Mon. Not. Roy. Astron. Soc.* **476**, 3861–3882 (2018), [arXiv:1707.00007 \[astro-ph.CO\]](#).
- [38] Hao-Yi Wu and Dragan Huterer, “Sample variance in the local measurements of the Hubble constant,” *Mon. Not. Roy. Astron. Soc.* **471**, 4946–4955 (2017), [arXiv:1706.09723 \[astro-ph.CO\]](#).
- [39] Anton Chudaykin, Dmitry Gorbunov, and Nikita Nedelko, “Combined analysis of Planck and SPTPol data favors the early dark energy models,” *JCAP* **08**, 013 (2020), [arXiv:2004.13046 \[astro-ph.CO\]](#).
- [40] G. Alestas, L. Kazantzidis, and L. Perivolaropoulos, “ H_0 Tension, Phantom Dark Energy and Cosmological Parameter Degeneracies,” *Phys. Rev. D* **101**, 123516 (2020), [arXiv:2004.08363 \[astro-ph.CO\]](#).
- [41] Moritz Haslbauer, Indranil Banik, and Pavel Kroupa, “The KBC void and Hubble tension contradict Λ CDM on a Gpc scale – Milgromian dynamics as a possible solution,” *Mon. Not. Roy. Astron. Soc.* **499**, 2845–2883 (2020), [arXiv:2009.11292 \[astro-ph.CO\]](#).
- [42] Tanvi Karwal and Marc Kamionkowski, “Dark energy at early times, the Hubble parameter, and the string axiverse,” *Phys. Rev. D* **94**, 103523 (2016), [arXiv:1608.01309 \[astro-ph.CO\]](#).
- [43] Vivian Poulin, Tristan L. Smith, Tanvi Karwal, and Marc Kamionkowski, “Early Dark Energy Can Resolve

- The Hubble Tension,” *Phys. Rev. Lett.* **122**, 221301 (2019), [arXiv:1811.04083 \[astro-ph.CO\]](#).
- [44] Prateek Agrawal, Francis-Yan Cyr-Racine, David Pinner, and Lisa Randall, “Rock ‘n’ Roll Solutions to the Hubble Tension,” (2019), [arXiv:1904.01016 \[astro-ph.CO\]](#).
- [45] Gen Ye and Yun-Song Piao, “Is the Hubble tension a hint of AdS phase around recombination?” *Phys. Rev. D* **101**, 083507 (2020), [arXiv:2001.02451 \[astro-ph.CO\]](#).
- [46] Eleonora Di Valentino, Alessandro Melchiorri, and Joseph Silk, “Reconciling Planck with the local value of H_0 in extended parameter space,” *Phys. Lett.* **B761**, 242–246 (2016), [arXiv:1606.00634 \[astro-ph.CO\]](#).
- [47] Robert R. Caldwell, William Komp, Leonard Parker, and Daniel A. T. Vanzella, “A Sudden gravitational transition,” *Phys. Rev. D* **73**, 023513 (2006), [arXiv:astro-ph/0507622](#).
- [48] Valerio Marra and Leandros Perivolaropoulos, “A rapid transition of G_{eff} at $z_t \simeq 0.01$ as a possible solution of the Hubble and growth tensions,” *Phys. Rev. D* **104**, L021303 (2021), [arXiv:2102.06012 \[astro-ph.CO\]](#).
- [49] Lavrentios Kazantzidis and Leandros Perivolaropoulos, “Is gravity getting weaker at low z ? Observational evidence and theoretical implications,” (2019), [arXiv:1907.03176 \[astro-ph.CO\]](#).
- [50] G. Alestas and L. Perivolaropoulos, “Late time approaches to the Hubble tension deforming $H(z)$, worsen the growth tension,” *Mon. Not. Roy. Astron. Soc.* **504**, 3956 (2021), [arXiv:2103.04045 \[astro-ph.CO\]](#).
- [51] Leandros Perivolaropoulos, “ H_0 Crisis: Systematics of distance calibrators or The End of Λ CDM?” <https://www.youtube.com/watch?v=RQ0DU88A2ik&t=15s>.
- [52] David Camarena and Valerio Marra, “Local determination of the Hubble constant and the deceleration parameter,” *Phys. Rev. Res.* **2**, 013028 (2020), [arXiv:1906.11814 \[astro-ph.CO\]](#).
- [53] David Camarena and Valerio Marra, “On the use of the local prior on the absolute magnitude of Type Ia supernovae in cosmological inference,” *Mon. Not. Roy. Astron. Soc.* **504**, 5164–5171 (2021), [arXiv:2101.08641 \[astro-ph.CO\]](#).
- [54] David Camarena and Valerio Marra, “A new method to build the (inverse) distance ladder,” *Mon. Not. Roy. Astron. Soc.* **495**, 2630–2644 (2020), [arXiv:1910.14125 \[astro-ph.CO\]](#).
- [55] George Alestas, Lavrentios Kazantzidis, and Leandros Perivolaropoulos, “ $w - M$ phantom transition at $z_t < 0.1$ as a resolution of the Hubble tension,” *Phys. Rev. D* **103**, 083517 (2021), [arXiv:2012.13932 \[astro-ph.CO\]](#).
- [56] L. Kazantzidis, H. Koo, S. Nesseris, L. Perivolaropoulos, and A. Shafieloo, “Hints for possible low redshift oscillation around the best-fitting Λ CDM model in the expansion history of the Universe,” *Mon. Not. Roy. Astron. Soc.* **501**, 3421–3426 (2021), [arXiv:2010.03491 \[astro-ph.CO\]](#).
- [57] L. Kazantzidis and L. Perivolaropoulos, “Hints of a Local Matter Underdensity or Modified Gravity in the Low z Pantheon data,” *Phys. Rev. D* **102**, 023520 (2020), [arXiv:2004.02155 \[astro-ph.CO\]](#).
- [58] Luca Amendola, Pier Stefano Corasaniti, and Franco Occhionero, “Time variability of the gravitational constant and type Ia supernovae,” (1999), [arXiv:astro-ph/9907222](#).
- [59] E. Gaztanaga, E. Garcia-Berro, J. Isern, E. Bravo, and I. Dominguez, “Bounds on the possible evolution of the gravitational constant from cosmological type Ia supernovae,” *Phys. Rev. D* **65**, 023506 (2002), [arXiv:astro-ph/0109299](#).
- [60] Bill S. Wright and Baojiu Li, “Type Ia supernovae, standardizable candles, and gravity,” *Phys. Rev. D* **97**, 083505 (2018), [arXiv:1710.07018 \[astro-ph.CO\]](#).
- [61] E. Garcia-Berro, E. Gaztanaga, J. Isern, O. Benvenuto, and L. Althaus, “On the evolution of cosmological type Ia supernovae and the gravitational constant,” (1999), [arXiv:astro-ph/9907440](#).
- [62] S. Nesseris and Leandros Perivolaropoulos, “Evolving newton’s constant, extended gravity theories and snia data analysis,” *Phys. Rev. D* **73**, 103511 (2006), [arXiv:astro-ph/0602053](#).
- [63] L. Kazantzidis, L. Perivolaropoulos, and F. Skara, “Constraining power of cosmological observables: blind redshift spots and optimal ranges,” *Phys. Rev. D* **99**, 063537 (2019), [arXiv:1812.05356 \[astro-ph.CO\]](#).
- [64] Catherine Heymans *et al.*, “KiDS-1000 Cosmology: Multi-probe weak gravitational lensing and spectroscopic galaxy clustering constraints,” *Astron. Astrophys.* **646**, A140 (2021), [arXiv:2007.15632 \[astro-ph.CO\]](#).
- [65] Savvas Nesseris, George Pantazis, and Leandros Perivolaropoulos, “Tension and constraints on modified gravity parametrizations of $G_{\text{eff}}(z)$ from growth rate and Planck data,” *Phys. Rev. D* **96**, 023542 (2017), [arXiv:1703.10538 \[astro-ph.CO\]](#).
- [66] Luca Amendola, Martin Kunz, Ippocratis D. Saltas, and Ignacy Sawicki, “Fate of Large-Scale Structure in Modified Gravity After GW170817 and GRB170817A,” *Phys. Rev. Lett.* **120**, 131101 (2018), [arXiv:1711.04825 \[astro-ph.CO\]](#).
- [67] Radouane Gannouji, Lavrentios Kazantzidis, Leandros Perivolaropoulos, and David Polarski, “Consistency of modified gravity with a decreasing $G_{\text{eff}}(z)$ in a Λ CDM background,” *Phys. Rev. D* **98**, 104044 (2018), [arXiv:1809.07034 \[gr-qc\]](#).
- [68] Lavrentios Kazantzidis and Leandros Perivolaropoulos, “Evolution of the $f\sigma_8$ tension with the Planck15/ Λ CDM determination and implications for modified gravity theories,” *Phys. Rev. D* **97**, 103503 (2018), [arXiv:1803.01337 \[astro-ph.CO\]](#).
- [69] Leandros Perivolaropoulos and Lavrentios Kazantzidis, “Hints of modified gravity in cosmos and in the lab?” *Int. J. Mod. Phys. D* **28**, 1942001 (2019), [arXiv:1904.09462 \[gr-qc\]](#).
- [70] F. Skara and L. Perivolaropoulos, “Tension of the E_G statistic and redshift space distortion data with the Planck - Λ CDM model and implications for weakening gravity,” *Phys. Rev. D* **101**, 063521 (2020), [arXiv:1911.10609 \[astro-ph.CO\]](#).
- [71] Radouane Gannouji, Leandros Perivolaropoulos, David Polarski, and Foteini Skara, “Weak gravity on a Λ CDM background,” *Phys. Rev. D* **103**, 063509 (2021), [arXiv:2011.01517 \[gr-qc\]](#).
- [72] George Alestas, Ioannis Antoniou, and Leandros Perivolaropoulos, “Hints for a gravitational constant transition in Tully-Fisher data,” (2021), [arXiv:2104.14481 \[astro-ph.CO\]](#).
- [73] Edvard Mortsell, Ariel Goobar, Joel Johansson, and Suhail Dhawan, “The Hubble Tension Bites the Dust: Sensitivity of the Hubble Constant Determination to

- Cepheid Color Calibration,” (2021), [arXiv:2105.11461 \[astro-ph.CO\]](#).
- [74] Scott Dodelson, *Modern Cosmology* (Academic Press, Amsterdam, 2003).
- [75] Leandros Perivolaropoulos, “Accelerating universe: observational status and theoretical implications,” *AIP Conf. Proc.* **848**, 698–712 (2006), [arXiv:astro-ph/0601014](#).
- [76] D. M. Scolnic *et al.*, “The Complete Light-curve Sample of Spectroscopically Confirmed SNe Ia from Pan-STARRS1 and Cosmological Constraints from the Combined Pantheon Sample,” *Astrophys. J.* **859**, 101 (2018), [arXiv:1710.00845 \[astro-ph.CO\]](#).
- [77] Bradley E. Schaefer, “The Hubble Diagram to Redshift >6 from 69 Gamma-Ray Bursts,” *Astrophys. J.* **660**, 16–46 (2007), [arXiv:astro-ph/0612285](#).
- [78] N. R. Tanvir *et al.*, “A gamma-ray burst at a redshift of $z \sim 8.2$,” *Nature* **461**, 1254–1257 (2009).
- [79] A. Cucchiara *et al.*, “A Photometric Redshift of $z \sim 9.4$ for GRB 090429B,” *Astrophys. J.* **736**, 7 (2011), [arXiv:1105.4915 \[astro-ph.CO\]](#).
- [80] J. S. Wang, F. Y. Wang, K. S. Cheng, and Z. G. Dai, “Measuring dark energy with the $E_{\text{iso}} - E_p$ correlation of gamma-ray bursts using model-independent methods,” *Astron. Astrophys.* **585**, A68 (2016), [arXiv:1509.08558 \[astro-ph.HE\]](#).
- [81] Marek Demianski, Ester Piedipalumbo, Disha Sawant, and Lorenzo Amati, “Cosmology with gamma-ray bursts: I. The Hubble diagram through the calibrated $E_{p,i} - E_{\text{iso}}$ correlation,” *Astron. Astrophys.* **598**, A112 (2017), [arXiv:1610.00854 \[astro-ph.CO\]](#).
- [82] Chen-Han Tang, Yong-Feng Huang, Jin-Jun Geng, and Zhi-Bin Zhang, “Statistical Study of Gamma-Ray Bursts with a Plateau Phase in the X-ray Afterglow,” *Astrophys. J. Suppl.* **245**, 1 (2019), [arXiv:1905.07929 \[astro-ph.HE\]](#).
- [83] M. M. Phillips, “The absolute magnitudes of Type Ia supernovae,” *Astrophys. J. Lett.* **413**, L105–L108 (1993).
- [84] Eoin Ó. Colgáin, “A hint of matter underdensity at low z ?” *JCAP* **09**, 006 (2019), [arXiv:1903.11743 \[astro-ph.CO\]](#).
- [85] Domenico Sapone, Savvas Nesseris, and Carlos A. P. Bengaly, “Is there any measurable redshift dependence on the SN Ia absolute magnitude?” *Phys. Dark Univ.* **32**, 100814 (2021), [arXiv:2006.05461 \[astro-ph.CO\]](#).
- [86] Hanwool Koo, Arman Shafieloo, Ryan E. Keeley, and Benjamin L’Huillier, “Model-independent Constraints on Type Ia Supernova Light-curve Hyperparameters and Reconstructions of the Expansion History of the Universe,” *Astrophys. J.* **899**, 9 (2020), [arXiv:2001.10887 \[astro-ph.CO\]](#).
- [87] Vladimir V. Luković, Balakrishna S. Haridasu, and Nicola Vittorio, “Exploring the evidence for a large local void with supernovae Ia data,” *Mon. Not. Roy. Astron. Soc.* **491**, 2075–2087 (2020), [arXiv:1907.11219 \[astro-ph.CO\]](#).
- [88] Isaac Tutusaus, Brahim Lamine, and Alain Blanchard, “Model-independent cosmic acceleration and redshift-dependent intrinsic luminosity in type-Ia supernovae,” *Astron. Astrophys.* **625**, A15 (2019), [arXiv:1803.06197 \[astro-ph.CO\]](#).
- [89] Isaac Tutusaus, Brahim Lamine, Arnaud Dupays, and Alain Blanchard, “Is cosmic acceleration proven by local cosmological probes?” *Astron. Astrophys.* **602**, A73 (2017), [arXiv:1706.05036 \[astro-ph.CO\]](#).
- [90] Persis S. Drell, Thomas J. Loredo, and Ira Wasserman, “Type Ia supernovae, evolution, and the cosmological constant,” *Astrophys. J.* **530**, 593 (2000), [arXiv:astro-ph/9905027](#).
- [91] Beatrice M. Tinsley, “Evolution of the Stars and Gas in Galaxies,” *Astroph. J.* **151**, 547 (1968).
- [92] Yijung Kang, Young-Wook Lee, Young-Lo Kim, Chul Chung, and Chang Hee Ree, “Early-type Host Galaxies of Type Ia Supernovae. II. Evidence for Luminosity Evolution in Supernova Cosmology,” *Astrophys. J.* **889**, 8 (2020), [arXiv:1912.04903 \[astro-ph.GA\]](#).
- [93] B. M. Rose, P. M. Garnavich, and M. A. Berg, “Think Global, Act Local: The Influence of Environment Age and Host Mass on Type Ia Supernova Light Curves,” *Astrophys. J.* **874**, 32 (2019), [arXiv:1902.01433 \[astro-ph.CO\]](#).
- [94] D. O. Jones *et al.*, “Should Type Ia Supernova Distances be Corrected for their Local Environments?” *Astrophys. J.* **867**, 108 (2018), [arXiv:1805.05911 \[astro-ph.CO\]](#).
- [95] M. Rigault *et al.* (Nearby Supernova Factory), “Strong Dependence of Type Ia Supernova Standardization on the Local Specific Star Formation Rate,” *Astron. Astrophys.* **644**, A176 (2020), [arXiv:1806.03849 \[astro-ph.CO\]](#).
- [96] Young-Lo Kim, Mathew Smith, Mark Sullivan, and Young-Wook Lee, “Environmental Dependence of Type Ia Supernova Luminosities from a Sample without a Local-Global Difference in Host Star Formation,” *Astroph. J.* **854**, 24 (2018), [arXiv:1801.01192 \[astro-ph.GA\]](#).
- [97] A. Sandage, G.A. Tammann, A. Saha, B. Reindl, F.D. Macchetto, and N. Panagia, “The Hubble Constant: A Summary of the HST Program for the Luminosity Calibration of Type Ia Supernovae by Means of Cepheids,” *Astrophys. J.* **653**, 843–860 (2006), [arXiv:astro-ph/0603647](#).
- [98] G. Fritz Benedict, Barbara E. McArthur, Michael W. Feast, Thomas G. Barnes, Thomas E. Harrison, Richard J. Patterson, John W. Menzies, Jacob L. Bean, and Wendy L. Freedman, “Hubble Space Telescope Fine Guidance Sensor Parallaxes of Galactic Cepheid Variable Stars: Period-Luminosity Relations,” *Astron. J.* **133**, 1810–1827 (2007), [Erratum: *Astron. J.* **133**, 2980 (2007)], [arXiv:astro-ph/0612465](#).
- [99] Floor van Leeuwen, Michael W. Feast, Patricia A. Whitelock, and Clifton D. Laney, “Cepheid Parallaxes and the Hubble Constant,” *Mon. Not. Roy. Astron. Soc.* **379**, 723–737 (2007), [arXiv:0705.1592 \[astro-ph\]](#).
- [100] Stefano Casertano *et al.*, “Parallax of Galactic Cepheids from Spatially Scanning the Wide Field Camera 3 on the Hubble Space Telescope: The Case of SS Canis Majoris,” *Astrophys. J.* **825**, 11 (2016), [arXiv:1512.09371 \[astro-ph.SR\]](#).
- [101] Adam G. Riess, Stefano Casertano, Jay Anderson, John Mackenty, and Alexei V. Filippenko, “Parallax Beyond a Kiloparsec from Spatially Scanning the Wide Field Camera 3 on the Hubble Space Telescope,” *Astrophys. J.* **785**, 161 (2014), [arXiv:1401.0484 \[astro-ph.IM\]](#).
- [102] L. Lindegren, U. Lammers, U. Bastian, and *et al.*, “Gaia Data Release 1. Astrometry: one billion positions, two million proper motions and parallaxes,”

- Astron. Astrophys.* **595**, A4 (2016), [arXiv:1609.04303 \[astro-ph.GA\]](#).
- [103] Adam G. Riess *et al.*, “Milky Way Cepheid Standards for Measuring Cosmic Distances and Application to Gaia DR2: Implications for the Hubble Constant,” *Astrophys. J.* **861**, 126 (2018), [arXiv:1804.10655 \[astro-ph.CO\]](#).
- [104] G. Pietrzyński, D. Graczyk, A. Gallette, W. Gieren, I. B. Thompson, B. Pilecki, P. Karczmarek, M. Górski, K. Suchomska, M. Taormina, B. Zgirski, P. Wielgórski, Z. Kołaczowski, P. Konorski, S. Villanova, N. Nardetto, P. Kervella, F. Bresolin, R. P. Kudritzki, J. Storm, R. Smolec, and W. Narloch, “A distance to the Large Magellanic Cloud that is precise to one per cent,” *Nature* **567**, 200–203 (2019), [arXiv:1903.08096 \[astro-ph.GA\]](#).
- [105] J. R. Herrnstein, J. M. Moran, L. J. Greenhill, P. J. Diamond, M. Inoue, N. Nakai, M. Miyoshi, C. Henkel, and A. Riess, “A Geometric distance to the galaxy NGC 4258 from orbital motions in a nuclear gas disk,” *Nature* **400**, 539–541 (1999), [arXiv:astro-ph/9907013](#).
- [106] E. M. L. Humphreys, Mark J. Reid, Jim M. Moran, Lincoln J. Greenhill, and Alice L. Argon, “Toward a New Geometric Distance to the Active Galaxy NGC 4258. III. Final Results and the Hubble Constant,” *Astrophys. J.* **775**, 13 (2013), [arXiv:1307.6031 \[astro-ph.CO\]](#).
- [107] M. J. Reid, D. W. Pesce, and A. G. Riess, “An Improved Distance to NGC 4258 and its Implications for the Hubble Constant,” *Astrophys. J. Lett.* **886**, L27 (2019), [arXiv:1908.05625 \[astro-ph.GA\]](#).
- [108] G. Pietrzyński *et al.*, “An eclipsing binary distance to the Large Magellanic Cloud accurate to 2 per cent,” *Nature* **495**, 76–79 (2013), [arXiv:1303.2063 \[astro-ph.GA\]](#).
- [109] Siyang Li, Adam G. Riess, Michael P. Busch, Stefano Casertano, Lucas M. Macri, and Wenlong Yuan, “A sub-2% Distance to M31 from Photometrically Homogeneous Near-Infrared Cepheid Period-Luminosity Relations Measured with the Hubble Space Telescope,” (2021), [arXiv:2107.08029 \[astro-ph.CO\]](#).
- [110] B. T. Draine, “Interstellar dust grains,” *Ann. Rev. Astron. Astrophys.* **41**, 241–289 (2003), [arXiv:astro-ph/0304489](#).
- [111] Bradley W. Carroll and Dale A. Ostlie, *An Introduction to Modern Astrophysics*, 2nd ed. (Cambridge University Press, 2017).
- [112] B. F. Madore, “The period-luminosity relation. IV. Intrinsic relations and reddenings for the Large Magellanic Cloud Cepheids,” *Astroph. J.* **253**, 575–579 (1982).
- [113] Edward L. Fitzpatrick, “Correcting for the effects of interstellar extinction,” *Publ. Astron. Soc. Pac.* **111**, 63–75 (1999), [arXiv:astro-ph/9809387](#).
- [114] R. McGonegal, C. W. McAlary, B. F. Madore, and R. A. McLaren, “The Cepheid distance scale - A new application for infrared photometry,” *Astroph. J.* **257**, L33–L36 (1982).
- [115] Wendy L. Freedman, Christine D. Wilson, and Barry F. Madore, “New Cepheid Distances to Nearby Galaxies Based on BVRI CCD Photometry. II. The Local Group Galaxy M33,” *Astroph. J.* **372**, 455 (1991).
- [116] Lucas M. Macri *et al.*, “NICMOS observations of extragalactic Cepheids. 1. Photometry database and a test of the standard extinction law,” *Astrophys. J.* **549**, 721 (2001), [arXiv:astro-ph/0102125](#).
- [117] Piotr Wielgórski, Grzegorz Pietrzyński, Wolfgang Gieren, Marek Górski, Rolf-Peter Kudritzki, Bartłomiej Zgirski, Fabio Bresolin, Jesper Storm, Noriyuki Matsunaga, Dariusz Graczyk, and Igor Soszyński, “A Precision Determination of the Effect of Metallicity on Cepheid Absolute Magnitudes in VIJHK Bands from Magellanic Cloud Cepheids,” *Astroph. J.* **842**, 116 (2017), [arXiv:1705.10855 \[astro-ph.SR\]](#).
- [118] W. Gieren, J. Storm, P. Konorski, M. Górski, B. Pilecki, I. Thompson, G. Pietrzyński, D. Graczyk, T. G. Barnes, P. Fouqué, N. Nardetto, A. Gallette, P. Karczmarek, K. Suchomska, P. Wielgórski, M. Taormina, and B. Zgirski, “The effect of metallicity on Cepheid period-luminosity relations from a Baade-Wesselink analysis of Cepheids in the Milky Way and Magellanic Clouds,” *Astron. Astrophys.* **620**, A99 (2018), [arXiv:1809.04073 \[astro-ph.SR\]](#).
- [119] M. A. T. Groenewegen, “The Cepheid period-luminosity-metallicity relation based on Gaia DR2 data,” *Astron. Astrophys.* **619**, A8 (2018), [arXiv:1808.05796 \[astro-ph.SR\]](#).
- [120] V. Ripepi, G. Catanzaro, R. Molinaro, M. Marconi, G. Clementini, F. Cusano, G. De Somma, S. Lecchia, I. Musella, and V. Testa, “Period-luminosity-metallicity relation of classical Cepheids,” *Astron. Astrophys.* **642**, A230 (2020), [arXiv:2008.04608 \[astro-ph.SR\]](#).
- [121] Louise Breuval, Pierre Kervella, Piotr Wielgórski, Wolfgang Gieren, Dariusz Graczyk, Boris Trahin, Grzegorz Pietrzyński, Frédéric Arenou, Behnam Javanmardi, and Bartłomiej Zgirski, “The Influence of Metallicity on the Leavitt Law from Geometrical Distances of Milky Way and Magellanic Cloud Cepheids,” *Astroph. J.* **913**, 38 (2021), [arXiv:2103.10894 \[astro-ph.GA\]](#).
- [122] Wendy L. Freedman, Barry F. Madore, Dylan Hatt, Taylor J. Hoyt, In Sung Jang, Rachael L. Beaton, Christopher R. Burns, Myung Gyoon Lee, Andrew J. Monson, Jillian R. Neeley, M. M. Phillips, Jeffrey A. Rich, and Mark Seibert, “The carnegie-chicago hubble program. VIII. an independent determination of the hubble constant based on the tip of the red giant branch,” *Astroph. J.* **882**, 34 (2019).
- [123] Adam G. Riess, Wenlong Yuan, Stefano Casertano, Lucas M. Macri, and Dan Scolnic, “The Accuracy of the Hubble Constant Measurement Verified through Cepheid Amplitudes,” *Astrophys. J.* **896**, L43 (2020), [arXiv:2005.02445 \[astro-ph.CO\]](#).
- [124] Wendy L. Freedman, “Measurements of the Hubble Constant: Tensions in Perspective,” (2021), [arXiv:2106.15656 \[astro-ph.CO\]](#).
- [125] J. D. Fernie, “The Structure of the Cepheid Instability Strip,” *Astroph. J.* **354**, 295 (1990).
- [126] Allan Sandage and G. A. Tammann, “Temperature Differences in the Cepheid Instability Strip Require Differences in the Period-Luminosity Relation in Slope and Zero Point,” *Astrophys. J.* **686**, 779–784 (2008), [arXiv:0803.3836 \[astro-ph\]](#).
- [127] Barry F. Madore, Wendy L. Freedman, and Sandy Moak, “A Method for Improving Galactic Cepheid Reddenings and Distances,” *Astroph. J.* **842**, 42 (2017).
- [128] Ondrej Pejcha and Christopher S. Kochanek, “A Global Physical Model for Cepheids,” *Astrophys. J.* **748**, 107 (2012), [arXiv:1112.3038 \[astro-ph.SR\]](#).
- [129] Gustav A. Tammann, Bernd Reindl, Frank Thim, Abhijit Saha, and Allan Sandage, “Cepheids, Supernovae,

- H_0 , and the Age of the Universe,” in *A New Era in Cosmology*, Astronomical Society of the Pacific Conference Series, Vol. 283, edited by Nigel Metcalfe and Tom Shanks (2002) p. 258, [arXiv:astro-ph/0112489](https://arxiv.org/abs/astro-ph/0112489) [astro-ph].
- [130] G. A. Tammann, A. Sandage, and Bernd Reindl, “New period - luminosity and period - color relations of classical Cepheids: 1. Cepheids in the Galaxy,” *Astron. Astrophys.* **404**, 423–448 (2003), [arXiv:astro-ph/0303378](https://arxiv.org/abs/astro-ph/0303378).
- [131] A. Sandage, G. A. Tammann, and Bernd Reindl, “New period - luminosity and period - color relations of classical Cepheids: 2. Cepheids in LMC,” *Astron. Astrophys.* **424**, 43–71 (2004), [arXiv:astro-ph/0402424](https://arxiv.org/abs/astro-ph/0402424).
- [132] Cow-Choong Ngeow, Shashi M. Kanbur, Sergei Nikolaev, John Buonaccorsi, Kem H. Cook, and Douglas L. Welch, “Further empirical evidence for the non-linearity of the period-luminosity relations as seen in the Large Magellanic Cloud Cepheids,” *Mon. Not. Roy. Astron. Soc.* **363**, 831–846 (2005), [arXiv:astro-ph/0507601](https://arxiv.org/abs/astro-ph/0507601).
- [133] A. Sandage, G. A. Tammann, and B. Reindl, “New period-luminosity and period-color relations of classical Cepheids: III. Cepheids in SMC,” *Astron. Astrophys.* **493**, 471–479 (2009), [arXiv:0810.1780](https://arxiv.org/abs/0810.1780) [astro-ph].
- [134] Anupam Bhardwaj, Shashi M. Kanbur, Lucas M. Macri, Harinder P. Singh, Chow-Choong Ngeow, and Emille E. O. Ishida, “Large Magellanic Cloud Near-Infrared Synoptic Survey - III. A statistical study of non-linearity in the Leavitt Laws,” *Mon. Not. Roy. Astron. Soc.* **457**, 1644–1665 (2016), [arXiv:1601.00953](https://arxiv.org/abs/1601.00953) [astro-ph.GA].
- [135] H. L. Johnson and J. Borgman, “The law of interstellar extinction,” *BAN* **17**, 115 (1963).
- [136] Kevin Krisciunas, Jose Luis Prieto, Peter M. Garnavich, Jessica-Lynn G. Riley, Armin Rest, Christopher Stubbs, and Russet McMillan, “Photometry of the type ia supernovae 1999cc, 1999cl, and 2000cf,” *Astron. J.* **131**, 1639–1647 (2006), [arXiv:astro-ph/0511162](https://arxiv.org/abs/astro-ph/0511162).
- [137] Serena Nobili and Ariel Goobar, “The colour-lightcurve shape relation of Type Ia supernovae and the reddening law,” *Astron. Astrophys.* **487**, 19 (2008), [arXiv:0712.1155](https://arxiv.org/abs/0712.1155) [astro-ph].
- [138] M. M. Fausnaugh, C. S. Kochanek, J. R. Gerke, L. M. Macri, A. G. Riess, and K. Z. Stanek, “The Cepheid distance to the maser-host galaxy NGC 4258: studying systematics with the Large Binocular Telescope,” *Mon. Not. Roy. Astron. Soc.* **450**, 3597–3619 (2015), <https://academic.oup.com/mnras/article-pdf/450/4/3597/5831120/stv881.pdf>.
- [139] Ariel Goobar, “Low R_v from circumstellar dust around supernovae,” *Astrophys. J. Lett.* **686**, L103–L106 (2008), [arXiv:0809.1094](https://arxiv.org/abs/0809.1094) [astro-ph].
- [140] Gaston Folatelli *et al.*, “The Carnegie Supernova Project: Analysis of the First Sample of Low-Redshift Type-Ia Supernovae,” *Astron. J.* **139**, 120–144 (2010), [arXiv:0910.3317](https://arxiv.org/abs/0910.3317) [astro-ph.CO].
- [141] Hubert Lampeitl *et al.* (SDSS), “The Effect of Host Galaxies on Type Ia Supernovae in the SDSS-II Supernova Survey,” *Astrophys. J.* **722**, 566–576 (2010), [arXiv:1005.4687](https://arxiv.org/abs/1005.4687) [astro-ph.CO].
- [142] A. Goobar *et al.*, “The Rise of SN 2014J in the Nearby Galaxy M82,” *Astrophys. J. Lett.* **784**, L12 (2014), [arXiv:1402.0849](https://arxiv.org/abs/1402.0849) [astro-ph.GA].
- [143] R. Amanullah *et al.*, “The peculiar extinction law of SN2014J measured with The Hubble Space Telescope,” *Astrophys. J. Lett.* **788**, L21 (2014), [arXiv:1404.2595](https://arxiv.org/abs/1404.2595) [astro-ph.HE].
- [144] R. Amanullah *et al.*, “Diversity in extinction laws of Type Ia supernovae measured between 0.2 and 2 μm ,” *Mon. Not. Roy. Astron. Soc.* **453**, 3300–3328 (2015), [arXiv:1504.02101](https://arxiv.org/abs/1504.02101) [astro-ph.HE].
- [145] Aleksandar Cikota, Susana Deustua, and Francine Marleau, “Determining Type Ia Supernovae Host galaxy extinction probabilities and a statistical approach to estimating the absorption-to-reddening ratio R_V ,” *Astrophys. J.* **819**, 152 (2016), [arXiv:1601.05659](https://arxiv.org/abs/1601.05659) [astro-ph.GA].
- [146] Rahul Biswas *et al.*, “Two c’s in a pod: Cosmology independent measurement of the Type Ia supernova colour-luminosity relation with a sibling pair,” (2021), [arXiv:2103.16978](https://arxiv.org/abs/2103.16978) [astro-ph.GA].
- [147] Jason A. Cardelli, Geoffrey C. Clayton, and John S. Mathis, “The relationship between infrared, optical, and ultraviolet extinction,” *Astrophys. J.* **345**, 245–256 (1989).
- [148] James E. O’Donnell, “ R_v -dependent Optical and Near-Ultraviolet Extinction,” *Astroph. J.* **422**, 158 (1994).
- [149] David M. Nataf *et al.*, “Interstellar extinction curve variations towards the inner Milky Way: a challenge to observational cosmology,” *Mon. Not. Roy. Astron. Soc.* **456**, 2692–2706 (2016), [arXiv:1510.01321](https://arxiv.org/abs/1510.01321) [astro-ph.SR].
- [150] Edvard Mortsell, Ariel Goobar, Joel Johansson, and Suhail Dhawan, “The Hubble Tension Revisited: Additional Local Distance Ladder Uncertainties,” (2021), [arXiv:2106.09400](https://arxiv.org/abs/2106.09400) [astro-ph.CO].
- [151] G. Efstathiou, “A Lockdown Perspective on the Hubble Tension (with comments from the SH0ES team),” (2020), [arXiv:2007.10716](https://arxiv.org/abs/2007.10716) [astro-ph.CO].
- [152] Samantha L. Hoffmann *et al.*, “Optical Identification of Cepheids in 19 Host Galaxies of Type Ia Supernovae and NGC 4258 with the Hubble Space Telescope,” *Astrophys. J.* **830**, 10 (2016), [arXiv:1607.08658](https://arxiv.org/abs/1607.08658) [astro-ph.SR].
- [153] Julien Guy, P. Astier, S. Nobili, N. Regnault, and R. Pain (SNLS), “SALT: A Spectral adaptive Light curve Template for Type Ia supernovae,” *Astron. Astrophys.* **443**, 781–791 (2005), [arXiv:astro-ph/0506583](https://arxiv.org/abs/astro-ph/0506583).
- [154] Julien Guy *et al.* (SNLS), “SALT2: Using distant supernovae to improve the use of Type Ia supernovae as distance indicators,” *Astron. Astrophys.* **466**, 11–21 (2007), [arXiv:astro-ph/0701828](https://arxiv.org/abs/astro-ph/0701828).
- [155] J. Guy *et al.* (SNLS), “The Supernova Legacy Survey 3-year sample: Type Ia Supernovae photometric distances and cosmological constraints,” *Astron. Astrophys.* **523**, A7 (2010), [arXiv:1010.4743](https://arxiv.org/abs/1010.4743) [astro-ph.CO].
- [156] J. Mosher *et al.*, “Cosmological Parameter Uncertainties from SALT-II Type Ia Supernova Light Curve Models,” *Astrophys. J.* **793**, 16 (2014), [arXiv:1401.4065](https://arxiv.org/abs/1401.4065) [astro-ph.CO].
- [157] <http://supernovae.in2p3.fr/salt/doku.php>.
- [158] M. Betoule *et al.* (SDSS), “Improved cosmological constraints from a joint analysis of the SDSS-II and SNLS supernova samples,” *Astron. Astrophys.* **568**, A22 (2014), [arXiv:1401.4064](https://arxiv.org/abs/1401.4064) [astro-ph.CO].
- [159] M. Romaniello, F. Primas, M. Mottini, S. Pedicelli, B. Lemasle, G. Bono, P. Francois, M. A. T. Groenewegen, and C. D. Laney, “The influence of chemical composition on the properties of Cepheid stars. II-The iron content,” *Astron. Astrophys.* **488**, 731 (2008), [arXiv:0807.1196](https://arxiv.org/abs/0807.1196) [astro-ph].
- [160] Samyaday Choudhury, Annapurni Subrama-

- niam, and Andrew A. Cole, “Photometric metallicity map of the Large Magellanic Cloud,” *Mon. Not. Roy. Astron. Soc.* **455**, 1855–1880 (2015), <https://academic.oup.com/mnras/article-pdf/455/2/1855/18513939/stv2414.pdf>.
- [161] https://github.com/FOTEINISKARA/Cepheid_SnIa_Calibrator_Data_Transition.
- [162] H. Jeffreys, *Theory of probability*, 3rd ed. (Oxford University Press, 1961).
- [163] Andrew R. Liddle, “How many cosmological parameters?” *Mon. Not. Roy. Astron. Soc.* **351**, L49–L53 (2004), [arXiv:astro-ph/0401198](https://arxiv.org/abs/astro-ph/0401198) [astro-ph].
- [164] Savvas Nesseris and Juan Garcia-Bellido, “Is the Jeffreys’ scale a reliable tool for Bayesian model comparison in cosmology?” *JCAP* **08**, 036 (2013), [arXiv:1210.7652](https://arxiv.org/abs/1210.7652) [astro-ph.CO].
- [165] Alexander Bonilla Rivera and Jorge Enrique García-Farieta, “Exploring the Dark Universe: constraints on dynamical Dark Energy models from CMB, BAO and growth rate measurements,” *Int. J. Mod. Phys. D* **28**, 1950118 (2019), [arXiv:1605.01984](https://arxiv.org/abs/1605.01984) [astro-ph.CO].
- [166] Judit Pérez-Romero and Savvas Nesseris, “Cosmological constraints and comparison of viable $f(R)$ models,” *Phys. Rev. D* **97**, 023525 (2018), [arXiv:1710.05634](https://arxiv.org/abs/1710.05634) [astro-ph.CO].
- [167] David Camarena and Valerio Marra, “Impact of the cosmic variance on H_0 on cosmological analyses,” *Phys. Rev. D* **98**, 023537 (2018), [arXiv:1805.09900](https://arxiv.org/abs/1805.09900) [astro-ph.CO].
- [168] H. Akaike, “A new look at the statistical model identification,” *IEEE Transactions on Automatic Control* **19**, 716–723.
- [169] Gideon Schwarz, “Estimating the Dimension of a Model,” *Annals Statist.* **6**, 461–464 (1978).
- [170] Andrew R Liddle, “Information criteria for astrophysical model selection,” *Mon. Not. Roy. Astron. Soc.* **377**, L74–L78 (2007), [arXiv:astro-ph/0701113](https://arxiv.org/abs/astro-ph/0701113) [astro-ph].
- [171] Fabiola Arevalo, Antonella Cid, and Jorge Moya, “AIC and BIC for cosmological interacting scenarios,” *Eur. Phys. J. C* **77**, 565 (2017), [arXiv:1610.09330](https://arxiv.org/abs/1610.09330) [astro-ph.CO].
- [172] Martin Kerscher and Jochen Weller, “On Model Selection in Cosmology,” *SciPost Phys. Lect. Notes* **9**, 1 (2019), [arXiv:1901.07726](https://arxiv.org/abs/1901.07726) [astro-ph.CO].
- [173] Moncy V. John and J. V. Narlikar, “Comparison of cosmological models using bayesian theory,” *Phys. Rev. D* **65**, 043506 (2002), [arXiv:astro-ph/0111122](https://arxiv.org/abs/astro-ph/0111122).
- [174] K. P Burnham and D. R. Anderson, *Model selection and multimodel inference*, 2nd ed. (Springer-Verlag, 2002).
- [175] K. P Burnham and D. R. Anderson, “Multimodel Inference: Understanding AIC and BIC in Model Selection,” *Sociol. Method.* **33**, 261 (2004).
- [176] Nariaki Sugiura, “Further analysts of the data by akaike’s information criterion and the finite corrections,” *Communications in Statistics - Theory and Methods* **7**, 13–26 (1978), <https://doi.org/10.1080/03610927808827599>.
- [177] Rubén Arjona, Wilmar Cardona, and Savvas Nesseris, “Unraveling the effective fluid approach for $f(R)$ models in the subhorizon approximation,” *Phys. Rev. D* **99**, 043516 (2019), [arXiv:1811.02469](https://arxiv.org/abs/1811.02469) [astro-ph.CO].
- [178] Mehdi Rezaei, Mohammad Malekjani, and Joan Sola, “Can dark energy be expressed as a power series of the Hubble parameter?” *Phys. Rev. D* **100**, 023539 (2019), [arXiv:1905.00100](https://arxiv.org/abs/1905.00100) [gr-qc].
- [179] Dillon Brout and Daniel Scolnic, “It’s Dust: Solving the Mysteries of the Intrinsic Scatter and Host-galaxy Dependence of Standardized Type Ia Supernova Brightnesses,” *Astrophys. J.* **909**, 26 (2021), [arXiv:2004.10206](https://arxiv.org/abs/2004.10206) [astro-ph.CO].
- [180] J. et al. Johansson, “Near-IR Type Ia SN distances: host galaxy extinction and mass-step corrections revisited,” (2021), [arXiv:2105.06236](https://arxiv.org/abs/2105.06236) [astro-ph.GA].
- [181] Mario Hamuy, M. M. Phillips, Jose Maza, Nicholas B. Suntzeff, R. A. Schommer, and R. Aviles, “A Hubble Diagram of Distant Type Ia Supernovae,” *Astron. J.* **109**, 1 (1995).
- [182] Mark Sullivan *et al.* (Supernova Cosmology Project), “The Hubble diagram of Type Ia supernovae as a function of host galaxy morphology,” *Mon. Not. Roy. Astron. Soc.* **340**, 1057 (2003), [arXiv:astro-ph/0211444](https://arxiv.org/abs/astro-ph/0211444).
- [183] M. J. Childress *et al.*, “Host Galaxy Properties and Hubble Residuals of Type Ia Supernovae from the Nearby Supernova Factory,” *Astrophys. J.* **770**, 108 (2013), [arXiv:1304.4720](https://arxiv.org/abs/1304.4720) [astro-ph.CO].
- [184] P. Wiseman *et al.* (DES), “Supernova Host Galaxies in the Dark Energy Survey: I. Deep Coadds, Photometry, and Stellar Masses,” *Mon. Not. Roy. Astron. Soc.* **495**, 4040–4060 (2020), [arXiv:2001.02640](https://arxiv.org/abs/2001.02640) [astro-ph.GA].
- [185] L. Kelsey *et al.* (DES), “Skip Nav Destination The effect of environment on Type Ia supernovae in the Dark Energy Survey three-year cosmological sample,” *Mon. Not. Roy. Astron. Soc.* **501**, 4861–4876 (2021), [arXiv:2008.12101](https://arxiv.org/abs/2008.12101) [astro-ph.CO].
- [186] Sara Mazrouei, Rebecca R. Ghent, William F. Bottke, Alex H. Parker, and Thomas M. Gernon, “Earth and moon impact flux increased at the end of the paleozoic,” *Science* **363**, 253–257 (2019).
- [187] P. Schulte *et al.*, “The chicxulub asteroid impact and mass extinction at the cretaceous-paleogene boundary,” *Science* **327**, 1214–1218 (2010).
- [188] Paul R. Renne, Alan L. Deino, Frederik J. Hilgen, Klaudia F. Kuiper, Darren F. Mark, William S. Mitchell, Leah E. Morgan, Roland Mundil, and Jan Smit, “Time scales of critical events around the cretaceous-paleogene boundary,” *Science* **339**, 684–687 (2013).
- [189] John Alroy, “Dynamics of origination and extinction in the marine fossil record,” *Proceedings of the National Academy of Sciences* **105**, 11536–11542 (2008).
- [190] Luis W. Alvarez, Walter Alvarez, Frank Asaro, and Helen V. Michel, “Extraterrestrial cause for the cretaceous-tertiary extinction,” *Science* **208**, 1095–1108 (1980).
- [191] Luis W. Alvarez, “Experimental Evidence that an Asteroid Impact Led to the Extinction of Many Species 65 Million Years Ago,” *Proceedings of the National Academy of Science* **80**, 627–642 (1983).
- [192] Rachael L. Beaton *et al.*, “The Carnegie-Chicago Hubble Program. I. An Independent Approach to the Extragalactic Distance Scale Using only Population II Distance Indicators,” *Astrophys. J.* **832**, 210 (2016), [arXiv:1604.01788](https://arxiv.org/abs/1604.01788) [astro-ph.CO].
- [193] S. Cassisi and M. Salaris, “A critical investigation on the discrepancy between the observational and theoretical red giant luminosity function bump,” *Mon. Not. Roy. Astron. Soc.* **285**, 593 (1997), [arXiv:astro-ph/9702029](https://arxiv.org/abs/astro-ph/9702029).
- [194] In Sung Jang and Myung Gyoon Lee, “The Tip of the Red Giant Branch Distances to Type Ia Supernova Host Galaxies. III. NGC 4038/39 and NGC 5584,” *Astroph.*

- J. **807**, 133 (2015), [arXiv:1506.03089 \[astro-ph.GA\]](#).
- [195] In Sung Jang and Myung Gyoon Lee, “The Tip of the Red Giant Branch Distances to Typa Ia Supernova Host Galaxies. V. NGC 3021, NGC 3370, and NGC 1309 and the Value of the Hubble Constant,” *Astrophys. J.* **836**, 74 (2017), [arXiv:1702.01118 \[astro-ph.CO\]](#).
- [196] Dylan Hatt *et al.*, “The Carnegie-Chicago Hubble Program. IV. The Distance to NGC 4424, NGC 4526, and NGC 4356 via the Tip of the Red Giant Branch,” *Astrophys. J.* **861**, 104 (2018), [arXiv:1806.02900 \[astro-ph.CO\]](#).
- [197] Dylan Hatt *et al.*, “The Carnegie–Chicago Hubble Program. V. The Distances to NGC 1448 and NGC 1316 via the Tip of the Red Giant Branch,” *Astrophys. J.* **866**, 145 (2018), [arXiv:1809.01741 \[astro-ph.GA\]](#).
- [198] Wendy L. Freedman *et al.*, “The Carnegie-Chicago Hubble Program. VIII. An Independent Determination of the Hubble Constant Based on the Tip of the Red Giant Branch,” (2019), [10.3847/1538-4357/ab2f73](#), [arXiv:1907.05922 \[astro-ph.CO\]](#).
- [199] Wendy L. Freedman, Barry F. Madore, Taylor Hoyt, In Sung Jang, Rachael Beaton, Myung Gyoon Lee, Andrew Monson, Jill Neeley, and Jeffrey Rich, “Calibration of the Tip of the Red Giant Branch (TRGB),” (2020), [arXiv:2002.01550 \[astro-ph.GA\]](#).
- [200] Sidney R. Coleman, “The Fate of the False Vacuum. 1. Semiclassical Theory,” *Phys. Rev. D* **15**, 2929–2936 (1977), [Erratum: *Phys.Rev.D* 16, 1248 (1977)].
- [201] Amol V. Patwardhan and George M. Fuller, “Late-time vacuum phase transitions: Connecting sub-eV scale physics with cosmological structure formation,” *Phys. Rev. D* **90**, 063009 (2014), [arXiv:1401.1923 \[astro-ph.CO\]](#).
- [202] Curtis G. Callan, Jr. and Sidney R. Coleman, “The Fate of the False Vacuum. 2. First Quantum Corrections,” *Phys. Rev. D* **16**, 1762–1768 (1977).
- [203] Michael Doran and Georg Robbers, “Early dark energy cosmologies,” *JCAP* **06**, 026 (2006), [arXiv:astro-ph/0601544](#).